Health Implications of Dounreay Fuel Fragments: Estimates of Doses and Risks

JD Harrison, TP Fell, AW Phipps, TJ Smith, M Ellender, GJ Ham, A Hodgson, BT Wilkins

Health Protection Agency, Radiation Protection Division, Chilton, Didcot, Oxon OX11 ORQ

MW Charles, PJ Darley, A Sh Aydarous

School of Physics & Astronomy, University of Birmingham, Edgbaston, Birmingham B15 2TT

This study was funded by the Scottish Environment Protection Agency.

Centre for Radiation, Chemical and Environmental Hazards
Radiation Protection Division
Chilton, Didcot, Oxfordshire OX11 0RQ

Approval: June 2005
Publication: June 2005

EXECUTIVE SUMMARY

Introduction

This report provides estimates of potential doses and risks from exposure to Dounreay fuel fragments. It concentrates on exposure to particles from the Materials Test Reactor (MTR) because these are most abundant and because assessments based on the characteristics of these particles are likely to be conservative when applied to particles from the Dounreay Fast Reactor (DFR). It includes measurements on MTR and DFR particles of surface dose rates, in vitro solubility in simulated gut fluids, and in vivo intestinal absorption. The main focus is the possibility of acute effects but risks of cancer and hereditary effects are also considered. Doses were estimated assuming that particles are spherical with a homogenous elemental composition of U/Al (15% U), and that they have a specific activity of 2 GBq ^{137}Cs g^{-1}, and activity ratios of 0.9 for ^{90}Sr/^{90}Y:^{137}Cs, 0.003 for ^{238}Pu:^{137}Cs, and 0.001 for both ^{239}Pu:^{137}Cs and ^{241}Am:^{137}Cs. This summary refers in particular to particles containing 10^5 Bq ^{137}Cs, representative of the highest activities found at Sandside Bay, and 10^8 Bq ^{137}Cs, corresponding to the highest activity particles recovered on the Dounreay foreshore.

Skin contact

For comparison with experimental data and international dose limits, acute effects are evaluated in relation to skin dose over an area of 1 cm^2 to the basal layer of the epidermis at a depth of 70 μm, although when considering ulceration involving sub-epidermal tissues it may be appropriate to consider dose to a greater depth. From measurements and calculations for 10^5 and 10^8 Bq ^{137}Cs particles (diameters of about 300 μm and 3mm), dose rates were estimated as about 0.3 Gy h^{-1} and about 70 - 140 Gy h^{-1}, respectively, for a depth of 70 μm, and about 0.1 Gy h^{-1} and 40 – 80 Gy h^{-1}, respectively, for a depth of 400 μm. On the basis of a threshold for skin damage of about 2 Gy, based on animal and human data, a 10^5 Bq ^{137}Cs particle would have to remain in stationary contact with skin for at least about 7 hours to cause any discernible effect. Movement of the particle by even a few mm during contact would substantially increase the time required for ulceration to occur. However, a 10^5 Bq particle trapped for longer periods of a day or two may cause a small ulceration, extending over an area of less than 1 cm^2 and healing within a few weeks. Such ulceration could occur following short periods of contact of 15 – 30 minutes or more to a 10^8 Bq ^{137}Cs particle and exposures of several hours would result in more serious ulceration that would take longer to heal. Similar considerations apply to a particle in contact with the skin of the external auditory canal of the ear or the corneal surface of the eye.

Ingestion

For ingestion of a particle, estimated doses are greatest for the rectosigmoid region of the colon and, assuming random movement of the particle within the lumen during transit, were calculated for a 10^8 Bq ^{137}Cs particle as 0.3 – 0.4 Gy in adults and 1 Gy in one year-old children. The maximum estimated doses, for a particle moving in contact with the wall, were about 1 – 2 Gy in adults and 4 Gy in young children. Estimated

doses for particles with a ^{137}Cs activity of 10^5 Bq, typical of the highest activity particles found at Sandside Bay, were less than 10 mGy in adults and 20 mGy in one year old children. Doses may typically be increased by a factor of 2 – 3 in constipated individuals. The estimated threshold dose for lethal damage to the colon from ingested radionuclides is 20 Gy.

An additional and potentially more important consideration for an ingested particle is that the flow of material through the colon is highly variable. Movement in the rectosigmoid in particular does not occur as a constant flow but rather as mass movements resulting from periodic contractions between longer periods of quiescence. Local doses within the rectosigmoid may therefore be substantially greater than the average dose within the region. For example, 10^5 Bq and 10^8 Bq particles held stationary against the lumenal wall of the rectosigmoid for 6 hours would deliver doses to 1 cm^2 of tissue of about 0.6 Gy and 240 Gy, respectively, based on calculations of skin doses to a depth of 400 μm. Doses of 200 – 300 Gy are likely to cause ulceration that might not repair readily in the environment of the large intestine while doses of less than 1 Gy will result in localised crypt sterilisation that should be replaceable by regeneration of new crypts.

Inhalation

Inhaled particles large enough to cause acute damage to the lungs are too large to reach the airways of the lungs and will deposit in the extrathoracic airways. For the purposes of assessment of possible effects of local irradiation within the extrathoracic airways, the epithelial lining can be regarded as similar to skin.

Committed doses

Committed equivalent doses to all body tissues and committed effective doses were calculated for ingestion of MTR particles of typical solubility: that is, assuming absorption to blood to be 1% for ^{137}Cs, 0.01% for ^{90}Sr and 0.001% for ^{238}Pu, ^{239}Pu, ^{241}Am and ^{90}Y. Committed effective dose following ingestion of 10^5 and 10^8 Bq ^{137}Cs particles was estimated as 0.1 mSv and 80 mSv, respectively, for an adult male, and 0.5 mSv and 300 mSv, respectively, for a one year-old child. For each of these values, the results showed that doses are dominated (>70%) by contributions from committed equivalent doses to the alimentary tract, particularly the colon. An important factor determining colon doses from ingested particles is the assumed transit time of material through the colon. Transit times are typically increased by a factor of 2 – 3 in constipated individuals and can be increased by factors of up to 10 in extreme cases. A threefold increase in the transit time of a 10^5 Bq ^{137}Cs particle through the colon of a one year-old child would increase the committed effective dose by a factor of two to 1 mSv and a tenfold increase would increase the dose by a factor of 6 to 3 mSv.

Committed equivalent and committed effective doses were also calculated for ingestion of a 10^5 Bq ^{137}Cs particle on the basis of the uncharacteristic solubility exhibited by one MTR particle in vitro. The data obtained suggested that more than half of the radionuclide content was dissolved from the particle and would therefore be available for intestinal absorption, compared with typical solubility of 1% or less. The committed effective dose to an adult male following ingestion of a 10^5 Bq ^{137}Cs particle of such high

solubility was estimated as about 2 mSv. In this case, committed equivalent doses to the alimentary tract contributed about 15% of the committed effective dose while skeletal tissues (red bone marrow and bone surfaces) contributed about 60%. Doses to a one year-old child would be about two to four times greater than to an adult male.

Conclusions

Analyses of possible doses and risks from exposure to Dounreay fuel fragments indicate that the principal concern following skin contact, ingestion or inhalation is the possibility of localised ulceration of skin or of the mucosal lining of the colon or extrathoracic airways. A 10^5 Bq ^{137}Cs MTR particle, typical of the more active particles found at Sandside Bay, would deliver skin doses of about 0.3 Gy h^{-1} (or 0.3 Sv h^{-1}; 1 cm^2, 70 μm). A 3 – 6 hour exposure to such a particle is not expected to result in any visible skin lesions. Stationary contact for longer periods of 15 hours or more might result in small lesions. More active particles have the potential to cause more serious ulceration.

ICRP recommends dose limits for localised skin exposure and for committed effective dose. These dose limits apply to controlled sources and are not intended to apply to existing situations in which the only available protective action takes the form of intervention, as is the case with potential exposure to Dounreay fuel fragments. Nevertheless, the limits provide values with which to compare possible doses from these particles. The dose limit for localised skin exposure of workers of 0.5 Sv (1 cm^2, 70 μm) can be regarded as conservative when applied to hot particle exposures since the threshold for effects is around 2 Sv. For the public, ICRP reduces the dose limit by a factor of ten to 50 mSv, although this reduction has no scientific basis and its use is questionable. At a dose rate of 0.3 Sv h^{-1}, a 10^5 Bq ^{137}Cs MTR particle held stationary on the skin would deliver doses corresponding to the ICRP worker and public dose limits in less than 2 hours and 10 minutes, respectively. The limit on committed effective dose to members of the public is 1 mSv. Doses from ingestion of 10^5Bq ^{137}Cs MTR particle are likely to be less than 1 mSv in adults and children, but slowed colonic transit or uncharacteristic particle solubility could result in doses of a few mSv.

It can be concluded that local skin dose from a 10^5Bq ^{137}Cs MTR particle is unlikely to cause ulceration, but the possibility of a small lesion cannot be ruled out for long residence times. More active particles are more likely to cause serious ulceration. Committed doses and cancer risks are of secondary importance. The extremely low probability of encountering a particle is considered in a separate analysis.

CONTENTS

1 INTRODUCTION

Discrete fragments of irradiated nuclear fuel have been discovered on the foreshore at the Dounreay Nuclear Power Development Establishment, offshore on the seabed, and at nearby Sandside beach to which members of the public have access. An inventory of these particles can be found at www.ukaea.org.uk/dounreay/particles.htm. The purpose of this report is to assess potential doses and risks to individuals from exposure to such particles. The likelihood of occurrence of exposures is considered in a separate report (Smith *et al*. 2005).

The fuel fragments vary substantially in size but are most typically similar in size to grains of sand (Bridges and Knill, 1995; COMARE, 1999). The principal radionuclides contained within the particles are the fission products ^{137}Cs and ^{90}Sr/^{90}Y and they also contain small amounts of ^{238}Pu, ^{239}Pu and ^{241}Am. Particles are generally characterised by their ^{137}Cs activity. For particles recovered to date, ^{137}Cs activities are within the range of 10^3 to 10^8 Bq. The most active particles found at Sandside Bay contain around 10^5 Bq ^{137}Cs.

There are two main types of particles, fragments of Materials Test Reactor (MTR) and Dounreay Fast Reactor (DFR) fuel. MTR particles are most abundant. They originated as swarf generated during milling to remove aluminium cases from fuel elements (Bridges and Knill, 1995). In some cases this process removed some of the underlying fuel plate so that the swarf contained fragments of fuel embedded in aluminium. DFR particles are identified by their niobium content. In general DFR particles have smaller proportions of ^{90}Sr/^{90}Y and the actinides, relative to ^{137}Cs, than MTR particles. They are also generally less soluble. In this report, dose and risk assessments relate primarily to MTR particles and are likely to be conservative when applied to DFR particles. In addition, a small number of ^{60}Co containing particles have been found.

Because of the high local dose rates delivered by the more active particles and because they are generally of low solubility, the principal concerns are possible skin contact and localised damage and possible ingestion and damage to the alimentary tract, particularly the large intestine. A previous assessment (Wilkins *et al*. 1998) considered both these possibilities but the dosimetric approaches used resulted in conservative estimates of doses and risks, by not taking account of self-absorption of energy within larger particles and applying the standard ICRP (1979) model of the alimentary tract (Darley *et al*. 2003). In this report, self-absorption within particles is taken into account and alimentary tract doses are calculated using a new ICRP model of the alimentary tract, due to be published later this year or in 2006. In addition, the possibility of inhalation of particles is addressed and absorption to blood and doses to all organs and tissues are considered in the context of risks of cancer and hereditary effects. Doses and risks are estimated for a range of particle sizes and activities, up to 10^8 Bq ^{137}Cs (taken to be a 3mm diameter particle) and where appropriate doses are calculated for a one year old child as well as for adults.

Chapter 2 considers doses to skin and the possibility of local acute effects. It includes consideration of the possibility of particles entering the ear or the eye. Chapter 3 provides an assessment of colon doses and their possible consequences, following

particle ingestion. Chapter 4 considers inhalation of particles, the probability of their depositing in different regions, and possible doses and effects. Doses to all tissues are addressed in Chapter 5, in the context of risks of cancer and hereditary effects. Committed equivalent and effective doses are calculated, concentrating on particle ingestion and considering the low solubility exhibited by most particles and also the possibility of substantial solubility and absorption from the alimentary tract.

2 FUEL FRAGMENTS ON SKIN

2.1 Introduction

When a "hot particle" such as a fuel fragment is localised on the skin surface the various layers of the epidermis and dermis are subject to a steep, three- dimensional dose gradient due to the predominant beta radiation component. This spatial variation of dose presents challenges for biological interpretation and for dose measurement. The ability of any given hot particle to damage the skin depends on the spatial distribution of radiation dose and the spatial location of target cells within the skin. It is therefore necessary to have some understanding of both the dosimetry of beta radiation sources (and in particular hot particles) and the structure and radiobiology of the skin. The possible biological effects arising from human exposure to Dounreay fuel fragments on the skin can be predicted on the basis of estimated dose rates from actual fuel fragments and the results of extensive experimental animal data for hot particle exposures. In this chapter, the results of calculated and directly measured doses for a number of Dounreay fuel fragments will be presented and used as the basis of evaluating likely biological effects, in the light of the available animal and clinical data. Consideration will be primarily concerned with the skin, but the possible effects of hot particle exposures of the ear and eye are also briefly considered. Due to the paucity of experimental data for hot particle exposures of other organs the response of the skin is used to provide guidance on possible effects.

2.2 Anatomy & radiobiology

2.2.1 Skin structure

The skin (Figure 2.1) consists of two distinct layers, the outermost epidermis and the underlying dermis. The epidermis varies in thickness according to body site (ICRP, 2002). As a generalisation, to include the majority of body sites, the International Commission on Radiological Protection (ICRP) has used an epidermal thickness range of 20 to 100 μm (2 - 10 mg cm^{-2})♣, although it maintains a nominal average value of 70 μm (ICRP, 1977, 1991a), as does the International Commission on Radiation

♣ Skin thickness is also often referred to in mass units of mg cm^{-2}. This is simply the product of physical thickness and the skin density. e.g., 70 μm ≈ 7 mg cm^{-2}.

Quantities and Units (ICRU) for general dosimetric purposes (ICRU, 1997). The outermost region of the epidermis (sometimes referred to as the stratum corneum) is composed of layers of dead, keratinized cells. The deepest layer of the epidermis (the so-called basal layer), is one cell thick, and is the layer where most cell division takes place. This process replaces the cells that are exfoliated continuously as part of the daily 'wear and tear' of the skin. The basal layer extends around the skin appendages, notably the shaft and base of the hair follicles that project deep into the dermis. At some sites on the body over 50% of the basal layer stem cells are associated with the hair follicles. Therefore, the depth of the basal layer is very variable. In most body areas it ranges from 20 to 100 μm deep in the inter-follicular sites, but exceptionally, e.g. in the finger-tips, it could be over 150 μm deep because of enhanced keratinisation. The soles of the feet and the palms of the hands are exceptional sites which have a much greater thickness, in excess of 500 μm, associated with a growth response due to prolonged pressure-related stimulation. The dermis is a thicker layer of connective tissue, up to 3-4 mm deep, again dependent on body site. There are three networks of blood vessels within the dermis in man. They are parallel to the surface and located at various depths. The dermis supports various structures such as hairs, sebaceous glands and sweat glands.

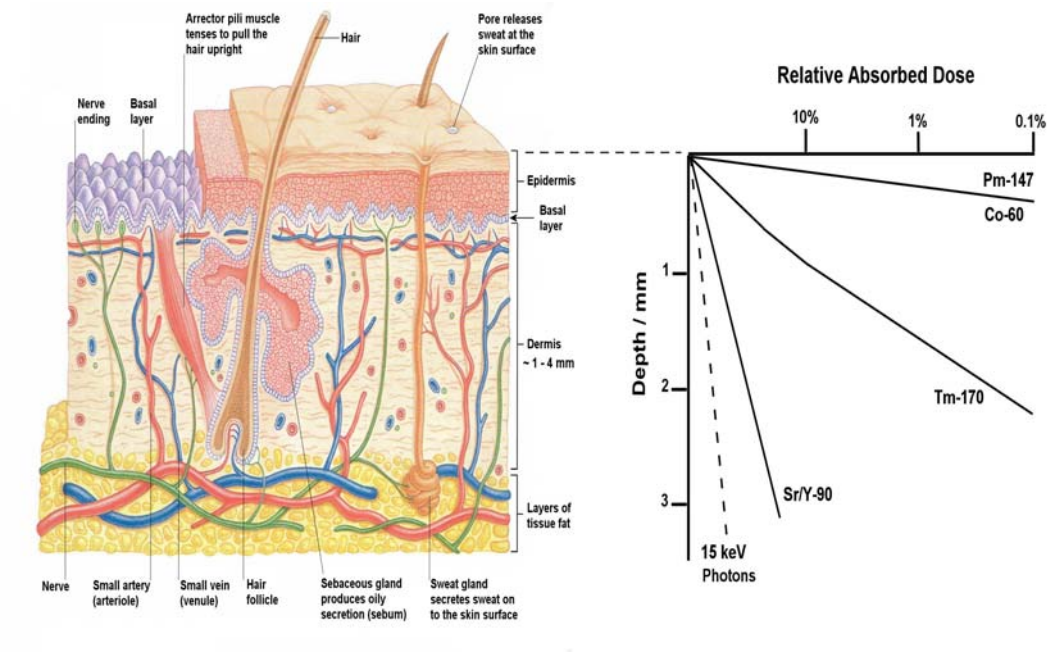

Figure 2.1. Schematic illustration of the relationship between the depths of important biological structures in the skin and the variation of absorbed dose with depth for beta radiations. The thickness of the epidermis is exaggerated for clarity – corresponding here to body regions such as the palm of the hand.

2.2.2 Target cells and stem cells

For the majority of radiation-induced biological effects in a particular tissue or organ there is generally an identifiable specific exposed cell population which plays a key, and often singular role. These cells are referred to as the target cells. In many cases the

target cells are the same as the so-called stem cells. Stem cells are the cells in tissue that are ultimately responsible for all the cell replacement (including their own replacement) which must take place in the tissue as part of normal tissue dynamics. Replacement is necessary because some cells die (naturally or due to external factors such as radiation exposure) and some differentiate into other forms of cells with a different function. The role of target cells will be illustrated below, with examples of radiation induced deterministic and stochastic effects in the skin.

2.2.3 Target cells for radiation induced deterministic effects in the skin

For deterministic effects involving gross tissue damage, it is not surprising that the target cells and stem cells are closely related. Under normal conditions in most tissues or organs there is a continual natural loss of cells which are replaced by cells from the stem cell pool. An external agent such as ionising radiation may lead to the death of some stem cells, together with other constituent cells in the tissue. The whole integrity of the tissue may be compromised unless the dead cells can be rapidly replaced. Killed cells can only be replaced, by definition, by stem cells. If the stem cell population falls below a critical value the loss of cells from the tissue as a whole cannot be counteracted before the tissue architecture breaks down. This is the origin of gross tissue damage and is the reason for the threshold response which is characteristic of acute or deterministic effects.

In the past 20 years, considerable light has been shed on the identification of target cells for deterministic effects in the skin. In particular, several extensive studies of radiation effects on pig skin have used a range of sizes of several different beta emitters (in the form of radioactive plaques) to probe the various depths of the skin. Pig skin is the nearest in structure and radiation response to human skin and is used widely for radiotherapy research. The effects produced involve damage to different target cells at different depths and with different radiosensitivities, and therefore depend strongly on beta energy since this dictates the penetration of radiation into the skin and the structures which can be damaged (Figure 2.1). A number of publications have described dose-response relationships for skin damage for a range of beta emitters with different energies, and for a range of source sizes, including hot particles. These studies have been reviewed extensively by ICRP (1991b) and the United States NCRP (1999). The main biological effects for large area sources (> 1 cm^2) are described below for low and high energy beta emitters.

Low energy beta emitters

Even up to high skin surface doses of about 100 Gy, only minimal erythema (reddening) in the skin is produced by low energy beta emitters such as ^{147}Pm (E_{max} ~ 0.25 MeV, range < 0.5 mm) for which beta particles penetrate barely into the superficial dermis. At higher doses, a unique response referred to as acute epidermal necrosis can be produced. This effect is similar to classical moist desquamation induced by more penetrating radiations, but occurs earlier (within about 10 days) and lasts for a shorter time. Because of their weak penetration, such low energy beta radiations do not produce any of the more severe skin responses which can be produced by more penetrating radiations which are described below.

High energy beta emitters
Several types of early deterministic effects can be produced by penetrating radiations such as high energy beta emitters (e.g. ^{90}Y ,E_{max} 2.3 MeV, range ~ 9 mm), which can penetrate well into the dermis:

(1) Transient erythema (skin reddening): caused by dilation of blood vessels following acute doses of several grays (Gy) or more to the superficial blood vessels of the upper dermis. Skin erythema induced as a result of x-ray exposures was one of the first biological effects of radiation to be studied and quantified by early radiation researchers. This classical skin erythema exhibits a temporal wave pattern of appearance: appearing, fading and reappearing several times over a period of hours or days, depending on dose.

(2) Moist desquamation: this is the result of death of the basal cells of the epidermis (including those around hair follicles) and damage to the superficial network of blood vessels. For pig skin it occurs ~ 4 - 6 weeks after exposure to acute doses in excess of ~12 Gy. Protraction of the exposure time significantly increases the threshold dose. The target depth for this effect is ~ 150 μm, corresponding approximately to the depth of the basal cell layer around the hair follicles. Healing can be rapidly achieved, providing that these deep epithelial cells survive to provide a source of cell repopulation.

(3) Dermal necrosis: this results from damage to the deep dermal vasculature, and occurs 2- 10 weeks after exposure. The target depth is > 1000 μm, so low energy beta rays do not produce this effect. Dermal necrosis was seen in some of the Chernobyl accident victims who received absorbed doses of 2 - 20 Gy from high energy beta radiation, at a depth of 1500 μm (Barabanova and Osanov, 1990).

(4) Dermal atrophy and damage to the deep vasculature, including telangiectasia (dilation of blood vessels): these are the main late effects following an acute exposure. They become apparent on a time scale of months or years. Dermal atrophy, detected as dermal thinning or as induration of the skin, has a target depth in the region of 300-500 μm. With fractionated x-ray exposures, the threshold absorbed dose for telangiectasia and late dermal atrophy is about 30-40 Gy.

2.2.4 Target cells for radiation induced skin cancer

The question as to which exposed cells in the skin play a dominant role in the induction of skin cancer has eluded a definitive answer. The basal layer of the epidermis (between 20-100 μm in man) has been chosen as the target cell layer by several authors, but more on the basis of conservatism than scientific evidence. The ICRP assume a nominal depth of 70 μm for general purposes.

The reasons for identifying the basal layer as the target cell layer for carcinogenesis is that it is thought to be the layer in which the stem cells for epidermal repopulation are found. However, not all basal cells are stem cells and there is some evidence (Hume and Potten, 1979), as discussed by ICRP (1991b), that the stem cells may be at the base of undulations in the basal layer - in the so called rete-pegs. This would give the stem cells a somewhat greater depth (~25%) than the nominal average depth of the

basal layer. There is also evidence that cells in the underlying dermis are implicated in skin cancer induction in animals (NCRP, 1989).

2.3 Biological effects of hot particle exposures to the skin

The biological effects following hot particle exposures are somewhat different to those that arise following more commonly encountered large, spatially uniform exposures, as for example used in radiotherapy.

Erythema can be produced by hot particle exposures but it is transient, extends over very small areas, and is subject to considerable variability and possible confusion with normal skin blemishes. The classical primary and secondary wave patterns (see Section 2.2.3), which are observed in radiotherapy, are not seen for hot particles. Hot particles do not induce the classical response of moist desquamation, as seen in radiotherapy, which occurs between 4-6 weeks after exposure. The nearest type of response is what has been termed acute epidermal necrosis, for exposure to low energy beta emitters which mainly irradiate the epidermis, or acute ulceration for higher energy beta emitters which irradiate down into the dermis (ICRP, 1991b). These effects involve interphase death (a rapid form of cell death following exposure to very high radiation doses) rather than cell death that takes place at the next cell division, as in the case of moist desquamation. These responses occur within a few days of exposure, are limited to very small areas, and readily heal at low doses. At very high doses these responses will take longer to heal and may produce small area scar tissue.

The most important deterministic effect that can be produced by radioactive particles, with radiations energetic enough to irradiate the dermis of the skin, is acute ulceration. Ulceration is a term that indicates breakdown of the skin structure that involves the dermal region that lies below the outermost epidermis. In the case of large area exposures, particularly to penetrating x- or gamma- radiations in radiotherapy, ulceration is potentially a serious response that may involve damage through the whole volume of skin. Healing may take a considerable time, with possible subsequent breakdown and recurrence. The formation of scar tissue may be debilitating – affecting mobility and causing pain, as well as being cosmetically detrimental. Frequent recurrence of ulceration and chronic infection may lead to a need for skin grafting. For ulceration induced by hot particles, the situation is quite different since the volume of damaged tissue is small, the majority of energy being deposited within a few mm^3. Cells will be killed within the small highly exposed area but viable cells around the periphery will be able to migrate to replace them. For large area exposures to penetrating radiations the detailed specification of dose is not critical, since it varies little with position in the radiation field. However, for hot particle exposures, the variation of dose with area and depth make it necessary to stipulate dose in terms of the area and depth over which it is averaged. Some hot particle studies on pig skin have used dose measurements over areas of 1.1 mm^2 at a depth of 16 μm. This apparently rather idiosyncratic measure of dose was the most convenient small-area measurement (using an ionisation chamber with a small electrode) which could be made in early radiobiological studies. A particularly convenient measure of hot particle dose which has been recommended by a

number of international organisations is the average over an area of 1 cm^2 at a depth of 70 μm. This will be referred to as skin dose (1 cm^2, 70 μm).

The depth of tissues that are subject to significant damage will depend on the level of exposure and the energy of the radiation involved. Typical fuel fragment particles, composed mainly of beta/gamma emitting radionuclides with beta energies up to about 2 MeV, may deliver very high doses to the few cells immediately beneath them in the skin. This dose is dramatically reduced at a few mm from the particle, towards the end of the range of the beta dose component. Fuel fragments may thus produce damage to the dermis of the skin, but over very small areas. Such effects may still be described by the term ulceration, even though their clinical significance is in no way comparable to that from an ulcerative response to a large area exposure from penetrating radiation, as in radiotherapy. The prefix 'acute' has been used by the ICRP (1991b) to refer to hot particle-induced ulceration.

There has been considerable research in the past 20 years in the UK and the USA to provide radiobiological data regarding skin exposure from hot particles in order to develop defensible dose limits. Data are available on pig skin exposures with various sizes of beta-emitting radionuclides such as ^{147}Pm (E max ~ 0.25 MeV), ^{60}Co (Emax ~ 0.32 MeV), ^{46}Sc (Emax ~ 0.35 MeV), ^{175}Yb (Emax ~ 0.47 MeV), ^{170}Tm (E max ~0.97 MeV), fissioned $^{235}UC_2$ microspheres (E max ~ 1.8 MeV), and $^{90}Sr/^{90}Y$ (E max ~ 2.3 MeV). The incidence of early and late acute effects such as acute epidermal necrosis, ulceration and dermal thinning has been scored, as well as the time-course, severity and healing outcome. This information has been used by the ICRP (1991a) and NCRP (1989, 1999) to provide dose limits for occupational exposures. The difficulties of evaluating the severity of the hot particle ulceration response has led the ICRP (1991a) to recommend an annual occupational dose limit of 0.5 Sv over an area of 1 cm^2 at a depth of 70 μm, whereas the NCRP (1999) have given a limit of 0.5 Sv averaged over an area of 10 cm^2 at a depth of 70 μm. For a single hot particle, the NCRP limit is equivalent to a dose of 5 Sv averaged over an area of 1 cm^2. This is 10 times the dose limit recommended by the ICRP. The ICRP limit is set to prevent acute ulceration, whereas the NCRP limit is at a level where transient ulceration would occur with a 10% probability. This level of effect is considered acceptable by the NCRP on the basis that it is said to be unlikely to give rise to a severe enough break in the skin barrier to lead to infection. The differences in dose limits set by the ICRP and NCRP reflect the difficult value judgement regarding the acceptability of the relatively minor, but possibly observable, skin lesions which may be produced at dose levels of about 5-10 Gy (1 cm^2, 70 μm). ICRP and NCRP also recommend dose limits for members of the public which are a factor of 10 less than those for occupational exposure. The rationale for this factor of 10 has not been fully described, but presumably represents a cautious approach to the exposure of members of the public who are not subject to the regulatory control or medical surveillance of radiation workers. It can be argued that no special dose limit is for members of the public is necessary because there is already sufficient conservatism in the chosen limit for workers (NRPB, 1997).

NCRP (1999) provided a particularly extensive review of the majority of published hot particle experimental studies, including those which extend to very high skin doses. Reece *et al*. (1994), for example, reported pig skin exposures at doses in the range of about 50 - 300 Gy (1 cm^2, 70 μm) from 3 mm diameter $^{90}Sr/^{90}Y$ disc sources. The

highest doses produced acute ulcerations that occurred within about 2-3 weeks of exposure, produced a scab after 4-5 weeks, and finally healed with a visible scar at about 12 – 16 weeks. Reece's view that such lesions were occupationally acceptable was not condoned by the ICRP or NCRP, who recommended dose limits at lower levels of acute response. However, Reece's results do indicate that if the skin is subjected to very high dose hot particle exposures, the resultant skin lesion should be clinically manageable, using normal wound treatment procedures, without recourse to surgery. Extensive studies in the UK (Hopewell *et al*. 1986) have included pig skin exposures with various sized, small beta-emitting sources of $^{90}Sr/^{90}Y$, ^{170}Tm, ^{147}Pm and ^{60}Co. Of particular relevance to Dounreay fuel fragments were the exposures using 1 mm diameter $^{90}Sr/^{90}Y$ at doses up to about 50 Gy (1 cm^2, 70 μm). The highest doses produced acute ulcerations within a few days, which healed within 1.5 – 3 weeks. Another extensive pig skin study, commissioned by the US Nuclear Regulatory Commission, has been published by Kaurin *et al*. (2001a,b). Of particular interest are the results for hot particles of neutron irradiated uranium carbide spheres of diameter 150 –300 μm. Kaurin reports ulcerations that healed with a scab formation. Scab diameters were large enough to be measurable above doses of about 5 Sv (1 cm^2, 70 μm) and increased in size to about 1 cm at doses of about 500 Sv (1 cm^2, 70 μm). Lower energy beta emitters produced smaller, faster healing, lesions at the same dose levels.

The combination of UK and US data show remarkable consistency (Figure 2.2). When doses are averaged over an area of 1 cm^2 at a depth of 70 μm (as recommended by the ICRP), the ED_{10} and ED_{50} values (the doses to produce an incidence in effect of 10% and 50% respectively) for acute epidermal necrosis or acute ulceration vary by only a factor of ± 2 across a wide beta energy range. The ED_{50} values are approximately 15, 8, 12, 6, 6, 11, and 8 Gy for ^{147}Pm (E max ~ 0.25 MeV), ^{60}Co (Emax ~ 0.32 MeV), ^{46}Sc (Emax ~ 0.35 MeV), ^{175}Yb (Emax ~ 0.47 MeV), ^{170}Tm (E max ~0.97 MeV), fissioned $^{235}UC_2$ microspheres (E max ~ 1.8 MeV), and $^{90}Sr/^{90}Y$ (E max ~ 2.3 MeV), respectively. These data are for small sources (dimensions < 1mm) except for ^{147}Pm where the smallest source was 2 mm diameter. For sources larger than about 1mm the ED values are increased (Charles, 1990, 1991). In the case of higher energy beta sources with diameters of about 3mm (corresponding to the largest and most active of the Dounreay fuel fragments, 10^8 Bq ^{137}Cs) the increase in ED_{10} value is by a factor of about 2-3. It has been argued that hot particles which are spaced away from the skin (on clothing for example) might be more radiobiologically effective than particles in direct contact with the skin (NCRP, 1999). However, the evidence is weak and the magnitude of the effect is small.

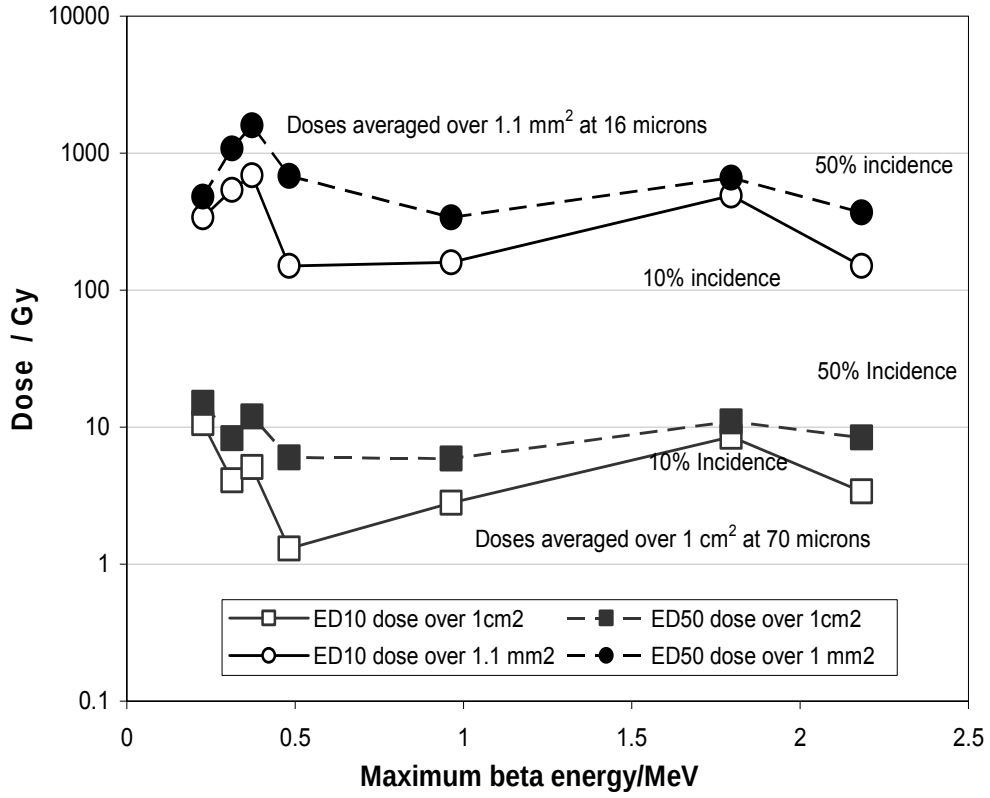

Figure 2.2. Variation in doses for 50% and 10% incidence (ED_{50} and ED_{10}) of acute ulceration of pig skin following hot particle exposures from specific radionuclides as a function of the maximum beta energy. Sources had dimensions < 1 mm (except ^{147}Pm – 2mm diameter). The radionuclides, in order of increasing maximum beta energy are: ^{147}Pm, ^{60}Co, ^{46}Sc, ^{175}Yb, ^{170}Tm, ^{235}U (fissioned) and $^{90}Sr/^{90}Y$. Data are shown for skin doses evaluated as averages over areas of 1.1 mm^2 and a depth of 16 μm (as used in various publications of experimental data) and averaged over an area of 1 cm^2 and a depth of 70 μm (as used in some publications of experimental data and by ICRP, NCRP and ICRU). Data are from ICRP (1991b), NCRP (1999) and Kaurin *et al*. (2001a,b).

Figure 2.2 includes skin doses in terms of an average over an area of 1.1 mm^2 at a depth of 16 μm as well as the conventional (1 cm^2, 70μm) value. The view is often expressed that a dose measurement over a small area is more appropriate for addressing hot particle effects than the conventional area of 1 cm^2. There is in fact reasonable consistency in the ED_{10} and ED_{50} values, for a wide range of beta energies, when dose is expressed in either conventional dose terms or when averaged over a smaller area (Figure 2.2). There is some practical advantage in attempting to find a particular area and depth for the measurement of skin dose which provides similar values for ED_{10} and ED_{50} for hot particle exposures. It enables a single value dose limit to be used that is equally appropriate for any energy of beta emitter and can be used for situations in which there is a mixture of different beta sources. An ICRP task group (ICRP 1991b) recommended that the best measurement of dose to achieve better consistency across the whole beta energy range was a dose measurement over an area of 1 cm^2 at a depth of 150 μm. However, the ICRP Main Commission recommended a dose measurement over an area of 1 cm^2 at a depth of 70μm – presumably on the basis of simplicity and conformity with long standing advice for general measurements of skin

dose in radiological protection. For the prediction of biological effects following a hot particle exposure it is possible to use a range of possible dose parameters – providing they are applied consistently to dose measurements and related experimental data. In this report we have followed the standard international practice of calculating and measuring skin dose (1 cm^2, 70μm) and we have used ED_{10} and ED_{50} values (from pig skin studies) which are based on the same dose parameter. This also enables us to compare exposures with international dose limits, which are expressed in terms of conventional skin dose (1 cm^2, 70μm).

There are few well documented reports of exposure of human skin to radioactive particles. However, one case has been reported by Dean *et al*. (1970). One of the authors exposed the skin of their own forearm to a uranium carbide sphere (160 μm diameter) which had been subjected to a reactor neutron exposure.

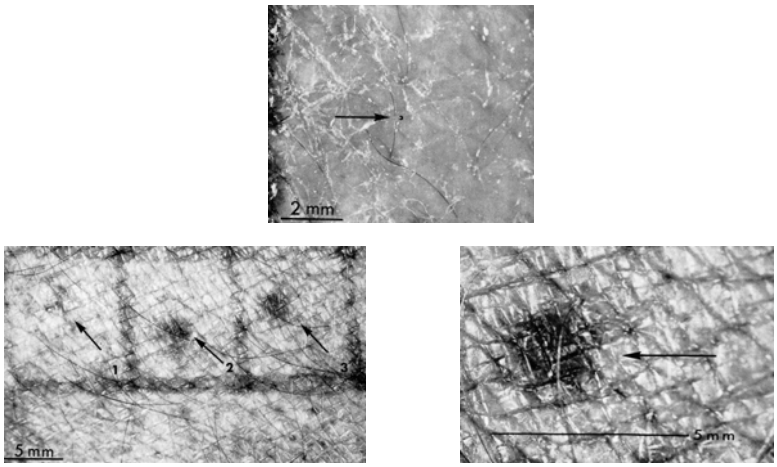

Figure 2.3. Top: Fissioned $^{235}UC_2$ particle (160 μm diameter) on human skin (Dean *et al*. 1970). Bottom left: Response after 28 days. Peak doses in the basal layer at 3 exposure sites: 1, 2 & 3: 142, 400 and 540 Gy, respectively. Average doses over 1 cm^2 are a factor of ~ 60 lower i.e., 2.4, 6.7 and 9 Gy. Bottom right: Skin response at 28 days for site 3.

The skin responses 28 days after exposure are shown in figure 2.3. Peak doses in the basal layer were recorded for 3 sites of 142, 400 and 540 Gy. Similar exposures were used for pig skin by Kaurin *et al*. (2001) and similar responses were observed. The dose estimates averaged over 1 cm^2 are a factor of about 60 less than the peak dose (Kaurin *et al*. 1997).

2.4 Dounreay fuel fragment dosimetry

The estimation of doses from Dounreay fuel fragments has previously been based largely on calculations which have necessitated a number of assumptions, such as particle density, composition and radionuclide contents. In this section the results are presented of direct depth-dose distribution measurements made around a number of

particles using radiochromic dye films (RDF). This technique eliminates the need for assumptions regarding particle properties. Monte Carlo (MCNP code) calculations have also been made to model the particles using the best available information regarding their composition.

2.4.1 Radiochromic Dye Film (RDF) depth-dose distribution measurements

The dose distribution measurements for fuel fragments, over various areas and at several depths, were carried out using the radiochromic dye film (RDF) technique (Aydarous *et al*. 2001). RDF provides a means of obtaining dose distributions with high spatial resolution. The GAFChromic^{TM} radiochromic dye films type HD-810 used in the present study have a 7 μm radiation sensitive surface layer. The total mass thickness of one RDF is approximately 15 mg cm^{-2}. The films develop a distinctive and characteristic blue colour upon exposure to ionising radiation and become progressively darker with increasing absorbed dose. Measurement of the optical density provides a measure of the absorbed dose. Exposure of a suitably calibrated stack of films enables 3-dimensional isodose distributions to be obtained.

For doses from 5 Gy to 800 Gy, a set of films was calibrated against a standard ion chamber using a ^{60}Co teletherapy source. For higher doses (800-5500 Gy), further sets of films from the same batch were exposed using a large area ^{90}Sr/^{90}Y beta source (5.18 GBq) cross calibrated using the ^{60}Co calibration. The experimental set up for the depth-dose measurement using the RDF is shown in figure 2.4. A limitation, for low activity fuel fragments, is the high threshold dose of the RDF technique (a few Gy), which necessitates long exposure times for low dose rate sources. The required exposure times for the particles varied from a few hours to a few weeks, for activities ranging from 10^7 Bq to 10^5 Bq. Figure 2.5 (A) shows a 2-dimensional false colour optical density map produced by RDF, read out using a Microtek film scanner, for a Sandside MTR fuel fragment (the highest activity found there to date). The cross lines represents the dose centroid from which the radial dose distributions and average doses are determined over selected areas at various depths. Dose calculations and image manipulations were provided by the program RADODS, developed for this project. The results enable dose distributions to be evaluated and average doses to be calculated over various chosen areas at selected depths as required. Doses averaged over an area of 1 cm^2 at a depth of 70 μm (7 mg cm^{-2}) are particularly appropriate for comparison with radiobiological data and are reported here. The peak dose immediately beneath the fragment is 15 times higher than the average dose (Figure 2.5B). Scanning electron microscopy can provide images (Figure 2.5C) which enable size and approximate shape to be evaluated. Associated energy-dispersive x-ray analysis (EDX) can provide the elemental composition and allow DFR and MTR fragments to be differentiated (DFR fragments have a characteristic niobium content).

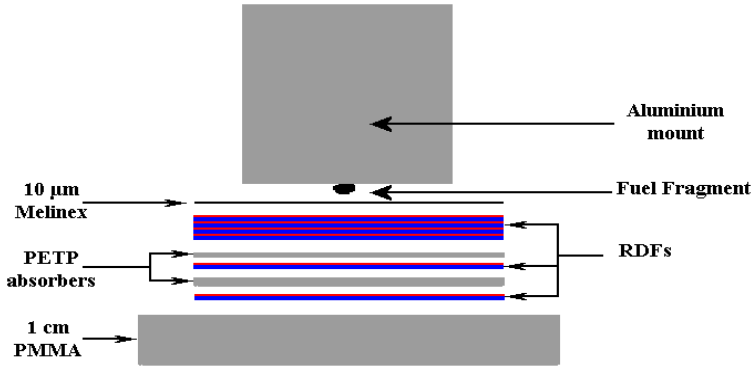

Figure 2.4. Schematic view of the experimental set up for depth dose measurements using a stack of radiochromic dye films (RDF). Polyethylene-terephthalate (PETP) absorbers and polymethyl methacrylate (PMMA) backscatter material were used to provide measurements over a wide depth range.

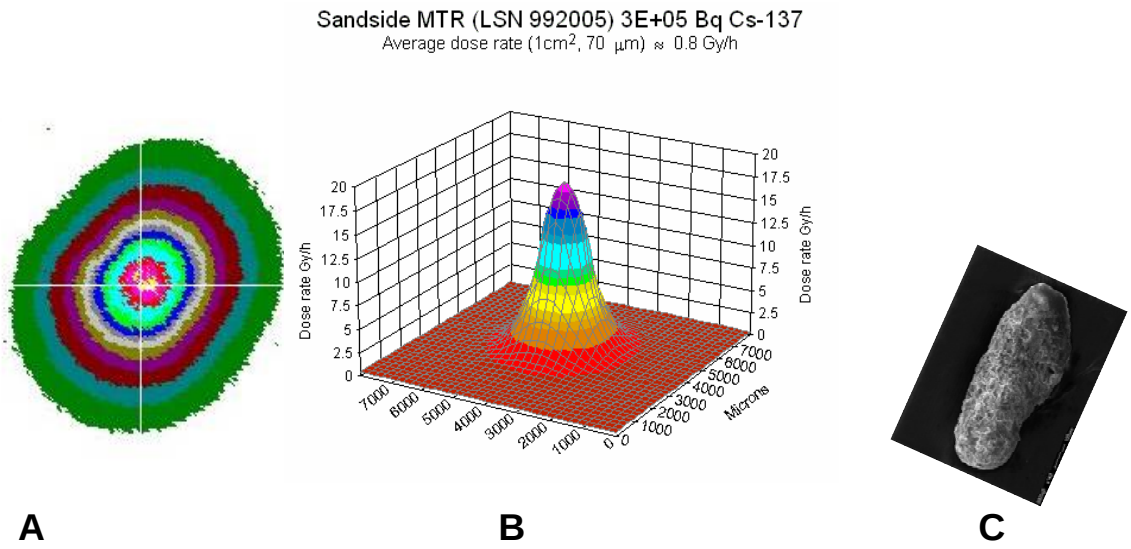

Figure 2.5. Sandside MTR fuel fragment (LSN889005) Activity: 3 x 10^5 Bq ^{137}Cs. Mass: 1.2 x 10^{-3} g, ~ 0.7 mm long and ~ 0.3 mm 'diameter' ('volume' shape).

A: Two-dimensional false colour optical density map produced by RDF. The cross lines represents the dose centroid from which the radial dose distributions and average doses are determined over selected areas at various depths.

B: 3D visualisation of the dose distribution around the source using the image A

C: Scanning Electron Microscope image

Thirty seven fuel fragments were selected for dose measurements. In order to make comparisons between measured doses and Monte Carlo calculated doses, the particles were limited to those which had been subject to prior scanning electron

microscope/EDX characterisation and ^{137}Cs activity determination. The 37 particles are categorised in Table 2.1 on the basis of MTR or DFR origin and on the site of discovery.

Table 2.1. Particles selected for radiochromic dye film depth-dose distribution measurements.

Site	MTR	DFR
Seabed	13	7
Foreshore	8	1
Sandside	6	2

Doses were measured as averages over various areas at several depths.

2.4.2 Dose calculations

Calculations of skin dose were made using the MCNP♥ Monte Carlo radiation transport code. Monte Carlo calculations for MTR particles assumed a density of 3.1 g cm^{-3}, ^{137}Cs and ^{90}Sr/^{90}Y specific activities 2 and 1.8 GBq g^{-1} respectively, and the fundamental radiation emission data given in Table 2.2. Data on radionuclide composition and physical density are not available to enable doses to be calculated for DFR particles.

Table 2.2. Radiation emission data for ^{90}Sr, ^{90}Y and ^{137}Cs

Radionuclide	Emission	Energy (MeV)	Relative abundance
^{90}Sr	Beta	Emax= 0.546	1.0
^{90}Y	Beta	Emax= 2.281	1.0
^{137}Cs	Beta	Emax= 0.514	0.944
		Emax= 1.175	0.056
	γ –ray	0.662	0.851
	X-Ray	0.0045	0.01
		0.032	0.0558
		0.036	0.0132
	Conversion electron	0.624	0.0766
		0.656	0.0139

Details of the Monte Carlo code calculations are given in the PhD thesis of Aydarous (2001).

Dose measurements were made using radiochromic dye film (RDF) stacks in contact with Dounreay fuel fragments mounted on an aluminium stub (Figure 2.6C). Parallel calculations (Figure 2.6A) were made using the MCNP code for this geometry and also for a geometry without an aluminium stub (Figure 2.6B). The calculations and measurements for the situation with an aluminium stub (Figure 2.6C) are appropriate for the practical situation where tissue is in contact with a particle on a sand surface. Calculations for the situation where no aluminium stub is present (Figure 2.6B) are

♥ MCNP (Monte Carlo N-Particle) – a widely used Monte Carlo radiation transport computer code

appropriate for the practical situation where a particle is resident on the skin with no other backscatter material other than the surrounding air.

For large fuel fragments (10^8 Bq Cs-137, ~ 3mm diameter), the particles themselves produce significant backscatter. There is therefore little additional contribution (~9 %) to skin dose (1 cm^2, 70 μm) from the additional aluminium stub, compared to air. For smaller particles (10^5 Bq Cs-137, ~ 300 μm diameter) the self-backscatter effect is smaller and the aluminium stub provides a significant additional contribution to skin dose (~30%).

A further practical situation can be envisaged which is intermediate between the two previously described - where a particle is sandwiched between tissue layers or between two layers that have properties similar to tissue. This will be the situation for example when a particle passes through the alimentary tract. In this case the backscatter will be intermediary between the two situations considered above and dose rates will be between those given for the two geometries in Figure 2.6A.

On the basis of these calculations the skin dose measurements which were made with particles mounted on an aluminium stub are thus likely to be higher than those that would actually be delivered by a particle on the skin. For the highest activity particles the over-estimates will be a few percent. For the lower activity particles the over-estimate may be up to about 15-30%.

All of the calculated doses in the following figures are for the geometry shown in Figure 2.6B – relevant to particles on the skin, with air backscatter.

2.4.3 Comparisons of calculated and measured doses

The measured and calculated skin dose rates (1 cm^2, 70 μm) as a function of the ^{137}Cs activity, are given in Figure 2.7. Calculations assume spherical geometry. The activities have been decay corrected to the date of dose measurement, assuming that the particle activity was measured by the UKAEA soon after the find date (which is recorded in the UKAEA database). Activity decay factors (based on a 30 year half-life) were on average less than 10%. Figure 2.7 also indicates the origin of particles, their type and MCNP-calculated skin doses. The dotted line indicates a linear extrapolation of the dose rate with particle activity, based on the lowest activity particles, making no allowance for self-absorption in larger particles. Overall, the measured skin dose values for MTR particles are in good agreement with MCNP calculations, particularly for the low activity particles. For the higher activity MTR particles the measured dose rates are between the MCNP calculations and the linear extrapolation from the low activity particles, a reflection of differing extents of self-absorption depending on particle shape.

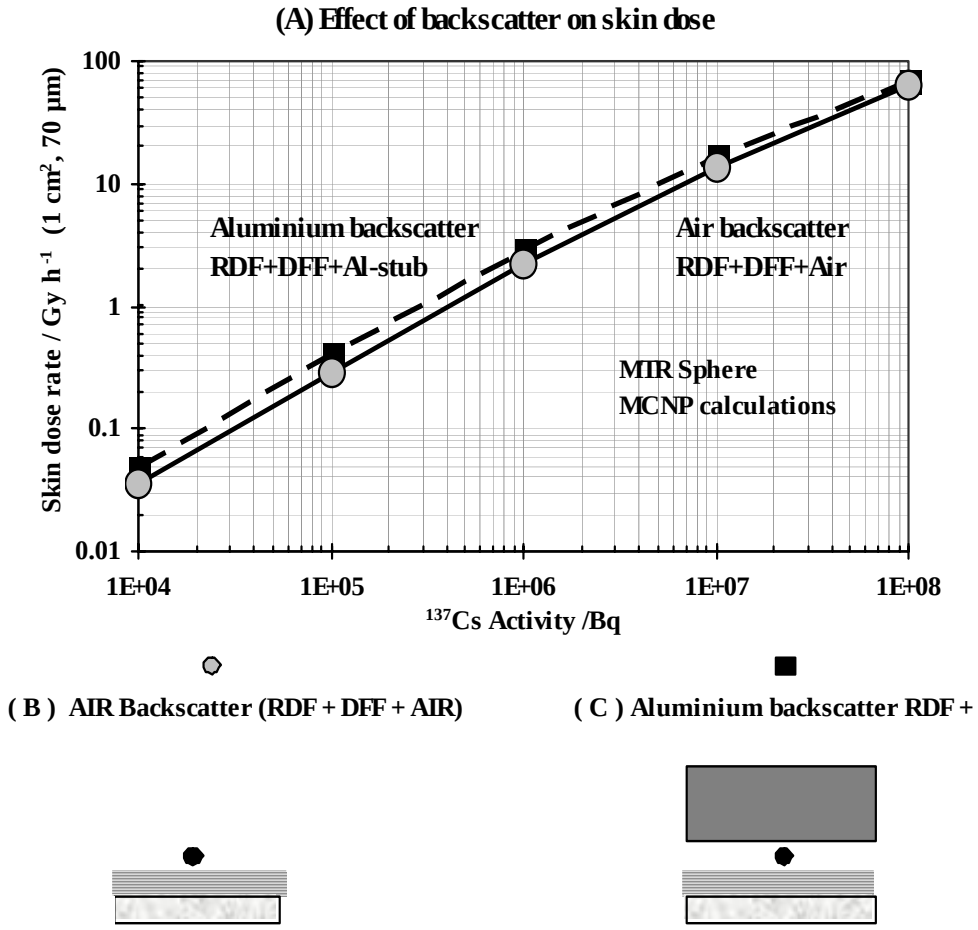

Figure 2.6. A shows MCNP calculations of skin dose for 2 geometries:

DFF in contact with layers of RDF(Figure 2.5 B)

DFFs mounted on an aluminium stub in contact with layers of RDF (Figure 2.5 C).

In both cases the RDF dosemeters were mounted on a 1 cm Perspex base. The extra backscatter from the aluminium stub produces a slightly higher skin dose than with air backscatter.

Figure 2.7 indicates that all of the 10 measured values of dose rate for DFR particles (solid symbols) are less than the MCNP calculations for MTR particles (for the same ^{137}Cs activity). The majority were in fact near to the predicted dose rates for calculations which assumed zero ^{90}Sr/^{90}Y content (Figure 2.7, dashed line). This indicates that the use of calculated doses for MTR particles will be conservative if applied to DFR particles of the same ^{137}Cs activity. In figure 2.7, the Sandside particles are indicated by solid and open squares. These include the highest activity fragment found to date (~ 3 x 10^5 Bq ^{137}Cs at time of find) – details of which are given in Figure 2.5. Also shown in Figure 2.7 are the dose rates assumed by Wilkins *et al*. (1998) for MTR particles in a previous

assessment, taking no account of self-absorption of energy within larger particles and assuming a $^{90}Sr/^{90}Y$: ^{137}Cs ratio of 2.1 (upper solid line).

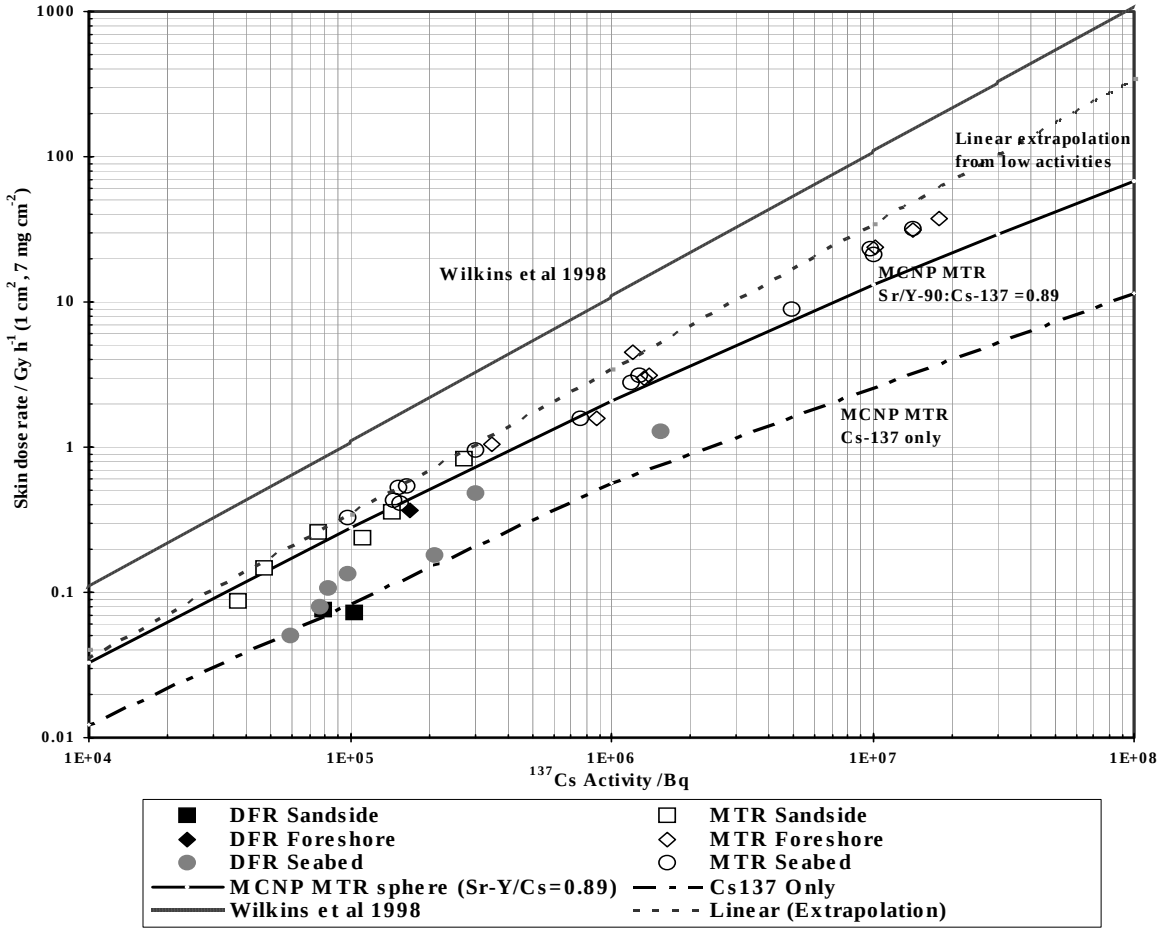

Figure 2.7. Skin dose rates for MTR and DFR fuel fragments (activity corrected to date of dose measurement).

Figure 2.8 presents the data in terms of particle shape for 18 selected MTR fuel fragments. They have been crudely categorised, using Scanning Electron Microscopy (SEM), as volume, cylindrical or disk. It is difficult to do this with any precision but, crudely, the classification is based on the ratio of x:y:z dimensions:

Volume, x~y~z; Cylindrical, x~y << z; Disc, x~y >>z. The symbols >> and << represent ratios of dimensions of 5-10; ~ represents a ratio ≤ 3. None of the particles could be reasonably described as spherical. Monte Carlo calculations have also been carried out using idealised cylindrical and disc geometries to mimic non-spherical sources. Results for an extreme assumption of a diameter/height ratio of 10 are given in Figure 2.8 (the effect of varying this ratio for cylindrical or disc geometries is similar). All dose rate measurements lie within the calculated range for spherical, elongated or plate sources.

Non–spherical sources produce higher dose rates than spherical sources due to reduced self-absorption.

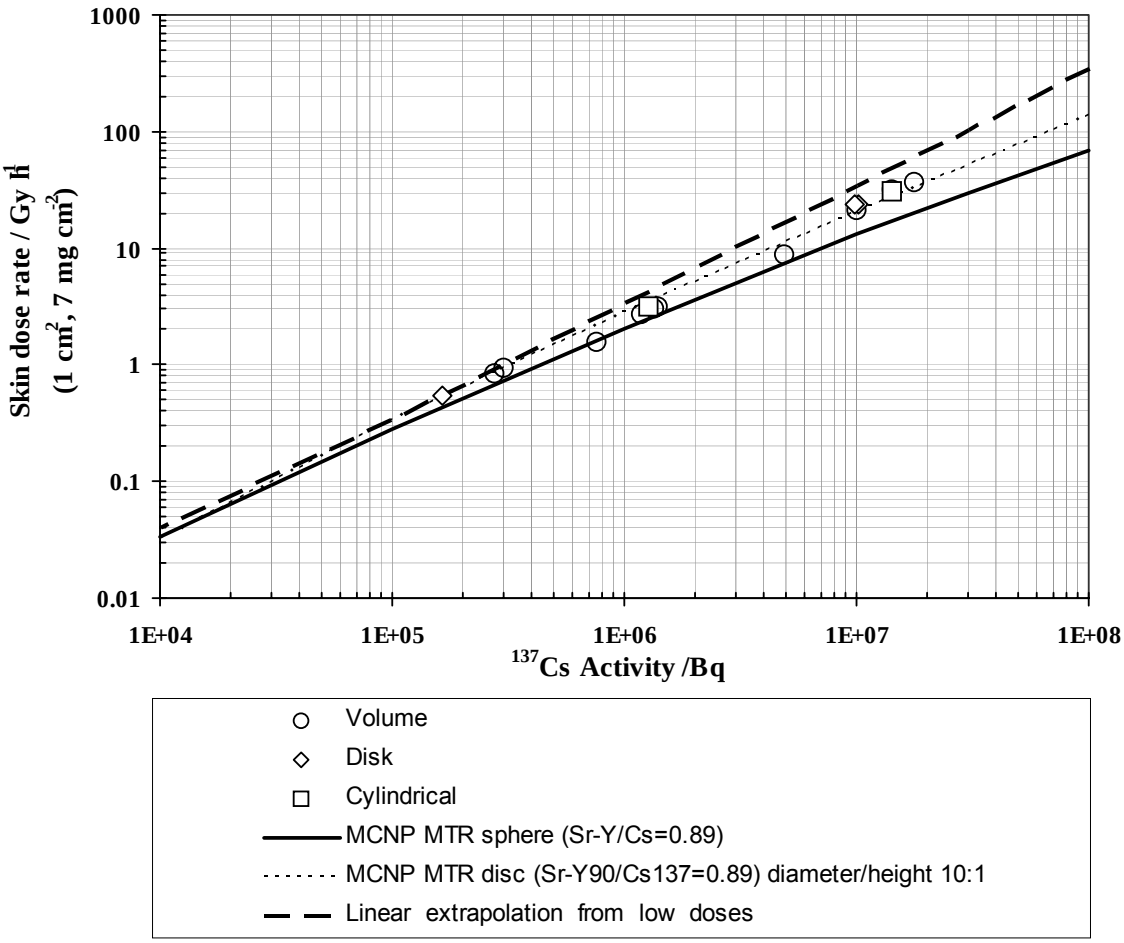

Figure 2.8. Dependence of skin dose on shape of 15 MTR Dounreay fuel fragments (activity corrected to date of measurement).

Figure 2.9 presents a comparison between the depth doses♠ for 6 DFR particles and 11 MTR particles. The more rapid reduction in dose with depth for all of the DFR particles could be explained by a reduced proportion of the higher energy beta emitter $^{90}Sr/^{90}Y$ compared with the lower energy beta emitter ^{137}Cs. A higher fragment density in DFR

♠ The normalised central axis depth dose has been plotted in Figure 2.9. Doses are those estimated over a very small area at various depths, normalised to the surface dose. Small area, central axis doses were chosen to highlight potential differences in depth doses due to differences in beta energy between the sources.

particles could also be a possible contributing factor via effects of self-absorption – although this is unlikely to be a major factor for most of these low activity DFR fragments. A reduced $^{90}Sr/^{90}Y$: ^{137}Cs ratio for DFR particles is also in agreement with the lower skin doses seen in Figure 2.7 (dashed line for zero $^{90}Sr/^{90}Y$ content). The consistency in depth dose measurements within the MTR and the DFR groupings is indicative of broadly similar radionuclide compositions within the two separate categories.

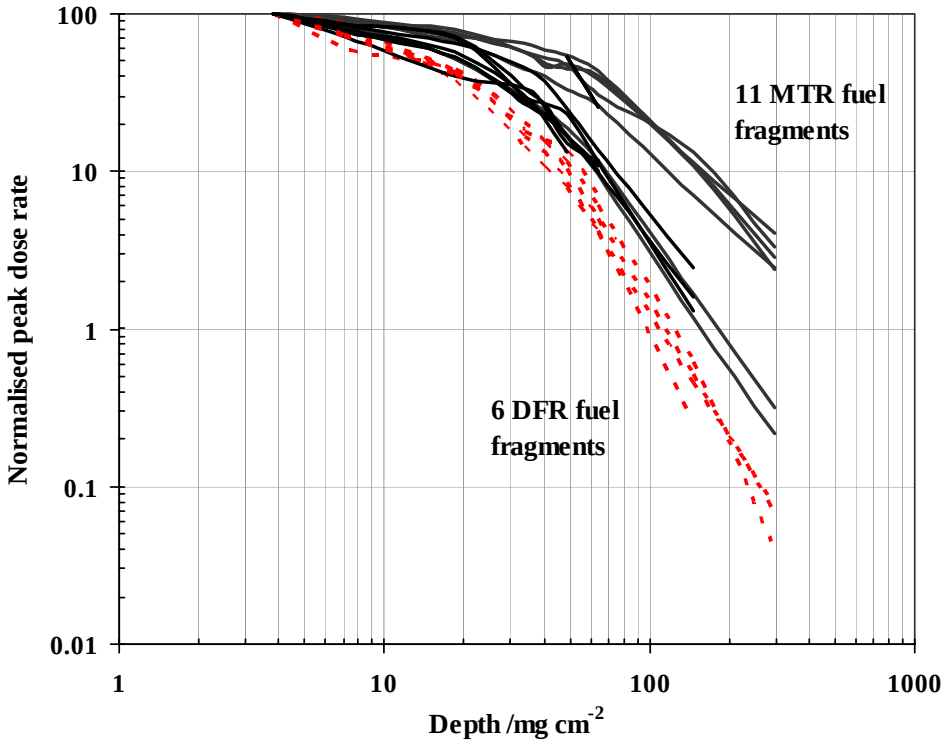

Figure 2.9. Normalised peak dose rates vs. depth for MTR and DFR fuel fragments.

2.5 Possible biological effects of Dounreay fuel fragments on the skin

Possible biological effects from Dounreay fuel fragments in contact with the skin can be predicted on the basis of estimated skin dose rates and the results of the extensive published animal data summarised above (Section 2.3). Such predictions are difficult to make for low activity particles, at low dose rates, because of the paucity or absence of experimental data. Low dose rate skin exposures with hot particles have not been systematically studied in any of the experimental programmes set up to study hot particle effects. This is due to the great difficulty of carrying out animal experiments in which movement of the particle on the skin must be prevented. Experiments would be required under anaesthesia for unacceptably long periods. The majority of published hot particle animal studies have involved exposures of no more than 1-2 hours, often much less. Physical attachment of sources to animals to facilitate long-term exposures are

problematic and involve some attachment method that may be likely itself to cause skin damage or possible skin infection, and invalidate the results. This highlights the point that, in practice, particles are unlikely to remain stationary for any extended period of time at most body sites. If particles do move, relative to the skin surface (for example, if they are located on clothing or are subject to physical movement across the skin surface) then the radiation energy will be delivered over a more extended area than if the particle remained stationary. The absorbed dose, averaged over an area of say 1 cm^2, will not be greatly affected if the particle movement is limited to say, a few mm. The spatial dose distribution will however be smeared out, and the peak dose immediately beneath the particle will be considerably reduced. The threshold dose (1 cm^2, 70μm) for biological effects under these circumstances would be expected to be increased by perhaps a factor of 2-3, just as the threshold dose for acute ulceration has been observed to increase as radioactive source size is increased for a range of beta emitting hot particle sources (Charles, 1990, 1991).

For low dose rate exposures the threshold dose for deterministic effects is likely to significantly increase due to cell repair and repopulation before damage becomes patent. Such increases have been observed for large area, low dose rate $^{90}Sr/^{90}Y$ sources on pig skin. The ED_{50} values for moist desquamation are about 27 Gy and 69 for dose rates of 180 Gy h^{-1} and 1.2 Gy h^{-1} respectively (Hopewell, 1991). Similar increases in ED_{50} values for hot particle exposures are to be expected. In fact much greater sparing at low dose rates might reasonably be expected for hot particles since wound healing by cell migration is likely to be very effective for the small lesion sizes involved. There may well be pseudo-threshold doses for very low dose rate exposures since cell repair and cell migration are likely to repopulate damaged tissues within the normal tissue turnover times – and the normal tissue architecture should be maintained.

Predicted skin dose rates (1 cm^2, 70 μm) from contact with the highest activity Dounreay fuel fragment particles found to date (~10^8 Bq ^{137}Cs) are about 60 Gy h^{-1}, for spherical particles (diameter ~ 3mm). Dose rates for elongated or disc particles of this activity may be a factor of 2 higher. At this dose rate, exposures for a few hours will produce lesions similar to those in high dose animal studies (Reece *et al*. 1994), i.e. ulcerations that are visible at 1-2 weeks, extend over areas of $\leq$ 1 cm^2, and may take several weeks to heal, probably with scar formation. In such cases infection is possible and medical treatment to control this may be required. Late dermal atrophy may also develop after 1-2 years due to a reduction in dermal thickness. These have the appearance of a small dimple (Hamlet *et al*. 1986). Exposure for about 30 minutes would produce skin doses at about the ED_{50} level, producing small lesions that would be visible within about 1-2 weeks and heal within a further 2-4 weeks with normal personal skin care. Shorter duration exposures (< 15 minutes, say) are unlikely to produce any significant observable effects.

The highest activity particles found to date at Sandside Bay (3 x 10^5 Bq ^{137}Cs) will deliver skin dose rates of about 1 Gy h^{-1} (1 cm^2, 70 μm). These particles are about 400 μm diameter. A 1-2 hour exposure from such a particle will not give rise to any visible skin lesion. Exposure times of 5 and 10 hours correspond to the ED_{10} and ED_{50} values for acute ulceration. These exposures might produce small lesions that would be visible within about 2-3 week and heal within a further 2-4 weeks with normal personal skin care. Particle movement across the skin of even a few mm during this extended

exposure period will significantly increase the threshold dose for ulceration. This would probably prevent the occurrence of any observable skin lesion. Exposure for 2 - 5 days (with the reservations regarding the likely sparing effect of low dose rate exposures and particle movement - discussed above) may produce subsequent ulceration of the skin within 2-3 weeks which would probably heal within a few weeks.

2.6 Possible biological effects of Dounreay fuel fragments on other organs

While concentrating on the most likely situations of hot particle exposures involving skin contact or ingestion, the NCRP (1999) review also considered possible effects of particle entry into the ear or eye. The following sections are based mainly on data presented and conclusions reached by NCRP (1999) but also refer to recent data on radiation-induced opacities of the lens.

2.6.1 Ear

The external ear consists of the auditory canal, which is terminated at the ear drum (the tympanum). There is little information regarding the skin response at these sites but even high doses of 60-70 Gy from low dose rate (0.3 – 0.9 Gy h^{-1}) ^{192}Ir interstitial radiotherapy sources produced little or no observable damage (Mazaron *et al*. 1986). The only known report of a radioactive particle in the ear is of a worker at an American nuclear plant (Horan, 1966). The particle was introduced into the ear in a blast of air and this appears to have caused the particle to impinge on the tympanic membrane. The worker reported an ear problem after 7 days, and was treated for ear infection. After 10 days the particle was removed, after a radiation survey. The mixed fission product particle was 70 μm in diameter. Dosimetry information for this exposure is difficult to interpret. Beta ray exposure to 'a small area' of the tympanic membrane was reported to be 'thousands of Roentgen'. NCRP (1999) considered that acute ulceration of the tympanic membrane had occurred, consistent with that reported experimentally for hot particle exposure of the skin. On the basis of similarities with skin responses the NCRP recommended a dose limit for the ear from a hot particle which is the same as they recommended for the skin (0.5 Gy averaged over 10 cm^2 at a depth of 70 μm, which is equivalent to a dose of 5 Gy over 1 cm^2). The likely residence times of particles in the ear are difficult to ascertain. Personal ear-cleaning habits are likely to vary widely. Ulceration of the skin of the ear is likely to lead to medical help which may include treatment for infection and ear syringing. NCRP consider that the limited beta radiation range in tissue will limit radiation effects to the skin of the ear or the tympanic membrane. Secondary infection of the middle ear could produce some hearing loss if infection in the tympanic membrane was untreated.

2.6.2 Eye

Figure 2.10 indicates the size and shape of the compartments of the anterior of the eye. Figure 2.11 puts the eye dimensions in the context of depth doses from a range of different penetrating radiations. For ^{90}Sr/^{90}Y beta radiation the dose to the eye lens is considerably smaller than the dose to the cornea.

There is a considerable literature on the exposure of the eye in radiotherapy to penetrating radiations (x- and gamma- radiation) and to various beta radiation sources. For short-term (acute) exposure to penetrating radiations the limiting biological effect for radiological protection considerations is the eye lens. Data reviewed by NCRP (1999) show that opacification of the lens can be produced after months/years following acute exposure at absorbed doses of greater than ~ 2 Gy. Opacities at these doses are likely to be small and cause little visual impairment. The incidence and severity of the opacification increases as dose increases and at doses in excess of ~ 5 Gy it causes severe detriment/blindness in most cases. Fractionation of the exposure over long periods of several months increases these doses by a factor of up to about 3.

Figure 2.10. Mean ocular dimensions for the unaccommodated eye. The equatorial epithelial cells (E) form a ring around the whole periphery of the lens. They are the target cells for

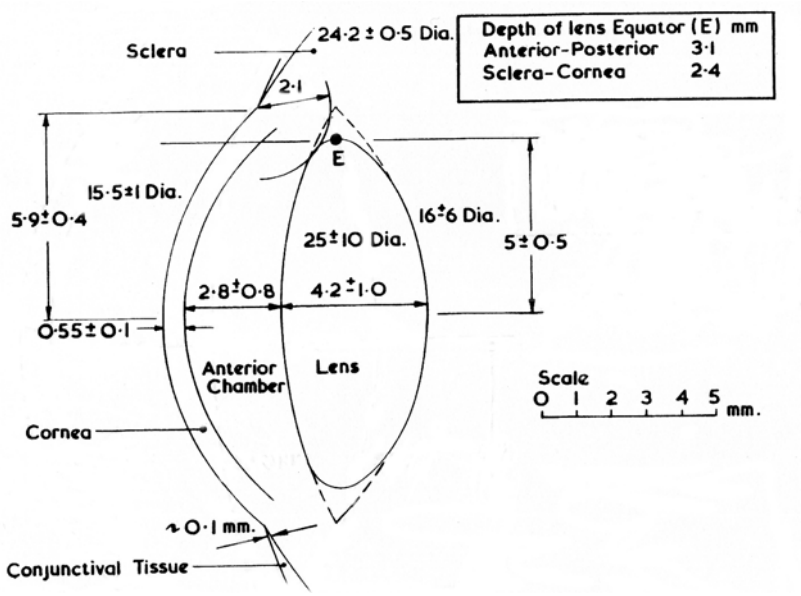

radiation-induced cataract. Dimensions are taken from slit lamp photographs. (Charles and Brown, 1975.)

The mechanism of cataract formation involves damage to a target population of equatorial epithelial cells around the periphery of the lens (marked E on Figure 2.10). Radiation exposure denatures proteins in these cells which then undergo opacification as they progress to the rear central region of the lens, as part of the continual slow process of lens growth. Cataracts can be removed with a minor operation, and vision can be restored with a lens implant. The ICRP (1991a) recommend annual dose limits for workers and members of the public of 150 and 15 mSv, respectively, on the basis that continuous, year-on-year, exposure at these dose limits should not produce impairment of vision from cataract induction. No justification is given for the factor of 10 reduction for members of the public.

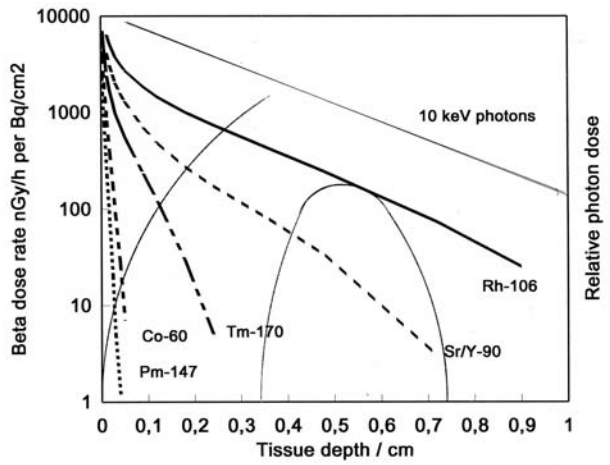

Figure 2.11. Depth doses in tissue for several large area beta sources and low energy photons. Superimposed, to scale, is a cross section of the anterior of a normal unaccommodated eye. (Charles, 1997.)

Recent studies discussed in a draft ICRP document on the biological effects of radiation (www.icrp.org) have suggested that the lens of the eye may be more sensitive than previously considered. In particular, among both A-bomb survivors (Minamoto *et al*. 2004) and a group of children treated for skin haemangioma (Hall *et al*. 1999), there is evidence of excesses of both cortical and posterior subcapsular cataract at doses somewhat lower than expected. The draft ICRP report suggests a threshold of about 1.5 Gy, while recognising uncertainties in the mechanisms of cataract formation. It is proposed that the dose limits of 150 mSv for workers and 15 mSv for members of the public should continue to apply and the sensitivity of the lens should be reviewed as new data are published.

The equatorial epithelial cells around the periphery of the lens lie at a depth of at least ~ 2.5 mm from the eye surface (Figure 2.10). For a hot particle at any position on the corneal surface the majority of the equatorial region of the eye is much deeper than this and the risk of cataract induction is small. Damage to the cornea is of primary concern. The cornea is approximately 0.5 mm (500 μm) thick and consists of connective tissue sandwiched between an outer epithelial layer and an inner endothelial layer. The outer epithelial layer is about 5 cells thick. It is a mucous type in contrast to the outer keratinised layer of the skin. The cellular turnover time (time for a cell in the basal layer to divide, differentiate, and migrate to the surface and desquamate) is about 1 week. The inner endothelial layer consists of a single layer of cells which repairs injury by the elongation and spreading of surviving adjacent cells.

There is a considerable literature regarding beta irradiation of the cornea in radiotherapy. It is used for example in conjunction with local surgery for the treatment of pterygium – a raised, wedge-shaped growth of the conjunctiva. Beta irradiation prevents the re-growth of pterygium after eye surgery. Single acute surface doses of 30 Gy and fractionated doses up to 60 Gy have been used for this treatment using large area $^{90}Sr/^{90}Y$ beta sources in contact with the cornea. These treatments are considered to be effective, with few complications or cataract induction (Jurgenliemk-Schulz *et al*. 2004).

A hot particle in the eye is likely to evoke a foreign body response that most people will have experienced from 'conventional' particles. However, according to NCRP (1999), there is considerable evidence that foreign body responses depend on a number of factors such as particle size, shape, composition and location – and some may be tolerated. There is insufficient experience or experimental data to definitively predict the outcome of a high dose delivered to a small area of the cornea. However, it is reasonable to assume that small area effects would not exceed the expectation of damage from the same dose delivered to a larger area. That is, if surface doses of at least 30-60 Gy to the cornea could be tolerated from large area exposures then similar doses from hot particles, measured over small areas in the vicinity of the hot particle, should also be tolerated. NCRP (1999) also considered that although 5 Gy (1cm^2, 70 μm) represents the ED_{50} for skin lesions, only a very small fraction of these would extend to depth equivalent to the full corneal thickness. Non-trans-corneal wounds would not be expected to produce other than very small imperfections in corneal topography, which would have little likelihood of influencing visual function or acuity. On this basis NCRP (1999) recommended for radiological purposes that eye dose from a hot particle should be limited to 5 Gy (1 cm^2, 70 μm) averaged over the most highly exposed 1 cm^2 of ocular tissue. This was considered adequate to prevent effects such as loss of visual function, breaching of the eye (e.g. resulting from severe damage of the cornea), or breakdown of the barrier function of the eye-related skin (e.g. lid) with consequent possibility of infection. Actual doses obviously depend on residence times of particles in the eye. The largest Dounreay fuel fragments found at Sandside Bay, which deliver dose rates of ~ 1 Gy (1cm^2, 70 μm) per hour, have diameters of about 0.4 mm. This is similar to a medium size grain of sand on the beach. It would seem reasonable to consider that toleration of this would not usually extend for more than a few hours, and early biological effects would be unlikely. Dose rates to the cornea are likely to be reduced due to particle movement around the eye, and movement of eye lids and eye ball. Extended corneal exposure to higher activity particles could produce corneal ulceration, which may require medical intervention and treatment, as in the case of side effects of high dose beta irradiation in ocular radiotherapy.

The only known report of a radioactive particle in the eye is that of a worker at a Finnish nuclear plant (Tossavainen, 1990). The 150 μm diameter particle was considered to have remained in the eye for 4 hours. No perceptible eye changes were seen. The activity of the particle was ~ 2 x 10^4 Bq of predominantly ^{95}Nb and ^{96}Zr, intermediate energy beta emitters. The surface dose was estimated as 1 Gy over an area of 1.4 mm^2.

2.7 Discussion

The available animal data on the effects of hot particle irradiation of skin, mainly from studies using pigs but supported by human data, allow the estimation of an ED_{50} value (1cm^2, 70 μm) for acute ulceration of about 10 Gy and a threshold of about 2 Gy. It is clear from these data, together with data for larger area skin exposures, that toleration of radiation will be increased when a particle moves during skin contact, by even a few mm, and when dose rates are low. Taking no account of this amelioration of their possible effect, Table 2.3 provides a summary of time taken for MTR particles to deliver

doses of 0.5 Gy, 2 Gy and 10 Gy, corresponding to the ICRP dose limit (see below), the estimated threshold and the ED_{50} value, respectively. The short times required for 10^8 Bq ^{137}Cs MTR particles to cause ulceration illustrate the high probability of such damage in the event of such contact. For 10^5 Bq ^{137}Cs MTR particles, typical of the most active particles found at Sandside Bay, stationary contact for more than 7 hours is required before ulceration is expected to occur. It can be concluded that contact with such particles is unlikely to cause ulceration, although a particle trapped against the skin for longer periods of a day or two may cause a small ulceration.

Table 2.3 includes estimates of time taken for particles to deliver a dose of 0.5 Gy, corresponding to the ICRP dose limit (0.5 Sv). This is the limit for localised skin exposure of workers and can be regarded as conservative when applied to hot particle exposures since the threshold for effects is around 2 Sv (NRPB, 1997). For the public, ICRP reduces the dose limit by a factor of ten to 50 mSv. However, this reduction has no scientific basis and it can be argued that no special limit for members of the public is necessary (NRPB, 1997). It should also be noted that ICRP (1991a) dose limits apply to controlled sources and are not intended to apply to existing situations in which the only available protective action takes the form of intervention, as would be the case for the pre-existing situation of environmental contamination with Dounreay particles.

Table 2.3. Estimates of time taken for MTR particles* to deliver doses corresponding to the ICRP dose limit, threshold and ED_{50} for acute ulceration

Activity	Dose rate†	Time to:		
Bq ^{137}Cs	Gy h^{-1}	ICRP limit: 0.5 Gy	Threshold: 2 Gy	ED_{50}: 10 Gy
10^4	0.03	17 hours	3 days	2 weeks
10^5	0.3	<2 hours	7 hours	33 hours
10^6	2 – 4	8 – 15 minutes	0.5 – 1 hours	2 – 5 hours
10^7	15 – 30	1 – 2 minutes	4 – 8 minutes	20 - 40minutes
10^8	70 - 140	<30 seconds	1 – 1.5 minutes	<10 minutes

*Applying standard assumptions used in this report including a specific activity of 2 GBq ^{137}Cs g^{-1} and an activity ratio of 0.9 for ^{90}Sr/^{90}Y:^{137}Cs.

†Dose rates from Figure 2.5; ranges take account of possible differences in shape and hence energy self-absorption within larger particles (see text).

The most comprehensive consideration of the possibility of hot particle damage to the ear or eye is that included in NCRP Report No. 130 (1999). As summarised above (Section 2.6), NCRP concluded that the same limits should apply to the skin lining the auditory canal and the ear drum as to other skin regions. They also concluded that the same limit should prevent damage to the cornea of eye, the site at greatest risk if a particle were to lodge in the eye.

3 INGESTION OF FUEL FRAGMENTS

3.1 Introduction

This chapter provides an assessment of possible acute radiation damage to the alimentary tract following the ingestion of fuel fragments, concentrating on the colon as the region receiving the greatest doses. Doses are calculated using a new ICRP model of the human alimentary tract which will be published this year or during 2006. It will replace the current ICRP Publication 30 model (ICRP, 1979). Section 3.2 of this chapter gives a brief description of the models and illustrates the effect of the new model on dose estimates.

An important development in the new ICRP model of the human alimentary tract (ICRP, 2005) is the explicit consideration of doses to target cells for radiation-induced cancer in the various regions. Section 3.3 includes a brief discussion of the location of target cells for cancer induction and acute effects and provides a summary of data on dose – response for acute intestinal damage from external acute exposures and ingested radionuclides.

Previous *in vitro* studies have shown that the particles are not readily soluble and are likely to pass through the alimentary tract with the loss of only a small proportion ($\leq$1%) of their radionuclide content (Wilkins *et al*. 1998). The results of more extensive *in vitro* and *in vivo* studies on a range of MTR and DFR particles are summarised in Section 3.4. In the *in vitro* studies, undertaken at the Scottish Universities Research and Reactor Centre (SURRC), four MTR and seven DFR particles were incubated in simulated stomach and duodenal fluids and the extent of radionuclide dissolution determined. In the *in vivo* studies, undertaken at NRPB, four MTR and four DFR particles were administered to adult rats and absorption to body tissues was measured. The results obtained from these studies provide information used in the dose assessments in this chapter and also in chapter 5 which considers doses to all tissues, and effective doses, in the context of cancer risk. Section 3.5 summarises data on the radionuclide content of particle, from these and previous studies.

Estimates of colon doses are presented in Section 3.6 for a range of particle activities from 10^3 to 10^8 Bq ^{137}Cs. Doses to the rectosigmoid are given because these will be greater than to other regions of the colon. In each case, estimates are given of the most likely 'expectation' doses for a particle moving randomly through the rectosigmoid and also the maximum dose for a particle moving along the interior wall of the rectosigmoid. The section includes consideration of the effect of changes in assumptions for: the location of target cells; colon dimensions; transit times; and, particle ^{137}Cs specific activity (Bq g^{-1}) and ^{90}Sr/^{90}Y:^{137}Cs ratios.

3.2 Alimentary tract models

3.2.1 ICRP Publication 30 model

The Publication 30 model (ICRP, 1979) of the gastrointestinal tract was developed specifically to calculate doses to workers, either from the direct ingestion of radionuclides or following their inhalation as particles with subsequent escalation from the lungs to the alimentary tract. The model took account of transit of ingested materials through four regions of the alimentary tract: the stomach, small intestine, upper large intestine and lower large intestine. The absorption of radionuclides to blood was specified by values of fractional uptake (f_1) from the small intestine. Transit times were based largely on information from clinical studies using barium meals; reference was also made to studies using materials labelled with iron-59 or lanthanum-140 (Eve, 1966). Mean residence times were taken to be 1 hour for the stomach, 4 hours for the small intestine, 13 hours for the upper large intestine and 24 hours for the lower large intestine.

In the Publication 30 model, doses were calculated separately for the mucosal layer of each of the four regions considered. For penetrating radiations, the average dose to the wall of each region was used as a measure of the dose to the mucosal layer. For non-penetrating radiations, the Specific Absorbed Fraction (see Section 3.2.3) for the mucosal layer was taken to be equal to 0.5v/M where M is the mass of the contents of that section of the tract and v is a factor between 0 and 1 representing the proportion of energy reaching sensitive cells. The factor of 0.5 was introduced because the dose at the surface of the contents will be approximately half that within the contents for non-penetrating radiations. For electrons (beta particles), v was taken to be 1. For alpha particles, a value of 0.01 was used on the basis of an acute toxicity study in rats in which the LD_{50} for ingested yttrium-91 was estimated as about 12 Gy, while an absorbed dose to the mucosal surface of more than 100 times greater from ^{239}Pu had no effect (Sullivan *et al*. 1960).

3.2.2 The new ICRP model (HATM)

The main features of the new ICRP Human Alimentary Tract Model, HATM (ICRP, 2005), can be summarised as follows:

- Inclusion of all alimentary tract regions. Doses are calculated for the oral cavity, oesophagus, stomach, small intestine, right colon, left colon and rectosigmoid (including the rectum). Colon doses are combined as a mass-weighted mean.
- Age-dependent parameter values for the dimensions of alimentary tract regions and associated transit times of contents through the regions.
- Gender-dependent parameter values of dimensions and transit times for adults.
- Transit times for food and liquids, as well as for total diet, for the mouth, oesophagus and stomach.
- Default assumption that total fractional absorption, f_A, of an element and its radioisotopes to blood occurs in the small intestine, i.e. $f_{SI} = f_A$.

- Model structure to allow for absorption in other regions, in situations where information is available (Figure 3.1).

- Model structure to allow for retention in the mucosal tissues of the walls of alimentary tract regions, and on teeth, in situations where information is available (Figure 3.1).

- Explicit calculations of dose to target regions for cancer induction within each alimentary tract region, considering doses from radionuclides in the contents of the regions, and considering mucosal retention of radionuclides where appropriate.

More extensive and reliable data on gut transit have become available since ICRP Publication 30 was issued, obtained by techniques including non-invasive scintigraphy (Stubbs, 1992). The oral cavity and oesophagus will normally receive very low doses from ingested radionuclides because mean transit times are fractions of a minute. However, these regions were included for completeness, because retention in the mouth, on teeth for example, can result in a substantial increase in dose to the oral mucosa, and because a specific tissue weighting factor, w_T, was assigned to the oesophagus in ICRP Publication 60 (1991a) to account for the risk of radiation-induced cancer (see Section 5.1). In general, however, the alimentary tract regions of greatest importance in terms of dose and cancer risk are the stomach and particularly the colon. While the small intestine may receive greater doses than the stomach, it is not sensitive to radiation-induced cancer and is not assigned a specific w_T value. The colon generally receives the highest doses because of long transit times and is of greatest importance when considering deterministic effects. Doses are calculated separately for the right colon, left colon and rectosigmoid. This partitioning of the colon for the purposes of dose calculations is predicated on the availability of transit time data. The rectum is taken to be part of the rectosigmoid because of difficulties in determining transit times separately and because the rectum does not have a specific w_T value. Table 3.1 summarises transit times used for the stomach, small intestine and colon in the HATM.

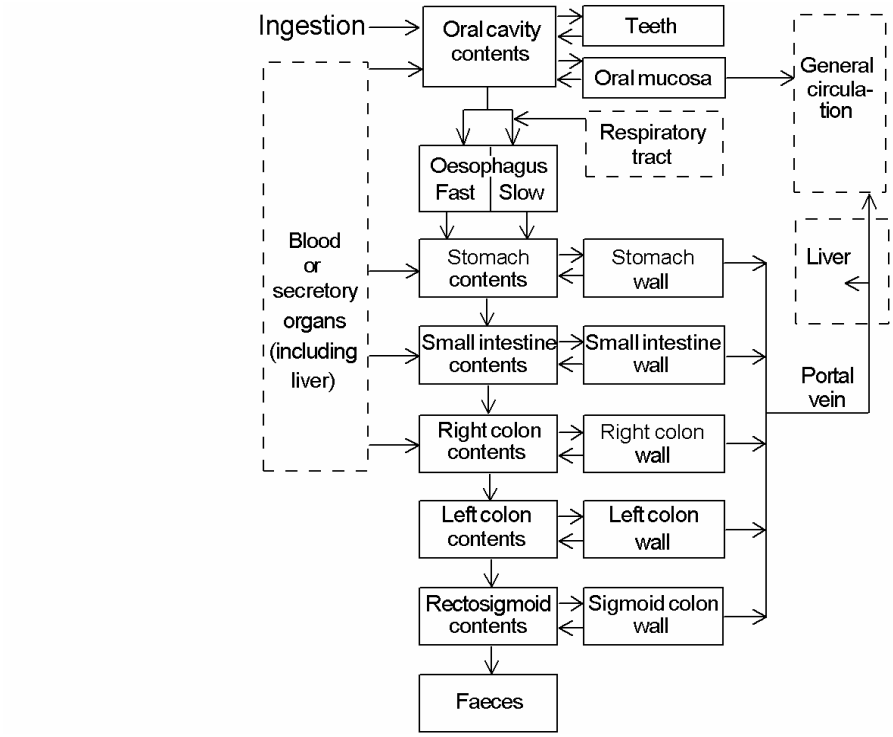

Figure 3.1. Structure of the ICRP human alimentary tract model (HATM). The dashed boxes are included to show connections with the respiratory tract model and systemic models.

Colon transit times are generally shorter in infants and children than in adults and, on this basis, the application of the Publication 30 model in a number of ICRP publications considering radionuclide ingestion by infants and children will have overestimated doses (e.g. ICRP, 1996). In adults, mean transit times for the stomach and colon are about one-third greater in females than males. Slightly smaller masses in females (e.g. 10% lower mass of colon tissue) will compound the resulting difference in dose.

An important development in the HATM is the methodology used to calculate doses in the various regions from non-penetrating alpha and electron radiations, taking account of the location of the target tissue in the mucosal layer of the wall of each region. The targets relating to cancer induction are taken in each case to be the epithelial stem cells, located in the basal layers of the stratified epithelia of the oral cavity and oesophagus and within the crypts that replenish the single cell layer epithelium of the stomach and small and large intestines (Potten, 1995). The epithelial stem cells are also taken to be the targets for deterministic effects (see Section 3.3). In the HATM, Absorbed Fractions for electrons were calculated using the MCNP general purpose Monte Carlo Code (Briesmeister, 1997) and for alpha particles on the basis of an algebraic relationship between stopping-power in soft tissue and alpha particle energy (Sontag, 1987). This was done using simple representations of alimentary tract anatomy. All tubular regions of the alimentary tract were treated as simple cylinders with target cells for cancer induction forming a continuous layer at a specified depth below the lumenal surface. The stomach was similarly treated as a sphere. Age-dependent dimensions were specified. Tables 3.2 – 3.4 give the values used in the HATM for the volume of the stomach and length and internal diameter of the regions of the large intestine. Table 3.5

shows the assumed target cell depths in each region and the mass of the target tissue in adult males.

Table 3.1. Mean transit times used in the new ICRP model of the human alimentary tract (HATM)

	Transit time, h				
Region	3-month infant	1 y	5-15 y	Adult male	Adult female
Stomach*	1.25	1.2	1.2	1.2	1.5
Small intestine	4	4	4	4	4
Right colon	8	10	11	12	16
Left colon	8	10	11	12	16
Rectosigmoid	12	12	12	12	16

*Values given for the stomach are for total diet: 75 min for infants, 95 min for adult females and 70 min for all other groups. The HATM report also gives separate values for solids and liquids for the stomach.

Table 3.2. ICRP Reference values for the volume of the stomach (cm^3)

Newborn	1 y	5 y	10 y	15 y	Adult
30	40	60	80	120	175

Table 3.3. ICRP Reference values for the length of the large intestine (cm)

					15 y		Adult	
Segmentntnt	Newborn	1 y	5 y	10 y	Male	Female	Male	Female
Right colon	14	18	23	28	30	30	34	30
Left colon	16	21	26	31	35	35	38	35
RS*	15	21	26	31	35	35	38	35
Total	45	60	75	90	100	100	110	100

*Rectosigmoid

Table 3.4. ICRP assumptions for the internal diameter of the large intestine (cm)

Segment	Newborn	1 y	5 y	10 y	15 y	Adult
Right colon	3	4	4.5	5	6	6
Left colon	2.5	3	3.5	4	5	5
Rectosigmoid	1.5	2	2.3	2.5	3	3

Table 3.5. Target cells depths* and masses for target each region of the HATM for adult males

Region	Target cell depth, μm	Target cell mass†, g
Oral cavity	190-200	0.23
Oesophagus	190-200	0.091
Stomach	60-100	0.62
Small intestine	130-150	3.6
Right colon	280-300	1.3
Left colon	280-300	1.2
Rectosigmoid	280-300	0.73

*Applied to all ages.

†computed from the length and diameter of each section (or radius for stomach) and the depth and thickness of the

target cells, assuming a tissue density of 1 g cm^{-3}.

Photon Absorbed Fractions were calculated in the HATM, as in the Publication 30 model (ICRP, 1979), as an average to the wall of each region, using mathematical models of the human body (see Section 5.3). Mathematical phantoms have been developed for adults, children and the pregnant woman (Cristy and Eckerman, 1987, 1993, Stabin *et al*., 1995) and these have been used in all calculations of ICRP dose coefficients (ICRP 1994b, 1996, 2001).

3.2.3 Changes in ICRP dose coefficients calculated using the HATM

The change in approach to the calculation of doses from non-penetrating radiations in the new ICRP model results in important changes in dose estimates. Figure 3.2 shows the variation of Specific Absorbed Fraction (SAF: Absorbed Fraction per unit mass) with electron energy for the example of the right colon of the HATM, compared with the energy-independent value for the upper large intestine (ULI) of the Publication 30 model. Above about 1 MeV, the HATM SAFs are about a factor of five lower than the Publication 30 value, with greater differences at lower energies. Comparisons for the stomach show much closer agreement between the two approaches (ICRP, 2005). Absorbed Fractions for alpha particles are zero for all sources within the lumen because alpha emissions from all important radionuclides (e.g. ^{239}Pu, ^{210}Po) have a track length of 50 μm or less in the body. The assumption for the stomach that target cells are closer to the lumenal surface (Table 3.5) might suggest that some energetic alpha particles could reach this layer. However, taking account of the presence of a protective mucus layer in the stomach, ignored in calculations for electrons, it appears reasonable to assume that Absorbed Fractions (AF) for alpha particles in the lumen are zero for all regions.

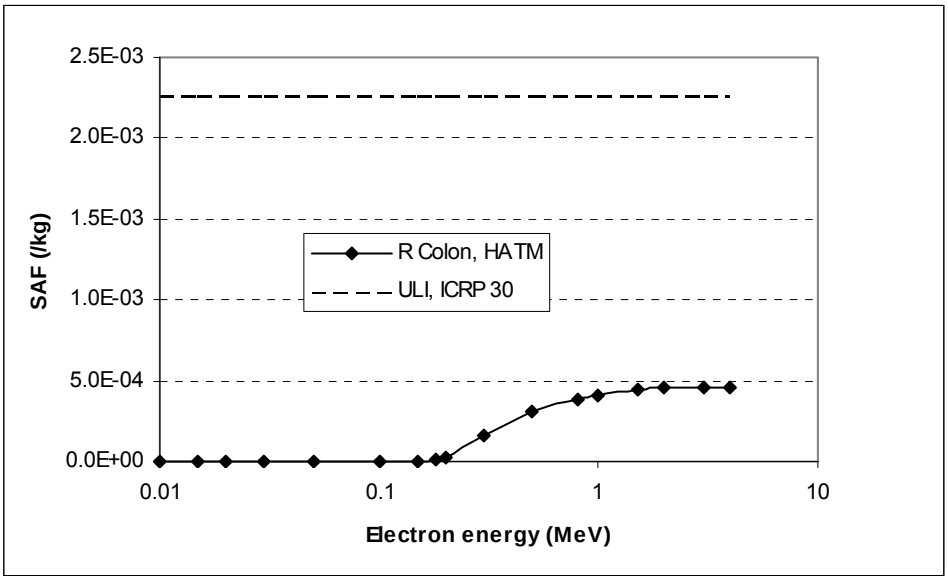

Figure 3.2. Comparison of values of Specific Absorbed Fraction (SAF) for a source in the lumen of the right colon (HATM) and upper large intestine (ULI, Publication 30) of adult males.

Table 3.6 compares doses calculated using the HATM and Publication 30 models for the examples of ingestion of ^{90}Sr and ^{239}Pu, considering committed equivalent doses to the stomach and colon and committed effective doses (see Secion 5.1), for ingestion of unit activity by adult males. In each case, standard systemic models were used to calculate doses to body tissues from the fraction of the ingested radionuclide absorbed to blood (ICRP, 1989, 1993; see Section 5.2). For the beta-emitting nuclide, ^{90}Sr, the substantial reduction in colon doses in the HATM reflects reduced SAFs (Figure 3.2). For ^{239}Pu, there is no direct dose to alimentary tract regions using the HATM; all dose is due to absorbed ^{239}Pu assigned to general soft tissues in the systemic model (see Section 5.2). The extent to which differences in equivalent doses to the tissues of the alimentary tract affects the effective dose, E, depends on the relative contribution of these tissues to E. For ^{90}Sr, E is dominated by skeletal doses (bone surfaces and red bone marrow; see Secfion 5.2) and there is little difference in values of E calculated using the HATM and Publication 30 model. For ^{239}Pu, doses to alimentary tract regions make only a small contribution to E, the dominant contributors being liver and skeletal tissues (see Section 5.2).

Table 3.6. Comparison[a] of ingestion dose coefficients derived using the HATM and ICRP Publication 30 model

	Equivalent dose		
Radionuclide	Stomach	Colon	Effective dose
^{90}Sr	1.0	0.2	-6%
^{239}Pu	0.8	0.3	Nil

[a]Equivalent doses compared as ratios, effective doses as fractional change (%).

3.3 Radiation effects

3.3.1 Target cells for acute damage and cancer induction

There is general agreement that acute damage within the alimentary tract relates to cell killing in the stem cell zone of the epithelial lining, such that renewal of the lining is prevented (ICRP, 2005). In addition to epithelial cells, targets may include vascular endothelial cells, mesenchymal fibroblasts and other cell types. However, as discussed below (this Section and 3.3.2), studies of epithelial repopulation in the small intestine of mice and acute effects of ingested radionuclides in dogs suggest that observed effects can be related to dose delivered at the stem cell positions in the small and large intestine (Cross *et al*. 1978; Sullivan *et al*. 1978). Cancers are also generally considered to originate from stem cells which may be transformed by carcinogenic agents so that their differentiation patterns are altered in such a way that cell renewal predominates over differentiation, leading to growth of an abnormal cell population.

Stem cells in stratified squamous epithelium, as in the lining of the mouth, the tongue and the oesophagus, are taken to be located in the basal cell layer adjacent to the basement membrane, as assumed for skin (ICRP, 2002; see Chapter 2). In the stomach, stem cells are thought to be located towards the upper regions of the gastric pits, renewing the epithelial layer by both upward flow of daughter cells towards the

lumenal surface of the stomach and downward flow into the gastric glands (Karam *et al*. 2003; Modlin *et al*. 2003).

Evidence for stem cell position in the small intestine was obtained from studies using short range electrons from a promethium-147 plaque to irradiate crypts in the mouse small intestine from the serosal surface towards the crypt base (Hendry *et al*. 1989). Efficient crypt sterilisation was achieved with doses calculated to cell positions 4-5 from the base, the stem-cell position above the Paneth cells. Dividing transit cells irradiated with much lower doses above the stem cell zone did not appear to contribute to repopulation of the damaged crypts. This lack of repopulation potential from daughter cells is in contrast to the positive contribution suggested from analyses of dose-response data obtained in other studies using high doses of penetrating irradiation in both small (Hendry *et al*. 1992; Roberts *et al*. 1995) and large (Cai *et al*. 1997) intestine. It was considered possible that daughter transit cells may be recruited into the stem cell population when there is sufficient cell damage and death in the crypt to allow cell migration against the normal direction of cell flow, thus allowing some of these mutated transit cells to reach the stem-cell zone. In a subsequent analysis, a different hypothesis was proposed, in which a secondary mechanism of injury either directly from damage to stem cells or indirectly from injured stromal cells, could explain the dose-response data without invoking down-migration of transit cells in the crypt (Roberts *et al*. 2003). On the basis of the above possibilities, it is considered here that the initial stem cell population is the most likely target-cell population for acute effects and carcinogenesis.

In the colon, the stem cells are situated at the very base of the crypts. This has been deduced from a variety of cell kinetic, mutational and regeneration studies in mouse models (Potten, 1995). Their position in man is likely to be qualitatively similar. The number of stem cells per colonic crypt in mice has been estimated to be in the range 1-8, and as colonic crypts in man are larger than in mice the number of stem cells per crypt may be greater in man.

In this report, as in the new ICRP report, the target for all effects is taken to be the epithelial stem cells. The possibility that a wider target is involved in the case of acute damage is addressed in Section 3.6.4.

3.3.2 Doses causing acute effects

The early effects of high doses of external radiation, involving gross cell killing in haemopoietic, intestinal or nervous tissue, are collectively referred to as the “acute radiation syndromes” and have been extensively reviewed (Bond *et al*., 1965; Young, 1987; UNSCEAR, 1988). Haemopoietic stem cells are more sensitive to radiation than intestinal stem cells but because of the more rapid cell division and renewal in the small intestine, sufficiently high acute doses (10 – 20 Gy) can cause death within 1 – 2 weeks due to breakdown of the intestinal epithelium. This destruction of the mucosal lining of the intestine results in fluid, protein and electrolyte loss, infection and haemorrhage. Survival depends on the presence of a sufficient number of stem cells to repopulate the epithelium, although, as discussed above (Section 3.3.1), it is possible that immediate daughter cells of stem cells may retain the potential to re-establish epithelial integrity. Delayed effects, involving other cell types including vascular endothelial cells and mesenchymal fibroblasts, may be seen in the small and large intestines and in other

regions of the alimentary tract. Effects include damage to blood vessels, such as endarteritis and fibrosis, excess collagen deposition in the submucosa and strictures.

Very few human data are available on gastrointestinal radiation damage. It is known, however, that cancer patients survived after whole body doses of 10 Gy or more, generally as a single dose delivered in about 4 hours in conjunction with bone marrow transplantation (Thomas *et al*. 1975). Extensive internal contamination with ^{137}CsCl (> 3.1 MBq) occurred in 22 persons in the Goiania accident in Brazil (IAEA, 1987). Eight individuals developed acute radiation syndrome, including symptoms such as nausea, vomiting, and watery diarrhoea during the prodromal phase. Doses received by these individuals were estimated using cytogenetic dosimetry to range between 3 and 7 Gy, accumulated over a period of 2 weeks. In four persons who died after receiving doses estimated as between 4 and 6 Gy, intestinal bleeding was found at autopsy, although the primary cause of death was bone marrow insufficiency and sepsis (IAEA, 1987; Brandao-Mello *et al*., 1991).

Dose-effect relationships for intestinal damage have been obtained from animal data; this is considered reasonable because different mammals respond in a similar way to irradiation of the gut (Bond *et al*., 1965; Maisin *et al*., 1971). Clonogenic studies of damage to the intestinal mucosa in mice, in terms of cell apoptosis, have shown cell killing and crypt sterilisation at doses between 1 – 10 Gy (Potten, 1990). Data obtained from studies in which the alimentary tract of rats was exposed to X-irradiation, either *in situ* or surgically exteriorised, indicated an LD_{50} (death of 50% of animals) of about 15 Gy for acute exposure (Sullivan *et al*., 1959). Values of LD_{50} of about 33 Gy for rats (25 - 41 Gy) and 40 Gy for dogs (20 - 52 Gy) were obtained in experiments in which rats ingested either ^{106}Ru/^{106}Rh (average 1.4 MeV beta) or ^{147}Pm (average 0.06 MeV beta) and dogs were given ^{106}Ru/^{106}Rh (Sullivan *et al*., 1978; Cross *et al*., 1978). The estimated dose to crypt cells in rats was the same for both ^{106}Ru/^{106}Rh and ^{147}Pm, about 35 Gy, although the dose to the mucosal surface was about 35 times greater for ^{147}Pm than for ^{106}Ru/^{106}Rh. This dose is comparable to a dose of about 13 Gy of external irradiation delivered acutely and is consistent with an expected reduction in effect at lower dose rate. Death was due to damage to the large intestine in both rats and dogs. Based on these data, an LD_{50} of 35 Gy has been suggested for human exposures, with a simple linear function with a threshold (LD_0) of 20 Gy and an LD_{100} of 50 Gy (Stather *et al*. 1988; NRPB, 1996). Evans *et al*. (1993) adopted a value for LD_{50} of 15 Gy for acute external irradiation and 35 Gy for protracted internal irradiation.

3.4 Radionuclide absorption to blood following fuel fragment ingestion

3.4.1 *In vitro* dissolution in simulated gut fluids

The studies summarised in this section were undertaken at the Scottish Universities Research and Reactor Centre (SURRC). Advice on experimental procedures was provided by Professor David Taylor of the University of Wales, Cardiff. On the basis of previous work in his laboratory (Taylor *et al*. 1986; Webb, 1998; Jones *et al*. 2001), the composition of simulated stomach and small intestinal fluids used in the SURRC study were as shown in Tables 3.7 and 3.8.

Table 3.7. Composition of the 'Stomach' solution

Compound	g dm^{-3}	Mmol.dm^{-3}
Calcium carbonate (Anhydr.)	0.200	Ca^{2+} 2.0
Magnesium carbonate	0.200	Mg^{2+} 2.1
Potassium chloride	*0.670*	K^{+} 9.0; Cl^{-} 9.0
Sodium chloride	2.800	Na^{+} 48.0; Cl^{-} 48.0
Sodium Lactate	0.250	Na^{+} 2.2; $(lact)^{-1}$ 2.2
Citric acid	0.040	2.1 x 10^{-1}
Urea	0.300	5.0
Pepsin (powder)	1.000	–

Table 3.8. Composition of the 'Small intestine' solution

Compound	g dm^{-3}	mmol.dm^{-3}
Calcium carbonate (Anhydr.)	0.200	Ca^{2+} 2.0
Magnesium carbonate	0.200	Mg^{2+} 2.1 x 10^{-3}
Potassium chloride	*0.670*	K^{+} 9.0; Cl^{-} 9.0
Sodium chloride	2.800	Na^{+} 48.0; Cl^{-} 48.0
Sodium Lactate	0.250	Na^{+} 2.22; $(lact)^{-1}$ 2.22
Citric acid	0.040	2.1 x 10^{-1}
Urea	0.800	13.3
Ox Gall	2.000	
Glucose	0.400	2.2
Pancreatin	2.000	–

The stomach solution was prepared by dissolving the chemicals listed in Table 3.7 in ~ 500 cm^3 of distilled water and adjusting to pH 2 using hydrochloric acid for a final volume of 1dm^3. For the small intestinal solution, the components listed in Table 3.8 were dissolved in water, adjusted to pH 7 with 5 M sodium hydroxide solution to produce a final volume of 1 dm^3. Fuel fragments were suspended separately in 250 cm^3 of Stomach solution and incubated at 37° C, with constant mixing. After 1 hour, a 100 cm^3 sub-sample was removed, filtered through a 0.22 μm filter and subsequently analysed. The volume was immediately made to 250 cm^3 with fresh solution and incubated for a further 1 hour, after which a further 100 cm^3 sub-sample was removed, filtered and analysed. Again, the volume was immediately re-made to 250 cm^3 with fresh solution and the entire stomach compartment solution was transferred to an equal volume of Small intestine solution, and pH adjusted to ~7.0 with 5 M sodium hydroxide solution. This final mixture was incubated for a further 4 hours. At the end of the final incubation, the entire solution was filtered and analysed.

Analyses were performed using standard techniques, as detailed in the contract report to SEPA (Stewart *et al*. 2003). A non-standard aspect of the procedures was that dissolution of the residual particles proved difficult and time-consuming. Dissolution was achieved using hydrofluoric acid (HF) at 100^0C in a Parr high pressure digestion bomb.

Results for the total dissolution of radionuclides from the particles are summarised in Table 3.9. Examination of the contributions of the stomach and small intestine

compartments to total dissolution did not show a consistent pattern, although in general it appeared that dissolution occurred in both fluids. In a number of cases, analytical results were given as "less than" values and percentage dissolution values are not included here. A surprising aspect of the results is that the actinides appear to be more readily dissolved from the particles than are ^{137}Cs and ^{90}Sr; this is contrary to expectations based on the chemical properties of the elements. One particle, MTR113, showed a high level of solubility, with consistent results for each radionuclide. One particle (MTR150) was found to contain only ^{60}Co; total dissolution was about 0.003%.

Table 3.9. Total % dissolution of radionuclides from fuel fragments in simulated gut fluids

Particle	^{137}Cs	^{90}Sr	$^{238,239/240}$Pu	^{241}Am
MTR 002	0.30	0.09	2.9	7.1
MTR 113	59.4	43.5	40.5	45.8
MTR 132	0.16	0.05	-	0.5
MTR 138	0.02	0.03	0.4	-
DFR 111	0.005	0.02	0.1	2.8
DFR 107	0.04	0.002	2.4	-
DFR 125	0.001	0.06	-	-
DFR 128	0.02	0.01	0.3	-
DFR 134	0.001	-	-	-
DFR 135	0.001	-	-	-
DFR 136	0.02	0.01	-	5.0

3.4.2 *In vivo* absorption to blood

In a study at NRPB, 8 particles were administered to rats in order to estimate *in vivo* absorption to blood. The particles were suspended in a small volume of isotonic saline solution and administered by intragastric intubation. Six particles were eliminated within 16 hours, but one rat retained its particle for about 24 hours and one for about 40 hours. The rats were sacrificed after particle elimination for analysis of the radionuclide content of tissues. The procedure adopted for tissue dissection involved removal of the pelt, head, lower limbs and alimentary tract, as described by Harrison and Stather (1982). This procedure avoids possible contamination of tissues with unabsorbed radionuclides passing through the alimentary tract or adhering to skin, particularly important in measurements of very low levels of actinide absorption.

The alimentary tract removed from each animal was separated at the gastro-duodenal junction into small intestine, caecum and colon, and the small intestine was divided further into four equal segments – duodenum, jejunum, proximal ileum and distal ileum. Representative samples were taken from each segment and fixed in phosphate buffered formol saline pH 7.2-7.4 (VWR International Ltd., Merck House, Poole, Dorset). The samples were processed using standard histological techniques (Culling, 1974), embedding in wax and cutting 5 μm sections for staining using Haematoxylin and Eosin. Histopathological examination of the 6 representative tissue samples from the each region of the small and large intestine showed no tissue damage.

Particles eliminated from the animals, having passed through their alimentary tracts, were sent to the National Nuclear Corporation (NNC) Ltd for analysis. There was no evidence of fragmentation of the particles, as determined by measurements of residual ^{137}Cs activity in the gastrointestinal tract. Rat tissues were analysed by the Environmental Investigations Group at NRPB as one sample. Radiochemical analyses were performed under the Group's UKAS accreditation number 1269; other procedures including dissection and interpretation of results fall outside the accreditation. Briefly the gamma emitting radionuclides were determined using high resolution mass spectrometry, ^{90}Sr was determined via its ^{90}Y progeny and plutonium, americium and uranium were determined by ion exchange separation and alpha spectrometry. The mass of tissue analysed represented about 75% of the animals' body weight (mean of 76.5%; range 75.5 – 77.8%).

Table 3.10 shows the radionuclide content of the eliminated particles, analysed by NNC. Table 3.11 shows the results obtained at NRPB for radionuclide retention in rat tissues. Table 3.12 expresses tissue retention as a percentage of activity in the eliminated particles. Since tissue retention was a small proportion of activity in the particles, the values in Table 3.12 can be taken as the percentage of ingested activity retained in the measured tissues. For ^{239}Pu, the results in Table 3.11 show that for three of the DFR particles (055, 098, 106), the tissue retention values were not significantly greater than control values; these results were not, therefore, used to estimate absorption. Similarly, all results in Table 3.11 for ^{241}Am and U isotopes are not greater than controls and were not used.

The results in Table 3.12 relate to tissues accounting for about 75% of body weight and excretion of absorbed ^{137}Cs, ^{90}Sr and ^{239}Pu before the animal were sacrificed is likely to have been less than 10% (Gran, 1960; Furchner and Richmond, 1962; Harrison and Stather, 1982). Taking account of the known tissue distribution of the radionuclides, it is therefore reasonable to assume that total absorption was less than 50% greater than the values given for tissue retention.

Table 3.10. Radionuclide content of particles, Bq

Particle	^{137}Cs	^{90}Sr	^{239}Pu	^{241}Am	^{238}U	^{235}U	^{234}U
MTR101	3.19×10^{6}	2.86×10^{6}	1278	3.75×10^{3}	1.34	21.4	1120
MTR109	1.33×10^{7}	1.21×10^{7}	2200	9.5×10^{3}	6.1	77	4700
MTR154	1.21×10^{5}	1.12×10^{5}	47	81.4	0.036	0.32	24
MTR157	5.80×10^{5}	5.34×10^{5}	333	211.4	0.730	13.7	520
DFR055	7.68×10^{4}	1.57×10^{4}	0.774	0.045	1.002	0.084	2.84
DFR082	1.90×10^{5}	1.45×10^{5}	93.8	0.553	0.138	1.28	49
DFR098	1.86×10^{5}	2.9×10^{4}	23.2	0.172	0.164	1.84	70
DFR106	1.54×10^{5}	1.68×10^{4}	18.7	-	0.100	0.53	20.3

Table 3.11. Radionuclide content of rat tissue, mBq

Particle	^{137}Cs	^{90}Sr	^{239}Pu	^{241}Am	^{238}U	^{235}U	^{234}U

MTR101	$2.6x10^7$	$4.3x10^5$	0.7	2.1	1.5	<0.5	1.8
MTR109	$5.0x10^6$	$1.3x10^5$	1.2	1.1	1.3	<0.4	1.9
MTR154	$1.2x10^5$	$7.0x10^2$	0.8	0.8	1.8	0.6	2.2
MTR157	$8.0x10^6$	$5.6x10^4$	1.5	4.0	1.0	0.2	2.0
DFR055	$2.2x10^3$	$0.5x10^3$	0.5	1.2	1.2	<0.1	1.6
DFR082	$2.1x10^3$	$1.0x10^3$	1.1	0.6	1.0	0.1	1.2
DFR098	$2.0x10^2$	$3.0x10^2$	0.2	1.3	1.3	<0.2	1.2
DFR106	$1.0x10^2$	$3.0x10^2$	<0.01	0.7	1.6	<0.3	1.4
Control	$<1x10^2$	Lost	< 0.1	3.3	1.3	<0.3	1.4
Control	$1.0x10^2$	$4.0\ x10^2$	0.3	2.7	1.2	<0.6	1.0

Table 3.12. % retained in rat tissues

Particle	^{137}Cs	^{90}Sr	^{239}Pu
MTR101	0.82	0.02	$5x10^{-5}$
MTR109	0.038	0.001	$5x10^{-5}$
MTR154	0.10	0.0006	$2x10^{-3}$
MTR157	1.38	0.01	$5x10^{-4}$
DFR055	0.003	0.003	-
DFR082	0.001	0.007	0.001
DFR098	0.0001	0.001	-
DFR106	0.0001	0.002	-

3.4.3 Absorption to blood - assumptions for dose calculations

In comparing the results obtained in the *in vitro* dissolution study and the *in vivo* study (Tables 3.9 and 3.12), the normal absorption of soluble forms of the radionuclides needs to be taken into account. For ^{137}Cs, absorption of soluble forms is usually assumed to be complete (ICRP, 1989), so the results of the two studies can be compared directly. For ^{90}Sr, absorption of soluble forms is assumed by ICRP to be 30% of the ingested activity and for ^{239}Pu the corresponding value is 0.05% (ICRP, 1989, 1993). On the basis of the data obtained, the values of absorption considered appropriate for use in dose calculations are as shown in Table 3.13, giving single estimates and ranges. The values for ^{239}Pu are taken to apply to other actinides and to yttrium, on the basis of chemical analogy and observations of similarly low absorption in other studies. For MTR113, which proved to be highly soluble in the *in vitro* dissolution study, appropriate absorption assumptions are taken to be 60% ^{137}Cs, 15% ^{90}Sr and 0.03% for the actinides and yttrium.

Table 3.13. Interpretation of *in vitro* and *in vivo* data on absorption to blood to give values for use in dose calculations

	% absorption to blood		
Particle type	^{137}Cs	^{90}Sr	^{239}Pu
MTR	1 (0.02 - 2)	0.01 (0.001 - 0.03)	0.001 ($5x10^{-5}$ – $5x10^{-3}$)
DFR	0.03 (0.001 - 0.05)	0.003 (0.001 - 0.02)	0.001 ($5x10^{-5}$ – $5x10^{-3}$)

3.5 Radionuclide content of fuel fragments

Table 3.14 provides a compilation of available data on radionuclide ratios for MTR and DFR particles. The ^{90}Sr: ^{137}Cs ratios for MTR fragments are reasonably consistent with the exception of two apparent outliers from the *in vitro* experiments (particle numbers 132 and 138). These two smaller values are not consistent with observations on surface and depth dose rates made at the University of Birmingham. The Pu : ^{137}Cs ratios for MTR particles are mainly in the range 10^{-2} – 10^{-4}. Particle 113 dissolved rapidly during the *in vitro* study as discussed above (Section 3.4.1). For particles 132 and 138, the Pu : ^{137}Cs ratios were low and within the very large range observed for

Table 3.14. Radionuclide activity ratios in particles

Particle	^{90}Sr : ^{137}Cs	^{238}Pu : ^{137}Cs	^{239}Pu : ^{137}Cs
MTR#	1.0	0.01	0.004
MTR#	0.9	0.003	0.008
MTR#	0.8	0.0009	0.0005
MTR##	2.0	0.003	0.001
MTR 101**	0.9	0.007	0.0004
MTR 109**	0.9	0.001	0.0002
MTR 154**	0.9	0.003	0.0004
MTR 157**	0.9	0.006	0.0006
MTR 002*	1.4	0.003	0.0006
MTR 113*	0.5	Not calc'd	Not calc'd
MTR 132*	0.04	0.00001	0.00005
MTR 138*	0.05	0.000003	0.00004
DFR 055**	0.2	0.000002	0.00001
DFR 082**	0.2	0.00009	0.0005
DFR 098**	0.2	0.00002	0.0001
DFR 106**	0.1	0.00003	0.0001
DFR 111*	1.3	0.00002	0.00007
DFR 107*	2.9	0.00004	0.0002
DFR 125*	0.3	0.000004	0.00002
DFR 128*	0.2	0.00006	0.0002
DFR 134*	0.04	0.0000004	0.000001
DFR 135*	0.3	0.000002	0.000007
DFR 136*	0.5	0.0005	0.005

#NRPB data (Wilkins *et al*. 1998). ##AEA data averaged over 3 particles (Bridges and Knill, 1995). *SURRC *in vitro* data (Table 3.9). **NNC *in vivo* data (Table 3.10).

DFR fragments. On the basis of the data for MTR particles, excluding 132 and 138, the assumptions made for the purposes of dose calculations were a ^{90}Sr/^{90}Y:^{137}Cs ratio of 0.9, a ^{238}Pu:^{137}Cs ratio of 0.003, and a ^{239}Pu:^{137}Cs ratio of 0.001. A ratio of 0.001 was also used for ^{241}Am: ^{137}Cs. Doses calculated for MTR particles on the basis of these ratios are likely to be conservative when applied to DFR particles. A ^{90}Sr/^{90}Y:^{137}Cs ratio of 0.9 has been used in previous estimates of colon dose (Darley *et al*. 2003).

3.6 Colon doses

3.6.1 Dosimetric methodology

The risk of deterministic effects following fuel fragment ingestion has been determined on the basis of doses to the rectosigmoid region of the colon since this region of the alimentary tract receives the greatest doses. Doses from electron and photon emissions were calculated using the radiation transport code MCNP (Breismeister, 2000), as applied to the calculation of electron SAFs for the new ICRP model (see 3.2). In its application here to doses from fuel fragments, the method takes account of absorption of energy within the fragments. For dosimetric purposes, spherical U/Al particles of homogenous elemental composition and radionuclide distribution were assumed. For consistency with earlier work (Darley, 2001; Darley *et al*. 2003), the uranium content of particles was assumed to be 15% and the density to be 3.1 gcm^{-3}.

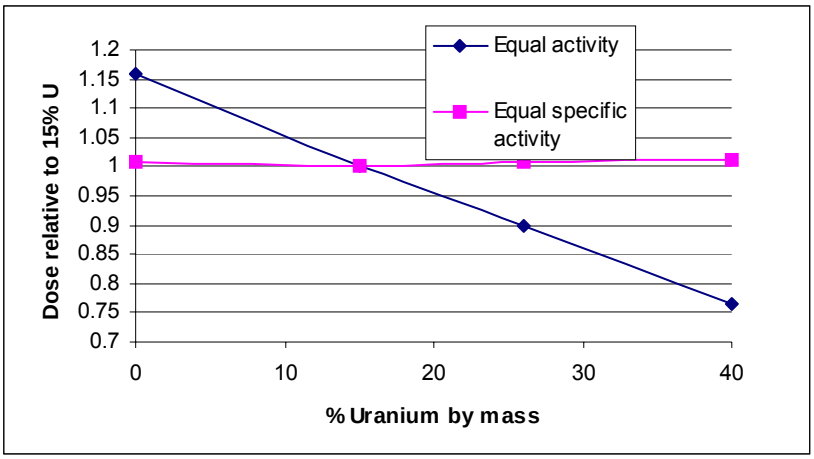

Figure 3.3. Relationship between U content of fuel fragments and ^{90}Y dose to the rectosigmoid

The precise values used for density and composition are not of critical importance, as illustrated in Figure 3.3. Considering a 3 mm particle and dominating emissions from ^{90}Y, the graph shows the effect of self-absorption on dose of variation in the %U content of the particle, normalised to 15%. Assuming that the specific activity is constant then the dose is practically independent of U content because of a trade-off between activity and self-absorption.

Doses have been calculated for ^{137}Cs and $^{90}Sr/^{90}Y$, assuming a ^{137}Cs specific activity of 2 GBq g^{-1}, characteristic of the most active particles analysed, and a Sr : Cs ratio of 0.9. Much lower (< 2 MBq g^{-1}) specific activities of ^{134}Cs and ^{106}Ru have not been included. Doses from alpha-emitting nuclides to the target layer at a depth of 280 – 300 μm will be zero (see Section 3.2.2). Initial beta spectra for ^{90}Sr, ^{90}Y and ^{137}Cs were taken from ICRU report 56 (1997); conversion electron and x and γ energies and abundances were as given in National Nuclear Data Centre NUDAT database (2000). Caesium-137 emits a combination of beta spectra (end-point energy 1.175 Mev), conversion electrons and

photons, while ^{90}Sr and ^{90}Y decay solely by beta emission with end-point energies of 0.546 MeV and 2.281 MeV, respectively.

3.6.2 Estimates of dose rate coefficients for the colon

Dose-rate coefficients (Gy h^{-1} Bq^{-1}) for the rectosigmoid wall were computed for fragments of various diameters located at a range of positions within the lumen, considering internal diameters of the rectosigmoid corresponding to adults and one year old children (see Table 3.4). Figure 3.4 shows the variation in dose rate to the adult rectosigmoid with fragment position, for the contributing radionuclides and the smallest and largest particles from the range considered. Figure 3.5 shows the corresponding graph for the one year old. Each point represents a single MCNP run with one million histories for electron emitters (^{90}Sr, ^{90}Y, ^{137}Cs beta) and ten million for photons (^{137}Cs photon). Only results complying with the MCNP 'reliable' category of precision are included based on a relative error of less than 0.1; results omitted on this criteria make no contribution to expectation dose because of their remoteness from the wall.

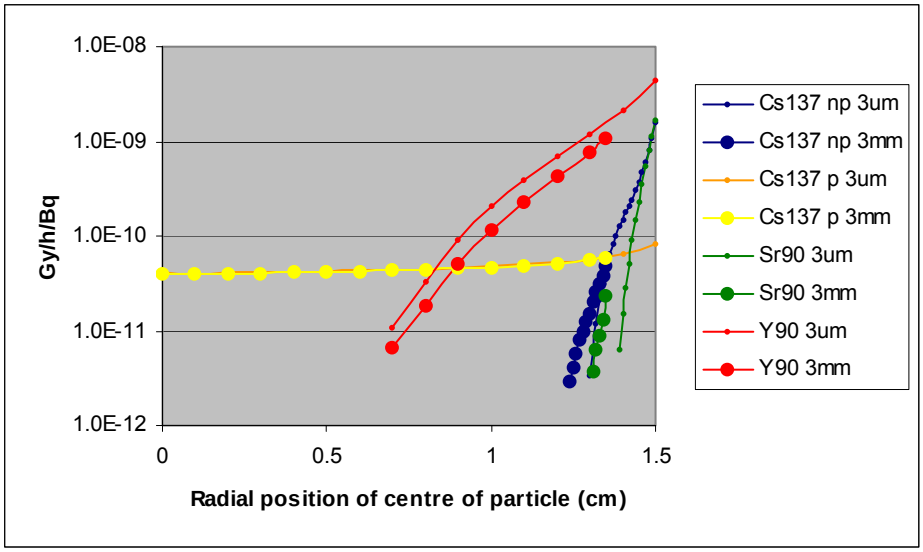

Figure 3.4. Dose rate coefficients for the adult male rectosigmoid for 3 μm (small circles) and 3 mm (large circles) diameter MTR fuel fragments. Radial position of fragment is measured from the axis of the lumen (3 cm diameter). Penetrating (photon) and non-penetrating (beta) components of ^{137}Cs emissions are designated p and np, respectively.

Figures 3.4 and 3.5 illustrate the insensitivity of ^{137}Cs photon dose to the position of the particle in the lumen, while the dose from non-penetrating radiations depends critically on distance from the wall, particularly for weak beta emissions from ^{90}Sr and ^{137}Cs. These calculations show that ^{90}Y contributions will dominate dose rate coefficients (Gy h^{-1} Bq^{-1}) averaged over all possible fragment positions within the lumen.

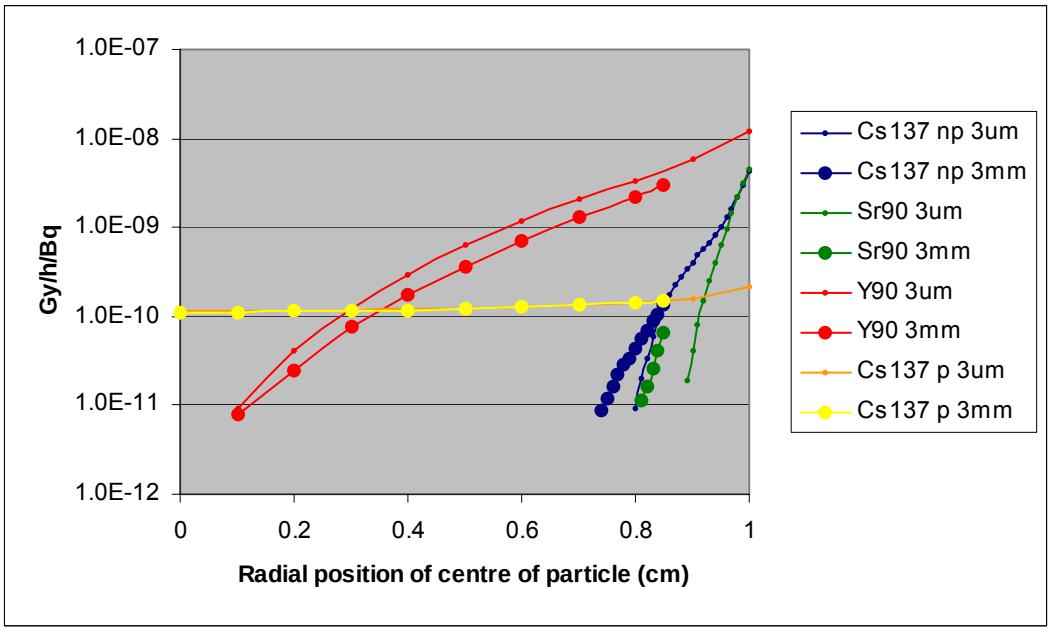

Figure 3.5. Dose rate coefficients for the one year old rectosigmoid for 3 μm (small circles) and 3mm (large circles) diameter MTR fission fragments. Radial position of fragment is measured from the axis of the lumen (2 cm diameter). Penetrating (photon) and non-penetrating (beta) components of ^{137}Cs emissions are designated p and np, respectively.

Particles in transit through the large intestine are unlikely to maintain a fixed radial position but can be expected to be randomly situated as they progress. In this case the probability of the fragment occupying a certain radial position R_p is proportional to R_p and the expectation value of the dose-rate coefficient <D> may be obtained by numerical integration of the predicted radial variation $D(R_p)$. Thus:

$$< D >= \int_0^{R_L - R} R_p D(R_p) dR_p \Big/ \int_0^{R_L - R} R_P dR_P$$

where R_L and R are the radius of the lumen and fragment respectively.

Assuming random movement throughout the lumen of the rectosigmoid, expectation dose rate coefficients as a function of particle size were calculated for each radionuclide and four fragment diameters (3 μm, 30 μm, 300 μm and 3mm), for the adult male and one year old child as shown in Figures 3.6 and 3.7.

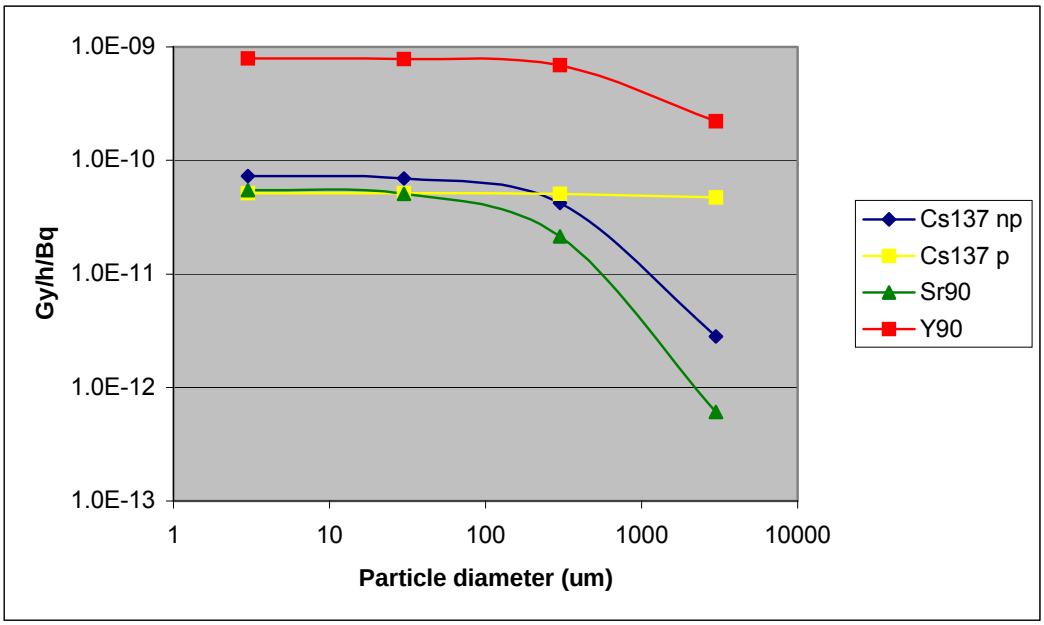

Figure 3.6. Expectation dose rate coefficients for the rectosigmoid of the adult male as a function of particle size. Penetrating (photon) and non-penetrating (beta) components of ^{137}Cs emissions are designated p and np, respectively.

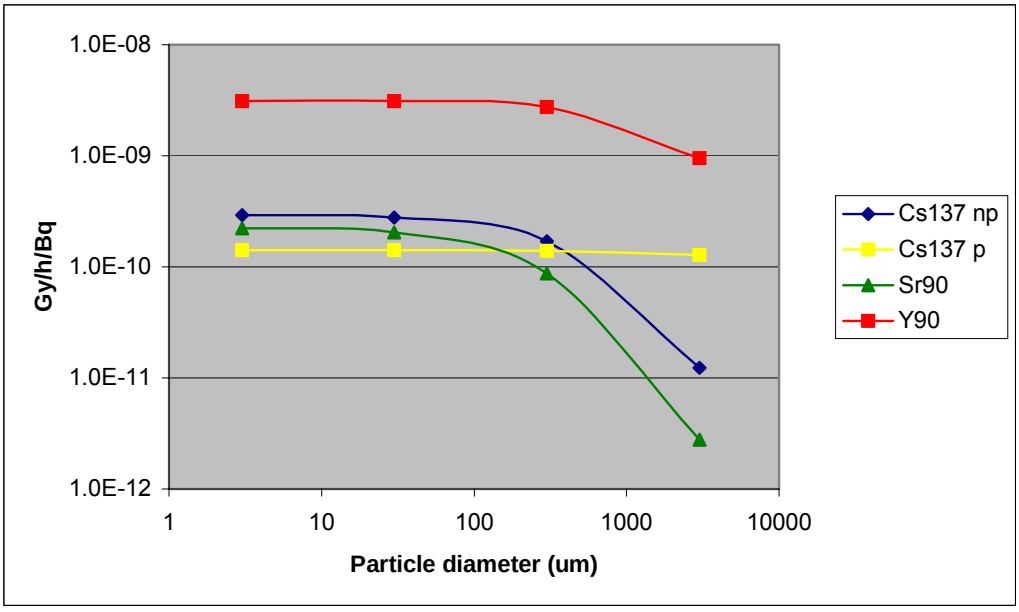

Figure 3.7. Expectation dose rate coefficients for the rectosigmoid of the one year old child as a function of particle size. Penetrating (photon) and non-penetrating (beta) components of ^{137}Cs emissions are designated p and np, respectively.

3.6.3 Estimates of colon doses

Using the dose rate coefficients discussed in the previous section, doses to the rectosigmoid were calculated for particles with ^{137}Cs activities ranging from 10^3 to 10^8 Bq, giving expectation values corresponding to random movement through the lumen and maximum values for particles remaining in contact with the wall during their transit. The results in Table 3.15 show that for the highest activity particles, the expectation doses are about 0.3 – 0.4 Gy for adults and 1 Gy in one year old children. The maximum estimated doses for a particle moving in contact with the wall, assuming standard transit times and other standard model parameter values, are about 1 – 2 Gy in adults and 4 Gy in one year old children. Estimated doses for particles with a ^{137}Cs activity of 10^5 Bq, typical of the highest activity particles found at Sandside Bay, are less than 10 mGy in adults and 20 mGy in one year old children. The relationships between particle activity and expectation doses are shown in Figure 3.8.

Table 3.15. Estimated doses to the rectosigmoid, mGy

Particle activity, Bq ^{137}Cs*	Particle diameter, μm†	Adult male		Adult female		One year old child	
		Random transit‡	Maximum§	Random transit	Maximum	Random transit	Maximum
10^3	67	0.01	0.08	0.01	0.1	0.04	0.2
10^4	150	0.1	0.7	0.1	1	0.4	2
10^5	310	0.9	6	1	8	3	16
10^6	680	7	40	10	60	27	110
10^7	1300	46	230	67	340	185	640
10^8	3100	290	1200	420	1800	1200	3500

*With ^{90}Sr/^{90}Y:^{137}Cs ratio of 0.9.

†Assuming a specific activity of 2 GBq ^{137}Cs g^{-1}.

‡Expectation value of dose based on random movement through the lumen.

§Dose for movement of particle immediately adjacent to the mucosal lining.

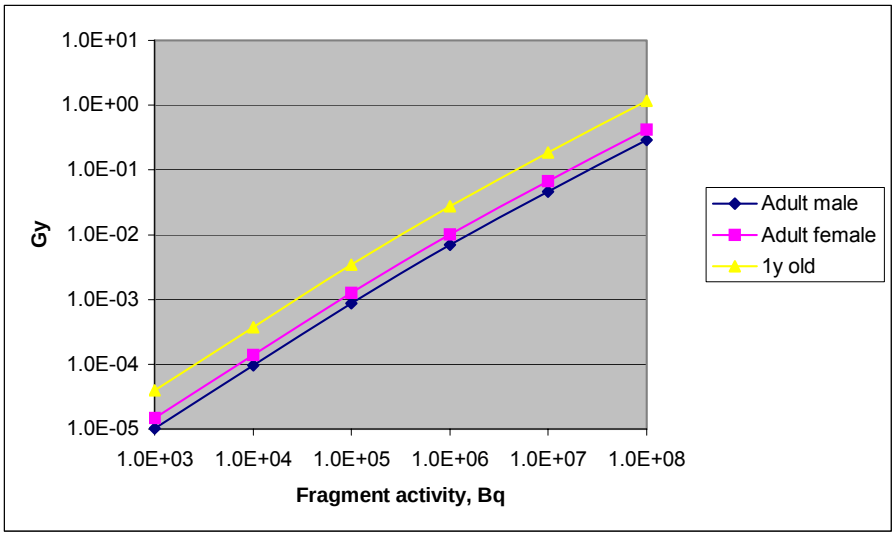

Figure 3.8. Relationship between particle ^{137}Cs activity and expectation dose for a particle moving randomly through the rectosigmoid.

3.6.4 Effect of assumed target cell depth

The dose estimates presented above relate to standard target cell assumptions in the new ICRP model (Section 3.2). That is, the targets for both cancer induction and acute effects are assumed to be the stem cells, which in the case of the large intestine are situated at the base of the crypts (Section 3.3). On the basis of measurements on human tissue (Potten, 2003), the depth of the cells are taken to be 280 – 300 μm from the lumenal surface. These measurements for adults were assumed to also apply to children, although there is evidence from comparisons for the small intestine that crypt depths may be greater in children (Stenling *et al*. 1984; Penna *et al*. 1981).

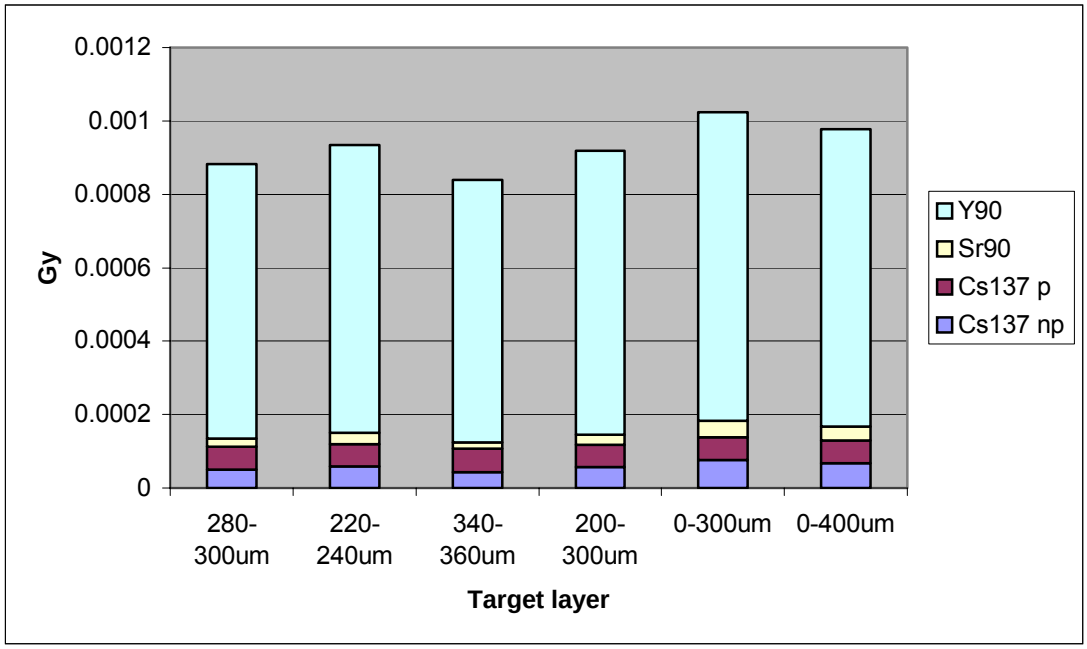

Figure 3.9. Expectation dose to the rectosigmoid of an adult male from a 10^5 Bq ^{137}Cs particle as a function of target assumptions.

Figures 3.9 and 3.10 show the effect of different assumptions regarding target depth on expectation and maximum doses to adult males from a 10^5 Bq ^{137}Cs particle (300 μm diameter) and Figures 3.11 and 3.12 make the corresponding comparisons for a 10^8 Bq ^{137}Cs particle (3mm diameter). Maximum dose refers here, as in the previous section, to a particle moving through the rectosigmoid in contact with the epithelial lining. In each case, the dose for the standard assumption of a target depth of 280 – 300 μm is shown together with doses that take account of uncertainty in crypt depth (220-240 μm and 340-360 μm) and allow for a wider target. A target width of 200 – 300 μm allows for the possibility that daughter cells may be recruited into the stem cell pool after acute damage (Roberts *et al*. 1995; Cai *et al*. 1997). Including all tissue to a depth of 300 μm is an extreme assumption that all epithelial cells may be capable of repopulating the epithelial layer and widening the target to 400 μm allows for the inclusion of other cell / tissue types, such as endothelial linings of blood vessels (see 3.3).

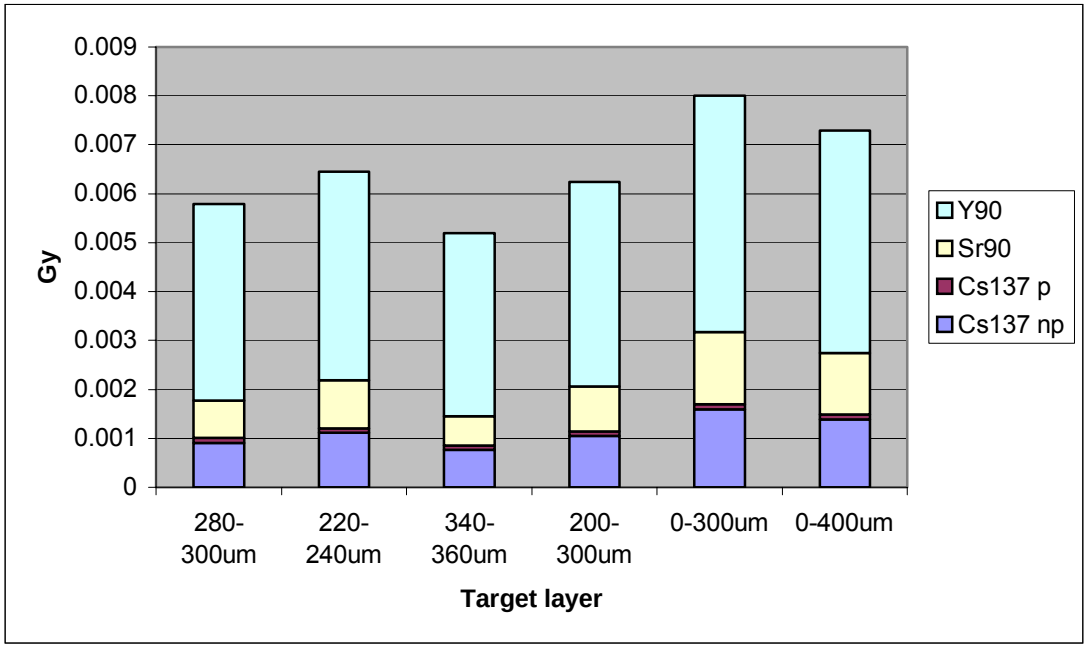

Figure 3.10. Maximum dose to the rectosigmoid of an adult male from a 10^5 Bq ^{137}Cs particle as a function of target assumptions (particle in contact with the mucosal lining of the rectosigmoid during transit).

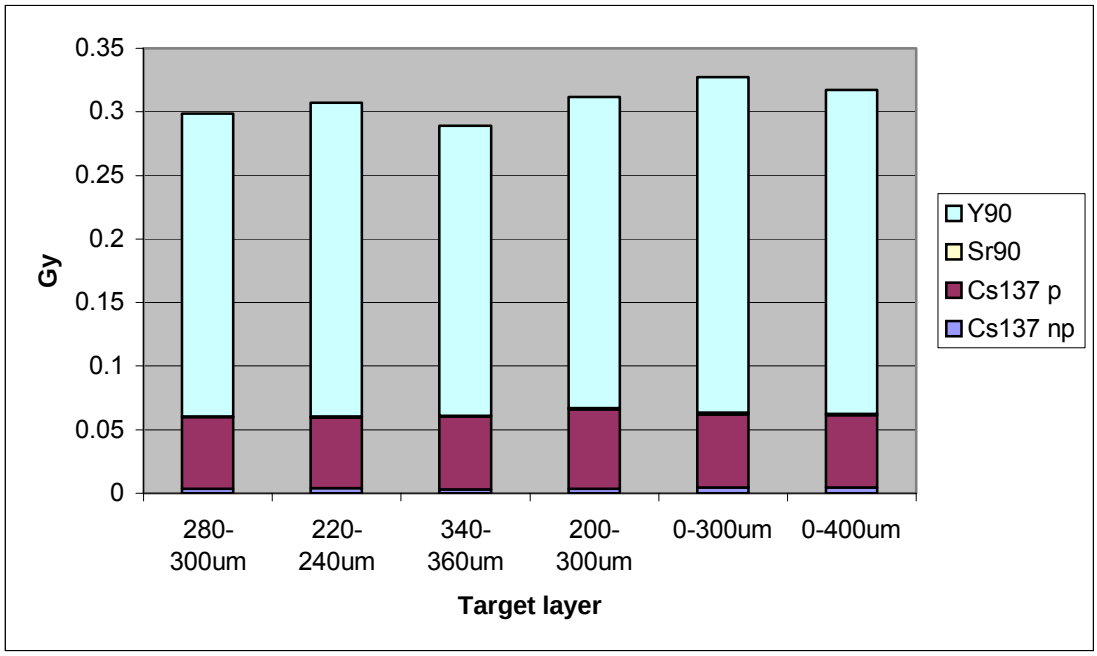

Figure 3.11. Expectation dose to the rectosigmoid of an adult male from a 10^8 Bq ^{137}Cs particle as a function of target assumptions.

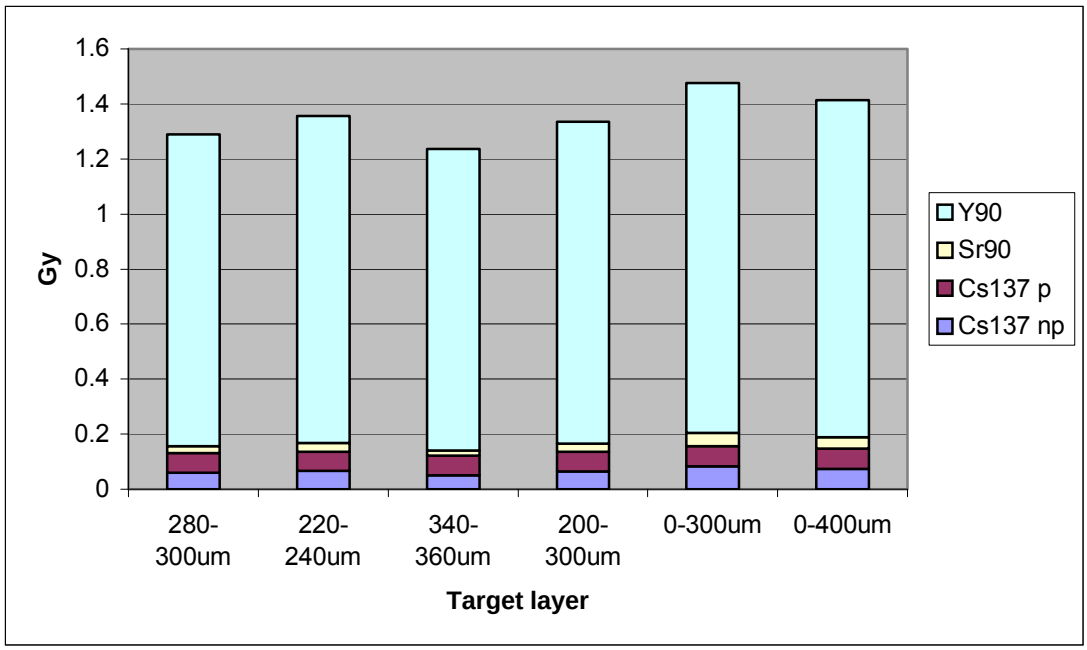

Figure 3.12. Maximum dose to the rectosigmoid of an adult male from a 10^8 Bq ^{137}Cs particle as a function of target assumptions (particle in contact with the mucosal lining of the rectosigmoid during transit).

As can be seen from Figures 3.9 – 3.12, doses from a 10^5 Bq ^{137}Cs particle are more sensitive to the effect of target assumptions than are doses from a 10^8 Bq ^{137}Cs particle. This is because the smaller size of the 10^5 Bq particles allows greater emission of low energy electrons resulting in greater sensitivity to target depth. As might be expected, maximum doses (for particles adjacent to the wall) are most sensitive to target cell assumptions. The observed variation in expectation doses resulting from these different target cell assumptions is 22% for 10^5 Bq particles and 13% for 10^8 particles, and the corresponding variations in maximum doses are 54% and 19%, respectively.

3.6.5 Effect of colon dimensions

The dose estimates presented above relate to standard assumptions regarding the length and internal diameter of the rectosigmoid in children and adult males and females. For the example of doses to the rectosigmoid of adult males from a 10^8 Bq ^{137}Cs particle, a change from the standard assumption of an internal diameter of 3 - 4 cm would decrease the expectation dose from 290 mSv by a factor of 1.5 to 190 mSv while a decrease in diameter to 2 cm would increase the dose by a factor of 2.2 to 640 mSv.

Changes in the assumed length of the rectosigmoid will result in corresponding changes in dose estimates: that is, a 10% increase in length will decrease the dose proportionately by increasing the mass of target tissue.

3.6.6 Effect of transit time

The dose estimates presented above relate to standard rectosigmoid transit times of 12 hours in adult males and in children and 16 hours in adult females. In each case, rectosigmoid transit times are taken to be one-third of the total colonic transit time (see Table 3.1). Reported central values for colonic transit are in the range 17 – 68 hours, with children tending to have shorter transit times and adult females having the longest transit times (Fallingborg *et al*. 1989, 1990; Bouchoucha and Thomas, 2000; Arhan *et al*. 1981; Rao *et al*. 1987). Values reported separately for the rectosigmoid colon show ranges in mean values of 9 – 14 hours for adult males and 12 – 22 hours for adult females (Metcalf *et al*. 1987; Bouchoucha and Thomas, 2000; Klauser *et al*. 1990).

Transit through the colon may be altered substantially by constipation or diarrhoea. For example, mean colonic transit times of 17.5 h and 118 h were determined for subjects with diarrhoea and constipation, respectively, but no significant difference in gastric emptying or small intestine transit was found between the two groups (Waller, 1975). The colonic transit time was prolonged in subjects with functional constipation (median, 50 h) but not in subjects with irritable bowel syndrome (median, 34 h), compared with control subjects (29 h) (Evans *et al*. 1998). In 13 adolescents with functional constipation, the estimated mean colonic transit time was 58 h, with segmental times of 16 h for the right colon, 15 h for the left colon, and 17 h for the rectosigmoid (Zaslavsky *et al*. 1998). In 7 children with constipation and abnormal morphology of the colon (dolichocolon), the estimated mean transit time was 114 h for the total colon, 40 h for the right colon, 43 h for the left colon, and 31 h for the rectosigmoid (Vattimo *et al*. 1993). Fourteen children with constipation secondary to myelomeningocele had a mean colon transit time of 60 h, with segmental times of 16 h for the right colon, 19 h for the left, and 25 h for the rectosigmoid (Bautista Casasnovas *et al*. 1991).

Slow-transit constipation occurs most frequently in women and is associated with markedly slowed transit in all colonic segments (Benninga *et al*. 1996). A mean colonic transit time of 120 h was determined in 11 women with slow-transit constipation (Ferrara *et al*. 1994). In 24 children with slow-transit constipation, the estimated median colonic transit time was 189 h (range, 104-384 h) (Benninga *et al*. 1996). Idiopathic slow transit constipation is a condition in which patients have varying sites and degrees of delayed intestinal transit (MacDonald *et al.* 1997). In 30 young patients with idiopathic constipation, the estimated mean colonic transit time was 61.4 h, with major delays occurring in the left colon and rectosigmoid (mean, 46 h) (Kolster *et al*. 1991).

The transit time through the colon may be altered substantially by drugs. For example, Senokot^{TM} may decrease colonic transit time by a factor of two or more, and conversely codeine or loperamide may increase transit time by a factor of two or more (Stephen *et al*. 1987). Administration of ondansetron appeared to increase the transit time of material through the left colon and rectosigmoid colon but not the right colon (Talley *et al*. 1990).

Doses to the rectosigmoid from fuel fragments in transit will be directly proportional to the assumed transit time. On the basis of the available data on transit times in constipated individuals, summarised above, it is clear that doses may typically be increased by factors of up to 2 – 3 but in extreme cases may be increased by factors of up to ten. For a 10^5 Bq ^{137}Cs particle, the data suggest that the maximum possible

doses to the rectosigmoid as a result of slow transit will be less than 100 mGy in adults and less than 200 mGy in one year old children. For a 10^8 Bq ^{137}Cs particle, doses might be increased by constipation to 1 – 5 Gy in adults and 2 – 10 Gy in one year old children. These estimates take account of slowed transit and the possibility that a particle might remain in contact with the wall of the colon throughout transit. A factor of ten increase in transit time would increase estimated doses from a 10^8 Bq ^{137}Cs particle to 3 – 4 Gy in adults and around 10 Gy in young children. The maximum possible dose estimates, the product of extreme assumptions of a ten-fold increase in transit time for a 10^8 Bq ^{137}Cs particle remaining in contact with the wall throughout transit, are about 10 – 20 Gy in adults and 35 Gy in young children.

An additional and potentially more important consideration is that the flow of material through the colon is highly variable. Movement in the rectosigmoid in particular does not occur as a constant flow but rather as mass movements resulting from periodic contractions between longer periods of quiescence. Local doses within the rectosigmoid may therefore be substantially greater than the average dose within the region. The dose to 1 cm^2 of tissue can be estimated from the results of calculations of dose to the skin to a depth of 400 μm, presented in Chapter 2 (see Section 2.4). Thus, for example, 10^5 Bq and 10^8 Bq particles held stationary against the lumenal wall of the rectosigmoid for 6 hours would deliver a dose to 1 cm^2 of tissue of about 0.6 Gy and 240 Gy, respectively.

3.6.7 Effect of ^{90}Sr : ^{137}Cs ratios, particle specific activity and comparison with doses from particles containing ^{60}Co

Doses have been calculated on the basis of a ^{90}Sr/^{90}Y : ^{137}Cs ratio of 0.9 (see Section 3.5). As shown in Table 3.14, this is typical of MTR particles, with values ranging from about 0.5 to 2. For the example of dose to the rectosigmoid of an adult male from a 10^8 Bq ^{137}Cs particle, changing the ratio to 0.5 would decrease expectation and maximum doses by factors of about 1.5 to about 190 mSv and 750 mSv, respectively, and changing to 2 would increase the dose by factors of about 2 to 570 mSv and 2600 mSv, respectively.

DFR particles generally contain a smaller proportion of ^{90}Sr/^{90}Y so that calculations performed for MTR particles will be conservative when applied to DFR particles.

All calculations have assumed a particle specific activity of 2 GBq ^{137}Cs g^{-1}, based on a range of 1 – 3 GBq g^{-1}. An increase to 3 GBq g^{-1}, with standard assumptions for the ^{90}Sr/^{90}Y : ^{137}Cs ratio, would increase the expectation and maximum doses to the rectosigmoid of an adult male for a 10^8 Bq ^{137}Cs particle by between about 10 and 20%, to 320 mSv and 1400 mSv, respectively.

Doses from ^{60}Co have been calculated using the ICRP HAT model as described in section 3.2. Since there have been few particles found containing significant activities of ^{60}Co, and because the emissions of ^{60}Co are dominated by energetic photons, the rigorous method using MCNP described in Section 3.6.1 for electron-emitters has not been applied to this radionuclide. Self-absorption within the particle has been ignored, and results for ^{60}Co are overestimates. Typically doses to the rectosigmoid per Bq ^{60}Co are about 70% of those calculated for unit activity of ^{137}Cs (together with the associated

activities of ^{90}Sr and ^{90}Y). Thus, for particles which contain only ^{60}Co (e.g. #86037, 8.5 x 10^6 Bq), doses can conservatively be taken to be approximately equal to the result for a particle of similar ^{137}Cs activity (Table 3.15).

3.7 Discussion

The estimates of colon doses, specifically rectosigmoid doses, presented in this chapter were obtained using a new ICRP model of the human alimentary tract which takes explicit account of the location of target cells within the walls of alimentary tract regions. In addition, account was taken of self-absorption of energy of radionuclide emissions within ingested particles. The methodology was as used by Darley *et al*. (2003), whereas previous estimates of colon doses by Wilkins *et al*. (1998) conservatively applied the ICRP Publication 30 (ICRP, 1979) model and took no account of self-absorption within particles. Thus, for example, Wilkins *et al*. (1998) gave an estimate of dose to the colon of an adult male following ingestion of a 10^8 Bq ^{137}Cs particle of about 7 Gy compared with a value of 0.3 Gy given in this report.

Rectosigmoid doses were calculated on the basis of the following assumptions:

spherical particles with a homogenous elemental composition of U/Al (15% U) and density 3.1 gcm^{-3}, as assumed previously (Darley *et al*. 2003);

particle specific activity of 2 GBq ^{137}Cs g^{-1}, characteristic of the most active MTR particles analysed (Darley *et al*. 2003);

particle activity ratios of 0.9 for ^{90}Sr/^{90}Y:^{137}Cs, 0.003 for ^{238}Pu:^{137}Cs, and 0.001 for ^{239}Pu:^{137}Cs and ^{241}Am:^{137}Cs, consistent with available data for MTR particles presented in this chapter (3.5);

radionuclide dissolution from particles of around 1% or less, as shown by *in vitro* and *in vivo* studies presented in this chapter (3.4), neglected for the purposes of calculating colon doses;

rectosigmoid as a uniform cylinder with internal diameter of 2 cm in one year-old children and 3 cm in adults and lengths of 21 cm in one year-old children, 35 cm in adult females and 38 cm in adult males (new ICRP model);

mean rectosigmoid transit times of 12 hours in one year-old children and adult males and 16 hours in adult females (new ICRP model); and

target cells at a depth of 280 – 300 μm from the lumenal surface.

On this basis and assuming random movement of a particle within the lumen of the rectosigmoid during transit, doses for the highest activity particles considered, 10^8 Bq ^{137}Cs, are estimated to be 0.3 – 0.4 Gy for adults and 1 Gy in one year old children. The maximum estimated doses, for a particle moving in contact with the wall, are about 1 – 2 Gy in adults and 4 Gy in one year old children. Estimated doses for particles with a ^{137}Cs activity of 10^5 Bq, typical of the highest activity particles found at Sandside Bay, are less than 10 mGy in adults and 20 mGy in one year old children.

Consideration of the possible effect on doses of changes in the assumptions made in the calculations showed that variations in transit times are of greatest importance. Doses to the rectosigmoid from fuel fragments in transit will be directly proportional to the assumed transit time. It is noteworthy that in a group of eight normal adult rats given fuel fragments by gastric intubation (Section 3.4), transit took 2.5 times longer in one rat than in the majority. On the basis of the available human data on transit times in constipated individuals, it is clear that doses may typically be increased by factors of up to 2 – 3. For 10^8 Bq ^{137}Cs particles, doses might be increased by constipation to 1 – 5 Gy in adults and 2 – 10 Gy in one year old children. These estimates take account of slowed transit and the possibility that a particle might remain in contact with the wall of the colon throughout transit. In extreme clinical conditions transit may be increased by factors of up to ten. A factor of ten increase in transit time would increase estimated doses from a 10^8 Bq ^{137}Cs particle to 3 – 4 Gy in adults and around 10 Gy in young children. The maximum possible dose estimates, the product of extreme assumptions of a ten-fold increase in transit time for a 10^8 Bq ^{137}Cs particle remaining in contact with the wall throughout transit, are about 10 – 20 Gy in adults and 35 Gy in young children. Even with such extreme asumptions, the maximum estimated doses from a 10^5 Bq ^{137}Cs particle are less than 100 mGy in adults and less than 200 mGy in young children.

The threshold dose for acute damage to the colon resulting in death, following protracted irradiation from ingested radionuclides passing through the gut, has been estimated on the basis of available animal data as 20 Gy, with an LD_{50} of 35 Gy (Section 3.3). These are average doses to the whole colon whereas the dose estimates presented in this report are for the rectosigmoid as the region receiving the greatest doses. On the basis of these data, it appears highly unlikely that ingestion of even a 10^8 Bq ^{137}Cs particle could result in death. However, the possibility, although judged to be extremely small, cannot be totally ruled out in the case of a young child. Doses from 10^5 Bq ^{137}Cs particles and intermediate activity particles (10^6 and 10^7 Bq) can be regarded as below the threshold for lethality resulting from damage to the colon.

An additional consideration is that the flow of material through the colon is highly variable. Movement in the rectosigmoid in particular does not occur as a constant flow but rather as mass movements resulting from periodic contractions between longer periods of quiescence. Local doses within the rectosigmoid may therefore be substantially greater than the average dose within the region. The dose to 1 cm^2 of tissue can be estimated from the results of calculations of dose to the skin to a depth of 400 μm, presented in Chapter 2 (see Section 2.4). Thus, for example, 10^5 Bq and 10^8 Bq particles held stationary against the lumenal wall of the rectosigmoid for 6 hours would deliver a dose to 1 cm^2 of tissue of about 0.6 Gy and 240 Gy, respectively. By analogy with effects observed following localised irradiation of animal skin (chapter 2), and from information on intestinal crypt survival in mice, it appears reasonable to assume that doses of 200 – 300 Gy will result in ulceration that might not be easy to repair while localised doses or below 1 Gy will result in localised crypt sterilisation that should be replaceable by regeneration of new crypts.

4 INHALATION OF FUEL FRAGMENTS

4.1 Introduction

This report is concerned mainly with the possible consequences of skin contact or ingestion of Dounreay fuel fragments. However, this chapter provides a less detailed assessment of doses and possible acute damage to the respiratory tract following the inhalation of particles. It begins with a description of the ICRP model of the human respiratory tract (ICRP, 1994a). This is followed in Section 4.3 by a brief summary of information on cells at risk for acute effects and cancer induction and dose – response data on acute effects following irradiation of the lung. Sections 4.4 provides estimates of the probability of particles of different sizes depositing in the extrathoracic airways and in regions of the lungs, and the possible consequences of the resulting doses.

4.2 Respiratory tract model

The ICRP Human Respiratory Tract Model (HRTM) has been used, with certain modifications, to calculate doses to the regions of the respiratory tract from inhaled fuel fragments. The model is described in full in ICRP Publication 66 (ICRP, 1994a) and is summarised in ICRP Publications 68 (ICRP 1994b) and 71 (ICRP 1995). A brief summary of the main features of the model is given here.

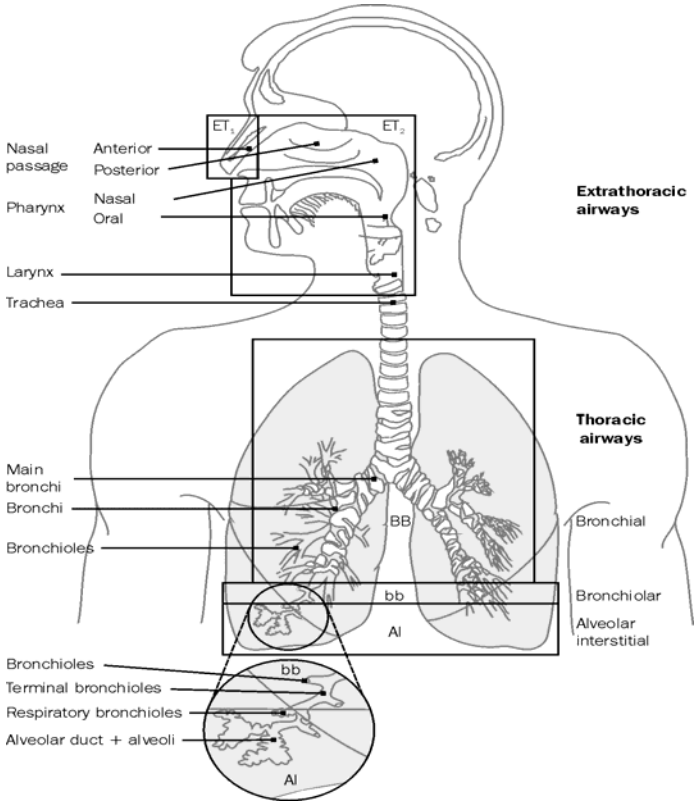

Figure 4.1. The ICRP Human Respiratory Tract Model (HRTM).

In the HRTM, the respiratory tract is represented by five regions (Figure 4.1). The extrathoracic (ET) airways are divided into ET_1, the anterior nasal passage, and ET_2, which consists of the posterior nasal and oral passages, the pharynx and larynx. The thoracic regions are the bronchial airways (BB: trachea, generation 0 and bronchi, generations 1-8), bronchiolar airways (bb: airway generations 9-15), and the alveolar-interstitial region (AI: the gas exchange region). Lymphatic tissue is associated with the extrathoracic and thoracic airways (LN_{ET} and LN_{TH} respectively).

The model is able to calculate doses per unit exposure to radionuclides in air as well as doses per unit intake (dose coefficients). Intake depends on ventilation, the product of the breathing frequency and tidal volume of the lungs, with comprehensive data available for children as well as male and female adults. Four levels of exercise are considered in the model: sleep, sitting, light exercise and heavy exercise; habit survey data are available for the proportion of time spent in each as a function of age and sex. These parameters are used to determine intake and are also used with the deposition model to determine regional deposition.

Deposition is calculated for each region of the respiratory tract taking account of both inhalation and exhalation. This is done as a function of particle size, density and shape, breathing parameters and/or work load, according to the age and sex of the subject. Deposition parameters for a particle size range of 0.006 μm AMTD* to 100 μm AMAD**. Default deposition parameters for individuals are given based on average daily patterns of activity.

Table 4.1 shows values for the regional deposition of aerosols in a reference adult male nose-breather engaged in light work, considering default aerosol sizes for environmental exposure (AMAD of 1 μm) and occupational exposure (AMAD of 5 μm). In general, deposition in the ET region increases for larger particles and, conversely, smaller particles are more able to reach the AI region.

Table 4.1. Deposition of inhaled aerosols in reference adult males, %

Region	AMAD 1 μm	AMAD 5 μm
ET_1	18	35
ET_2	23	41
BB	1.3	1.8
Bb	1.5	0.9
AI	9.9	4.5
Total	52	83

The model describes three clearance pathways. Material deposited in ET_1 (the front of the nose) is removed by extrinsic means such as nose-blowing. In other regions

*AMTD = Activity Median Thermodynamic Diameter, and

**AMAD = Activity Median Aerodynamic Diameter, are descriptions of the range of particle sizes in an aerosol. Thermodynamic processes dominate in determining particle description for small sizes (<0.5 μm) while aerodynamic processes (gravitational sedimentation, inertial impaction) dominate at larger sizes.

clearance is competitive between particle transport to the alimentary tract and lymphatics, and absorption into blood. Particle transport to the alimentary tract occurs by mucociliary clearance. It is assumed that particle transport rates are the same for all materials. Absorption to blood is material specific and is assumed to occur at the same rate in all regions except ET_1, where none occurs. Fractional clearance rates vary with time, but to facilitate calculations clearance is represented by combinations of compartments that clear at constant rates. It is assumed by ICRP and in this report that clearance rates by both processes are independent of age and gender.

The clearance rate constants (d^{-1}) shown in Figure 4.2 are reference values which, where possible, were derived from human studies, since particle transport rates are known to vary greatly between mammalian species. It is assumed that the AI deposit is divided between AI_1, AI_2 and AI_3 in the ratio 0.3:0.6:0.1 (half-times of about 30d, 700d and 7000d). The fraction of the deposit in bb and BB which moves slowly (bb_2 and BB_2) is particle size dependent (up to 50% for <2.5 μm) with 0.7% retained in the walls (bb_{seq} and BB_{seq}). A small fraction is retained in the wall in the ET_2 region (ETseq) and the rest is cleared rapidly to the GI tract. Simultaneous absorption to blood occurs as a competing process in all compartments except ET_1.

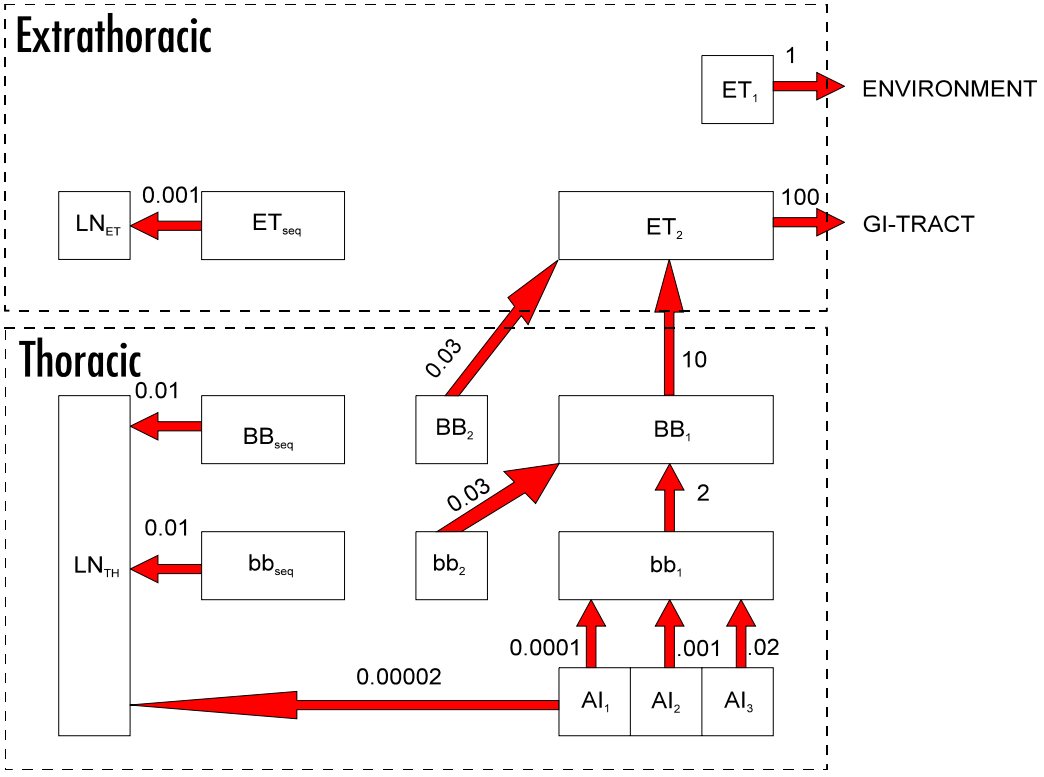

Figure 4.2. Compartment model for particle transport in the ICRP HRTM, showing clearance rate constants.

Absorption to blood depends on the chemical nature of the element and the chemical form deposited but is taken to be independent of deposition site (with the exception of ET_1). The model allows for changes in dissolution and absorption to blood with time. The use of material specific dissolution rates is encouraged but defaults are given.

These are type F (fast), M (medium) and S (slow) which, expressed as approximate half-times for one or two components of clearance, correspond to: Type F - 10 min (100%); Type M - 10 min (10%), 140d (90%); Type S - 10 min (0.1%), 7000d (99.9%). Maximum amounts reaching blood from the respiratory tract for the example of 1 μm AMAD aerosol can be calculated as 24% (F), 9% (M) and 1% (S) of the total inhaled. In each case, a further fraction of the inhaled material will reach blood by absorption from the gut after mechanical clearance and swallowing.

Doses are calculated separately for the ET1, ET2, BB, bb and AI regions of the HRTM. For ET_1, ET_2, BB and bb, the calculation of doses from non-penetrating radiations takes account of the assumed location of target cells in each region, as in the new ICRP model of the human alimentary tract (see Chapter 3). Thus, for example, the depth of the target in ET2 is taken to be a 10 μm layer of basal cells in the stratified squamous epithelium of the oropharynx and larynx at a depth of 40 μm (ICRP, 1994a). In the AI region, the interalveolar septa and the walls of blood and lymphatic vessels are sufficiently thin to ensure that target cells are distributed homogenously throughout the tissue mass. Therefore, it is assumed that the average dose received by the target cells is the same as that received by the whole tissue mass.

In the calculation of lung equivalent doses for the purposes of cancer risk estimation and the calculation of effective doses (see Chapter 5), regional doses to the BB, bb and AI are given equal weightings and added (ICRP, 1994a). Doses to ET regions are considered separately but are not important sites of radiation-induced cancer.

4.3 Radiation effects

4.3.1 Target cells for acute damage and cancer induction

The specification of target regions in the HRTM (ICRP, 1994a) was based on the assumed locations of cells considered likely to be sensitive to radiation-induced cancer. In both ET regions, the target is taken to be a 10 μm layer at a depth of 40 μm. For the BB region, the target is considered to include both columnar secretory and basal cells, in a 50 μm layer at a depth of 10 μm. The target secretory cells in the bb region are taken to form an 8 μm layer at a depth of 4 μm. As mentioned above, the AI region is treated as an homogenous mass of tissue with uniform distribution of dose and sensitive cells.

The targets for acute damage will include other cell types in addition to those considered in relation to cancer induction, including mesenchymal cells lineages in connective tissue and endothelial cells lining blood vessels. In considering gross lung damage, which relates largely to dose to the alveolar interstitial region that comprises the bulk of the tissue of the lung, the use of average dose will take account of dose to all cell types. For the ET, BB and bb regions, the doses calculated on the basis of standard HTRM assumptions may be an overestimate when considering the broader target relevant to acute effects. However, local doses from larger particles held stationary in the ET region have been based on skin dose estimates, considering a depth of 400 μm, as done for colon doses (see 3.6.6).

4.3.2 Doses causing acute effects

Damage to the lungs following exposure to high doses of radiation show two phases of damage: early pneumonitis and oedema starting within a few weeks of exposure and long-term changes including the development of fibrosis and the loss of alveoli which are replaced by collagen and connective tissue to form a scar. Such changes can result in impaired lung function and may lead to death at high doses. The overall response of the lung to radiation depends on both the dose and dose rate.

Human data from studies of patients treated with acute external irradiation for breast or lung tumours and other conditions have been interpreted as suggesting an LD_{50} of 10 Gy, with a threshold of about 5 Gy (Philips and Margolis, 1972; Van Dyk *et al*. 1981; Scott and Hahn, 1985; NRPB, 1996). Most information on the effect of dose rate comes from animal studies. Acute effects in animals have been studied after intratracheal injection of ^{144}Ce chloride (Cember and Stemmer, 1964) and inhalation of ^{144}Ce dioxide (Stuart *et al*. 1964; Thomas *et al*. 1972) and ^{90}Y in fused clay particles (Hobbs *et al*. 1977). Extensive long-term studies have been reported (McClellan *et al*. 1982) in which beagle dogs were exposed to aerosols of fused clay particles containing ^{90}Sr, ^{90}Y, ^{91}Y or ^{144}Ce to give different temporal patterns of radiation exposure. These data show that protracted irradiation of the lungs over a few weeks or a year or more are less effective in causing death from radiation pneumonitis than brief irradiation by factors of about 10 and 50, respectively. Thus, the LD_{50} for protracted irradiation over a few weeks was estimated to be about 100 Gy and the LD_0 can be taken to be similarly increased to about 50 Gy.

Measurements have also been made of the non-fatal acute effects of irradiation of the lungs. Respiratory impairment due to tissue fibrosis has been studied in dogs exposed to fused clay aerosols containing ^{90}Y or ^{144}Ce (Mauderley *et al*. 1973, 1980). On the basis of these studies, and similar studies using rats (Scott *et al*. 1988), it has been suggested that pulmonary injury can be detected at doses of about one-half to one-quarter of the LD_{50} (NRPB, 1996).

4.4 Respiratory tract doses

4.4.1 Dosimetric methodology

The ICRP HRTM considers the deposition and subsequent behaviour of inhaled aerosols of different particle sizes. As discussed above (Section 4.2), deposition in the different regions of the respiratory tract depends on particle size, shape and density, breathing rate and the tidal volume of the lungs. This report is concerned with the inhalation of single particles and thus fractional regional deposition is not meaningful. However, estimates of regional distribution can be interpreted in this application in terms of the probability of a particle depositing in the different regions.

Aerosols which contain a range of particle sizes are often described by their AMTD and AMAD (see Section 4.2), referring to median values from a distribution. Deposition of single particles of the sizes which are important in this study relates to their aerodynamic diameter (d_{ae}). This is given, approximately, by the equation:

$$d_{ae} = d_e \sqrt{\chi / \rho}$$

where ρ is the density of the particle, χ the shape factor, and d_e is the equivalent volume diameter, i.e. the diameter of the sphere which has the same volume as the particle under consideration (ICRP, 2002). Four fuel fragment particle sizes (d_e) are considered in this chapter, 3, 30, 300 µm and 3 mm, with corresponding aerodynamic diameters of 4.2, 42, 420 µm and 4.2 mm (using values of ρ and χ from Table 4.2*)*. A computer program implementation of the HRTM, LUDEP (Jarvis *et al*. 1996), has been used to calculate the probabilities of deposition given in Table 4.2.

Table 4.2 shows that the larger particles (300 µm and 3 mm) will be deposited in the extrathoracic airways before reaching the lungs, while there is a low probability that 30 µm particles will reach the upper bronchial airways. It is only for the 3 µm particles (d_{ae} of 4.2 µm) that there is a significant probability of the particle reaching the alveolar interstitial region of the lungs. It should be noted that the probability values given in Table 4.2 are calculated on the basis that the particle will be deposited and do not take account of the possibility of exhalation of smaller particles. Deposition values given by the HRTM for the inhalation of aerosols include consideration of exhalation and do not sum to 100%, as illustrated in Table 4.1.

Table 4.2. Probability of deposition in each HRTM region for four particle sizes*

	Probability (%) of deposition in region for particles of diameter:			
d_e†	3 µm	30 µm	300 µm	3 mm
d_{ae}‡	4.2 µm	42 µm	420 µm	4.2 mm
Activity§ (Bq)	<1	100	10^5	10^8
ET1	14.9	19.9	20	20
ET2	34.3	79.7	80	80
BB	16.4	0.4	0	0
Bb	8.4	0	0	0
AI	26.0	0	0	0

*Assuming breathing parameter values for an adult male undertaking light exercise while 'mouth breathing' and also assuming that the inhaled particle is deposited (see text). Note that 'mouth breathing' implies that 40% of the total volume inhaled passes through the mouth, while the remaining 60% passes through the nose.

†Equivalent diameter – as used throughout this report.

‡Aerodynamic diameter, assuming a shape factor of 1.5 (ICRP default) and density of 3.1 g cm^{-3} (typical of Dounreay particles).

§Approximate activity (Bq) of ^{137}Cs based on a specific activity of 2 GBq g^{-1}.

Standard HRTM parameter values have been used for particle clearance from the respiratory tract. Thus, loss from ET1 is assumed to occur at a rate of 1 d^{-1} and particle transport from other regions is taken to occur at the rates shown in Figure 4.2, with the exception of consideration of the possibility of sequestration of particles in ET2, BB and bb regions. In a review of available animal data, Bailey *et al*. (1997) concluded that the parameter values for long-term retention of particles applied in the HRTM to ET_2 should also be applied to retention in BB and bb regions. That is, the most appropriate interpretation of available data is that 0.05% of particles deposited in each region were

sequestered and subsequently transported to regional lymph nodes at a rate of 10^{-3} d^{-1}. Apart from questionable observations that pollen granules of 40 – 50 μm diameter may be retained in the nasal epithelium of guinea pigs (Stromme, 1955), data relating to particle sequestration in the respiratory tract derive from studies using particles in the submicron to 5 μm range (ICRP, 1994a; Bailey *et al*. 1997). Furthermore, the assumed mechanism of sequestration is uptake by macrophages and the site of accumulation is taken to be a 5-10 μm sub-epithelial layer in the lamina propria (ICRP, 1994a). In this report, it is assumed that the probability of sequestration is 0.05% for 3 μm (d_e) particles, and also conservatively for 30 μm particles, applying to deposition in ET_2, BB and bb regions. Uptake and retention of 300 μm and 3 mm particles in this way is considered here to be biologically implausible. However, the possibility that larger particles may become lodged and remain stationary in the extrathoracic airways is considered below.

The solubility of ingested Dounreay fuel fragments is low, as shown by both *in vivo* and *in vitro* studies (see Section 3.4). The results obtained suggest that dissolution within the stomach and intestine may typically account for of the order of 1% of the radionuclide content of particles. However, these data do not relate directly to solubility in lung fluids and do not allow the use of material-specific dissolution parameter values in the HRTM. The ICRP default values for Type S (slow clearance; see 4.2) materials are therefore adopted here.

As discussed above (4.3.2), acute damage to the lungs, as for other tissues, depends on the dose and dose rate. Considering a longer period allows more time for the dose to accumulate but effects decrease at lower dose rates. In a review of available data on deterministic effects in different tissues (NRPB, 1996), mathematical models were derived for the calculation of the risk of an effect occurring, taking account of dose, dose rate and dose-response functions. This methodology has been used to calculate the probability of pneumonitis and pulmonary fibrosis using dose integration periods of 1, 7 and 30 days, and 1 year, following inhalation of a particle containing ^{90}Sr and ^{90}Y. This comparison showed that an integration period of 30 days gives the highest risk of an effect for the particles of most interest and this integration period is used for the dose estimates presented here.

While self-absorption of energy within fuel fragments was calculated rigorously using MCNP methodology for the colon doses presented in Chapter 4, self-absorption for particles within the respiratory tract was estimated using ‘degraded’ beta spectra, as discussed in Chapter 5. The spectra calculated for spheres of diameters 3, 30, 300 μm and 3 mm are taken to apply to the particles of any shape which have these same equivalent volume diameters.

4.4.2 Dose estimates

Doses were calculated for each of the particle sizes (d_e = 3, 30, 300 μm and 3 mm) for deposition in each region of the HRTM (Figure 4.2) following inhalation by an adult male undertaking light exercise (see Table 4.2), giving doses to the region and doses to the AI in each case. Standard assumptions were made concerning particle composition in each case; that is, a specific activity of 2 GBq ^{137}Cs g^{-1} and a $^{90}Sr/^{90}Y$:^{137}Cs ratio of 0.9.

Doses from 3 μm particles to the AI region were less than 1 μSv in all cases. The greatest estimated doses to other regions from 3 μm particles were around 20 μGy for deposition in the BB region or sequestration in the BB or ET2 regions, each of which has a low probability of occurrence (estimated as probability of 8% for BB and <0.01% for BB_{seq} and ET_{seq}). Thus doses from 3 μm particles are considered to be insignificant and are not tabulated.

Tables 4.3 and 4.4 give dose estimates for inhaled 30 μm, 300 μm and 3 mm particles. Only doses which were estimated to have a finite probability of occurring are tabulated. The greatest AI doses are 3 mGy from 3 mm particles in the ET regions, due to photon irradiation. However, ET_1 doses were estimated as around 300 Gy for a 3 mm particle and 300 mGy for a 300 μm particle. These estimates are based on the standard HRTM assumption of a clearance half-time of one day and represent average dose to the target tissue in the region. Local doses within the ET region may be substantially greater than the average dose within the region. The dose to 1 cm^2 of tissue can be estimated from the results of calculations of dose to the skin to a depth of 400 μm, presented in Chapter 2 (see Section 2.4). Thus, for example, 300 μm (10^5 Bq) and 3 mm (10^8 Bq) particles held stationary against the ET epithelial lining for 12 hours would deliver a dose to 1 cm^2 of tissue of about 1 Gy and 500 Gy, respectively. These estimates of local dose apply to the possibility of larger particles lodging and remaining stationary at any position in the upper respiratory tract (ie, ET regions and BB).

Table 4.3. Estimated doses to the respiratory tract following inhalation of a 30 μm fuel fragment by an adult male, μGy

HRTM region	Dose to region	Dose to AI	Probability (%)*
ET1	1400	0.003	19.9
ET2	0.5	0.003	79.6
ET_{seq}	2000	0.1	0.04
BB_f	11	0.007	0.4
BB_{seq}	2500	1.5	0.0002

*Probability of deposition in each HRTM region.

Table 4.4. Estimated doses to the respiratory tract following inhalation of 300 μm and 3 mm fuel fragments by an adult male

	Dose to region		Dose to AI		
HRTM Region	300 μm	3 mm	300 μm	3 mm	Probability (%)
ET1	1 Gy	330 Gy	3 μGy	3 mGy	20
ET2	0.3 mGy	0.1 Gy	3 μGy	3 mGy	80

*Probability of deposition in each HRTM region.

Investigations using the deposition model of the HRTM as implemented in LUDEP (Jarvis *et al*. 1996) show that the maximum aerodynamic diameter (d_{ae}) particle which might penetrate to the AI region is about 20 μm (about 14 μm d_e). For the standard assumption of a specific activity of 2 GBq ^{137}Cs g^{-1}, this particle will have an activity of about 10 Bq ^{137}Cs. Estimated doses for a particle of this size and activity are of the

order of micrograys. The maximum aerodynamic diameter (d_{ae}) particle which might penetrate to the bronchial (BB) region is about 200 μm (about 140 μm d_e). Assuming a specific activity of 2 GBq ^{137}Cs g^{-1}, this particle will have an activity of about 10^4 Bq ^{137}Cs. The dose to the BB region from a particle of this size and activity is estimated as about 200 mGy, assuming standard HRTM clearance rates and integrating dose over a 30 day period (see 4.4.1). If clearance was impaired and the particle remained within the BB region, average dose to the region would increase to about 2.5 and 10 Gy over periods of 1 and 5 years, respectively. However, the probability of a particle of this aerodynamic diameter reaching the bronchial region is extremely small and the probability of retention in the region is even smaller.

4.5 Discussion

Acute effects associated with high radiation doses to the deep lung (AI region), ie. pneumonitis and pulmonary fibrosis, are extremely unlikely to occur following inhalation of a hot particle of Dounreay origin. This is because only particles of aerodynamic diameters less than about 20 μm can travel sufficiently deeply into the respiratory tract to be deposited in the AI region, and such particles are not sufficiently radioactive to produce the high doses associated with acute lung effects. Thus, the respiratory tract in effect operates a protection mechanism, whereby the particles of highest activity are prevented from reaching the deep lung (AI).

Large particles will deposit in the extrathoracic airways. Doses to the anterior nasal passages were estimated as around 300 Gy for a 3 mm particle (10^8 Bq ^{137}Cs) and 300 mGy for a 300 μm particle (10^5 Bq ^{137}Cs). These estimates are based on standard ICRP model assumptions including a clearance half-time of one day and represent average dose to the target tissue in the region. Potentially more important is the possibility of high local doses, as discussed for irradiation of the skin (chapter 2). Local doses within the ET region may be substantially greater than the average dose within the region. The dose to 1 cm^2 of tissue can be estimated from the results of calculations of dose to the skin to a depth of 400 μm. Thus, for example, 300 μm (10^5 Bq) and 3 mm (10^8 Bq) particles held stationary against the ET epithelial lining for 12 hours would deliver a dose to 1 cm^2 of tissue of about 1 Gy and 500 Gy, respectively. These estimates of local dose apply to the possibility of larger particles lodging and remaining stationary at any position in the upper respiratory tract (ie. ET regions and BB). Local doses of around 500 Gy will cause acute local ulceration; doses of around 1 Gy or less may cause only imperceptible damage.

5 EQUIVALENT AND EFFECTIVE DOSES

5.1 Introduction

The main objective of this report is to assess the possibility of acute tissue damage resulting from skin contact or ingestion of Dounreay fuel fragments, and a secondary issue was the possibility of damage to tissues of the respiratory tract following inhalation

of particles. This chapter provides estimates of dose relevant to the assessment of risks of cancer and hereditary effects, concentrating on particle ingestion but referring also to inhalation and particles on skin.

To provide a method for the interpretation of absorbed dose in different organs in terms of the total risk of cancer and hereditary effects, ICRP use the concepts of equivalent dose and effective dose (ICRP, 1991). Radiation weighting factors, w_R, take account of the relative biological effectiveness of different radiation types in causing malignancy or genetic damage. Thus, absorbed doses to organs and tissues in Gy are multiplied by a w_R of 20 for alpha irradiation and 1 for beta and gamma radiations to give equivalent doses in Sv. Tissue doses are commonly integrated over a 50 year period for adults or to age 70 years for children and the resulting values are referred to as committed equivalent doses. Tissue weighting factors are attributed to different tissues and organs, taking account of the incidence of fatal cancer and hereditary effects, weighted for the incidence of non-fatal disease and years of life lost (ICRP, 1991). The committed effective dose is then the sum of all committed equivalent doses multiplied by the appropriate tissue weighting factors. The tissue weighting factors (w_T) specified by ICRP in their 1990 recommendations (ICRP 1991) are given in Table 5.1. These are rounded values, corresponding to overall estimates of the risk of fatal cancer in the population of 0.05 Sv^{-1} and an estimate of total aggregated detriment of about 0.07 Sv^{-1}.

The use of effective dose allows the summation of doses from different radionuclides and from external sources and comparison with dose limits set on the basis of risk relating to whole body radiation exposure. The dose limit for members of the public, including children, is 1 mSv, although see the Discussion below (Section 5.5) regarding the relevance of the dose limit to possible exposure to Dounreay particles.

Table 5.1. ICRP (1991) Tissue Weighting Factors, w_T

Organ/Tissue	w_T
Skin, bone surfaces	0.01
Thyroid, Liver, Oesophagus, Breast, Bladder, Remainder	0.05
Lung, Red bone marrow, Stomach, Colon	0.12
Gonads	0.2
Total	1

Ingested or inhaled particles deliver a dose to the alimentary and respiratory tracts, as discussed in Chapters 3 and 4, and to other body organs in the case of penetrating photon radiations (gamma ray emissions). Radionuclides absorbed to blood, following ingestion or inhalation, will deposit in and irradiate other tissues, depending upon the elements concerned. The following section summarises the models used by ICRP for the systemic behaviour of Cs, Sr, Y, Co, Pu and Am. The subsequent section discusses dosimetric methodology applicable to the calculation of doses from ^{137}Cs, ^{90}Sr, ^{90}Y, ^{238}Pu, ^{239}Pu and ^{241}Am within particles in the alimentary and respiratory tract and absorbed to blood in soluble form.

5.2 Systemic biokinetic models

5.2.1 Caesium

The ICRP (1989) model assumes that absorbed Cs reaching blood is distributed uniformly throughout all body tissues; 10% is then assumed to be retained with a biological half-life of 2 days and 90% with 110 days. There is evidence that the rate of loss of Cs from the body is greater in children than adults and shorter retention times are applied in the ICRP model. Dose coefficients for ^{137}Cs are largely independent of age, the maximum difference being less than a factor of two, because the shorter biological half-times at younger ages counteract the effect of smaller body masses. For example, dose coefficients for ingestion are 1.4 x 10^{-8} Sv Bq^{-1} for adults and 1.2 x 10^{-8} Sv Bq^{-1} for one-year old children.

5.2.2 Strontium

The ICRP (1993) systemic model for strontium and related alkaline earth elements absorbed to blood is shown in Figure 5.1. It describes in detail the kinetics of alkaline earth elements in bone, which is a major site of deposition and retention, and also considers retention in soft tissues and routes of excretion. It takes account of initial uptake onto bone surfaces, transfer from surface to bone volume and recycling from bone and soft tissues to blood.

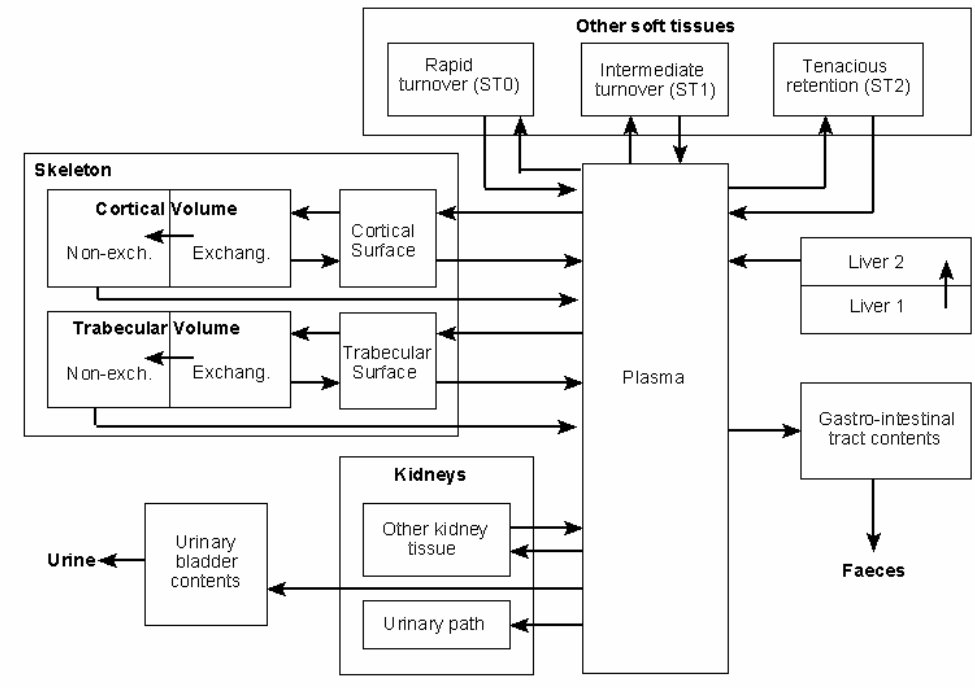

Figure 5.1. ICRP (1993) systemic model for alkaline earth elements.

There are good human and animal data indicating that early retention of the alkaline earth elements is greater in growing than in mature individuals and that much of the variation with age is due to elevated uptake by the immature skeleton. However, individuals exposed at younger ages also have a higher rate of loss of these elements from the skeleton than do mature individuals, due to a higher rate of bone turnover at younger ages. Accordingly, the most important changes in the ICRP model parameter values for intakes by children are increased initial deposition in the skeleton, relating to changes in skeletal uptake of Ca, and increased release of elements from non-exchangeable bone, proportional to the bone turnover rate.

5.2.3 Yttrium

The ICRP (1980) systemic model for Y assumes that 50% of yttrium absorbed to blood is taken up by bone, 15% by liver and 10% by other tissues, with 25% being promptly excreted. Due to the relatively short half-life of radioisotopes of yttrium, retention in these organs/tissues is taken to be indefinite. The same assumptions are taken to apply to children.

In keeping with dose calculation methods recommended by ICRP, the strontium model is applied to ^{90}Y formed in the body following intake of ^{90}Sr. This is regarded as a reasonable assumption in view of the relatively short physical half-life of ^{90}Y.

5.2.4 Cobalt

The ICRP (1993) systemic model for Co assumes that 5% of cobalt absorbed to blood is taken up by liver and 45% by other tissues, with 50% being promptly excreted. Activity is taken to be retained in tissues with half-times of 6 days (60%), 60 days (20%) and 800 days (20%) The same assumptions are taken to apply to children.

5.2.5 Actinides

The ICRP (1993) systemic model takes account of actinide deposition principally in the liver and skeleton and the recycling of elements from the skeleton and soft tissues to blood (Figure 5.2). Movement within the skeleton is modelled, taking account of burial of initial surface deposits and transfer from surfaces and bone volume to the marrow.

The main differences between Pu and the other actinides is in the parameter values used in the model for: rates of urinary and faecal excretion (eg. Pu < Am for urinary excretion); proportions deposited in the skeleton and liver; and, retention by the liver. The main age-dependent differences are greater initial uptake by the skeleton in children and more rapid loss from the skeleton in children due to greater bone turnover.

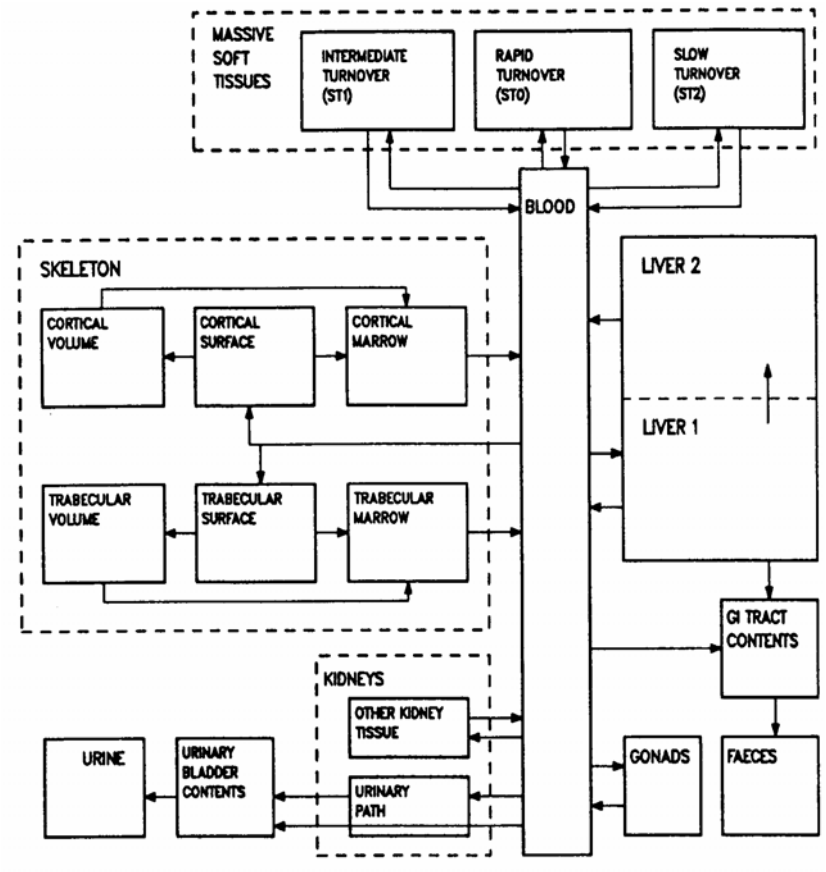

Figure 5.2. ICRP (1993) systemic model for actinide elements.

5.3 Dosimetric methodology

5.3.1 ICRP methodology

Biokinetic models for individual elements and their radioisotopes are used to calculate the total number of radioactive decays (transformations) occurring within specific tissues, organs or body regions (source regions) during a given period of time (usually to age 70y). Dosimetric models are used to calculate the deposition of energy in all important organs/tissues (targets) for each source region, taking account of the number of decays occurring in source regions and energy deposition in target regions.

Dose calculations involve the use of nuclear decay data (Eckerman *et al.* 1994; Endo *et al.* 2003, 2004) and anthropomorphic phantoms that describe geometric relationship between different tissues and organs. There are two main types of phantom – mathematical phantoms that approximate the sizes and shapes of organs mathematically (Cristy and Eckerman, 1987) and voxel phantoms that use tomographic data for real individuals obtained using computed tomography or magnetic resonance imaging (Zankl *et al*. 2002, 2003). ICRP currently uses mathematical phantoms that have been developed for adults and children of different ages (Eckerman, 1994). Voxel phantoms for a reference adult male and female are currently being developed for use by ICRP (Zankl *et al*. 2003; Fill *et al*. 2004).

Doses from “cross-fire” radiation between source and target tissues are important for penetrating photon radiation. For “non-penetrating” alpha and beta particle radiations, the general assumption is that energy will be largely deposited in the tissue in which the radionuclide is deposited and that dose can be calculated on the assumption of uniform distribution of the radionuclide and target cells. However, source and target considerations are taken into account for alpha and electron emissions in the case of doses to the walls of the alimentary and respiratory tracts from ingested and inhaled radionuclides, as discussed in Chapters 3 and 4. In addition, doses from the deposition of radionuclides in bone take account of their distribution on bone surfaces and within bone mineral and the relative position of target cells on inner bone surfaces and throughout red bone marrow. For all dose calculations, radionuclides are assumed to be uniformly distributed throughout systemic source regions, although these can be whole organs (e.g. liver) or a thin layer within a tissue (e.g. source regions within lung airways and on bone surfaces). Similarly, target cells are assumed to be uniformly distributed throughout target regions that vary in size from whole organs to layers of cells.

5.3.2 Methodology applied to Dounreay particles

For the purposes of calculating doses to all alimentary and respiratory tract regions from ingested or inhaled Dounreay fuel fragments, account was taken of self-absorption of energy within the particles using ‘degraded’ spectra. This approach was adopted because the rigorous approach applied to the calculation of doses to the skin and the rectosigmoid region of the colon (Chapters 2 and 3) would have been impossibly time-consuming and unwarranted on the basis of the level of precision required of dose estimates for other regions. Figures 5.3 – 5.5 show degraded beta spectra, computed using MCNP, for emissions from ^{90}Sr, ^{90}Y and ^{137}Cs from the surface of particles with diameters of from 3 μm to 3 mm. For particles in transit through regions of the alimentary tract, random traversal was simulated by sampling points uniformly within the interior. This method results in an overestimate of dose from larger particles when compared with the rigorous approach adopted in the calculation of colon dose in Chapter 3, since it ignores a geometrical effect which prevents close approach to the wall of most of the radioactivity contained in the larger particles. Thus, comparing expectation doses (see 3.6.3) to the rectosigmoid of an adult male from ^{90}Y for the two approaches shows that the dose estimates differ by 5% or less for particles of 300 μm diameter and smaller but indicates that the degraded spectra method overestimates dose by about 75% in the case of 3 mm diameter particles; this is acceptable in view of other uncertainties in dose calculations. The original un-degraded spectrum is used in calculating doses to systemic tissues.

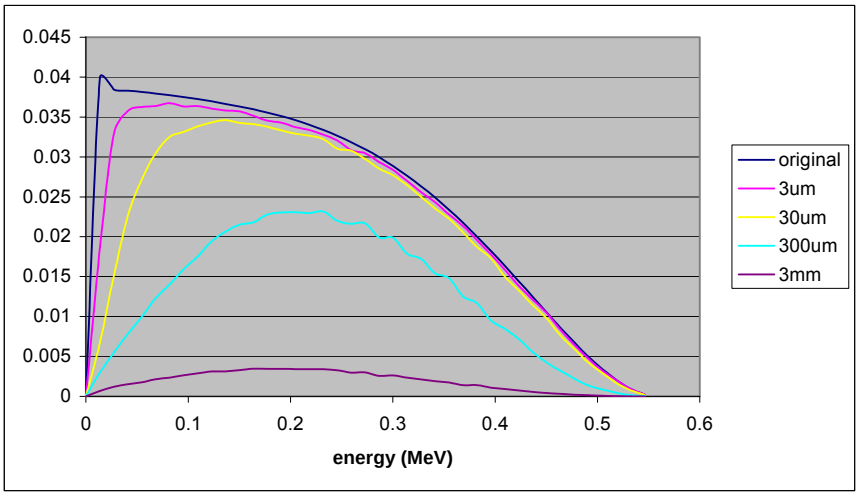

Figure 5.3. Degraded ^{90}Sr beta spectra escaping from the surface of MTR fragments of from 3μm to 3 mm diameter. The original spectrum is also shown.

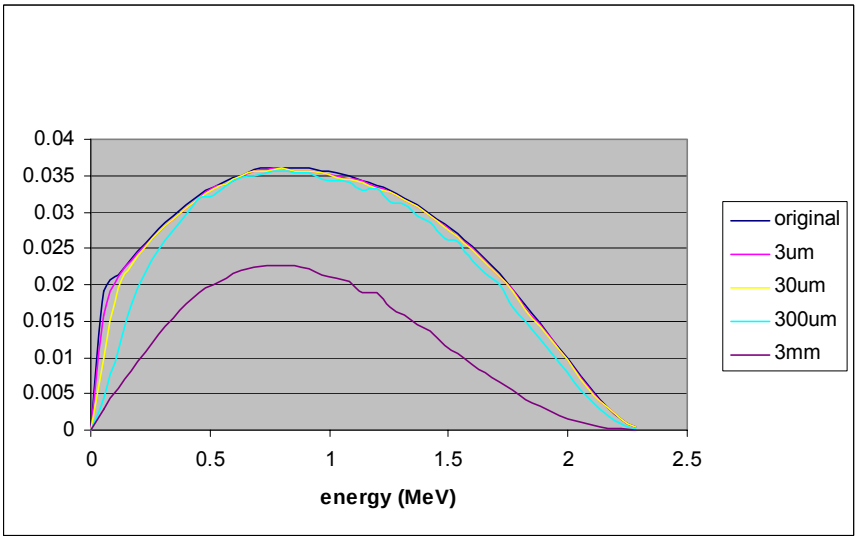

Figure 5.4. Degraded ^{90}Y beta spectra escaping from the surface of MTR fragments of from 3μm to 3 mm diameter. The original spectrum is also shown.

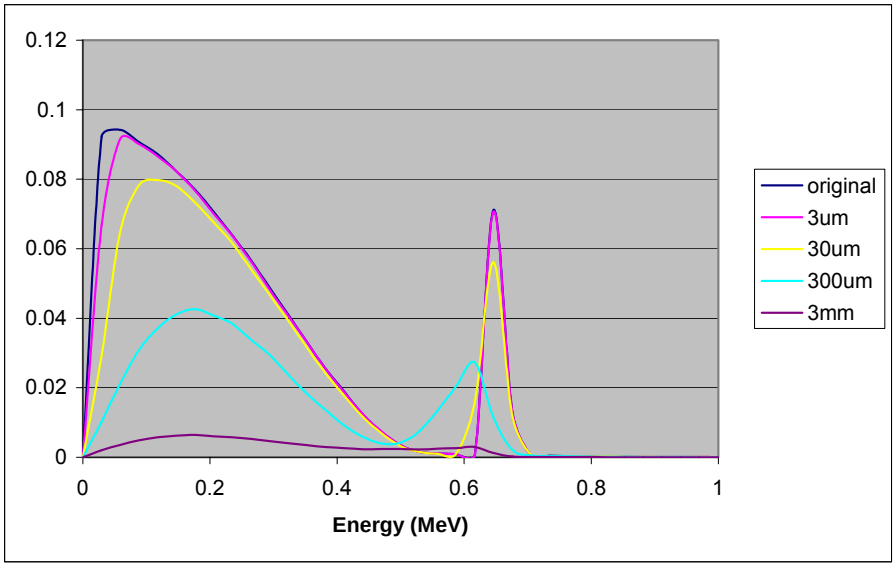

Figure 5.5. Degraded ^{137}Cs beta spectra escaping from the surface of MTR fragments of from 3μm to 3 mm diameter. The original spectrum is also shown.

The values used for the absorption of radionuclides from ingested particles were as given in section 3.4.3 for MTR particles. That is, absorption to blood as a percentage of activity in the ingested particle was assumed to be 1% for ^{137}Cs, 0.01% for ^{90}Sr and 0.001% for ^{239}Pu. The value for ^{239}Pu was taken to apply to ^{241}Am and ^{90}Y. As for the calculations in Chapters 3 and 4, the ^{90}Sr/^{90}Y:^{137}Cs ratio was taken to be 0.9. A ^{238}Pu:^{137}Cs ratio of 0.003 and ^{239}Pu:^{137}Cs and ^{241}Am:^{137}Cs ratios of 0.001 were used. Doses calculated for MTR particles on the basis of these assumptions are likely to be conservative when applied to DFR particles.

One MTR particle proved to be highly soluble in the *in vitro* dissolution study (3.4.1), suggesting that appropriate assumptions for absorption from the particle are 60% ^{137}Cs, 15% ^{90}Sr and 0.03% for the actinides and yttrium. This particle had a total activity of 8 x 10^4 Bq ^{137}Cs and a ^{90}Sr:^{137}Cs ratio of 0.5 but for the purposes of an illustrative dose calculation and comparison with other dose estimates, a particle activity of 10^5 Bq and a ^{90}Sr:^{137}Cs ratio of 0.9 have been assumed.

5.4 Estimates of equivalent and effective doses

5.4.1 Particle ingestion

Table 5.2 summarises the results of dose calculations for the examples of 10^5 and 10^8 Bq ^{137}Cs particles ingested by adult males and one year-old children. Assumptions regarding radionuclide ratios and levels of absorption to blood were those considered appropriate for MTR particles, as discussed above. The results show that estimates of committed effective doses from 10^5 Bq ^{137}Cs particles are about 0.1 mSv for an adult and 0.5 mSv for a one year-old child. The corresponding doses following ingestion of a 10^8 particle are about 80 mSv for an adult and 300 mSv for a one year-old child. In each case, the committed effective dose is dominated (>70%) by contributions from

committed equivalent doses to the alimentary tract, particularly the colon; these may be overestimated in the case of 10^8 Bq ^{137}Cs particles, as discussed above (see 5.3.2).

Table 5.2. Committed equivalent doses to organs / tissues and committed effective dose to adult males and one year-old children from the ingestion of fuel fragments, mSv[*]

	10^5 Bq ^{137}Cs particle (300 μm)		10^8 Bq ^{137}Cs particle (3mm)	
Organ/ Tissue	Adult	One year-old	Adult	One year-old
Stomach	0.22	0.94	120	460
Colon	0.61	2.4	350	1300
RBM[†]	0.03	0.06	34	57
BS[‡]	0.11	0.13	110	130
Liver	0.03	0.07	33	72
Gonads	0.08	0.31	77	310
E[§]	0.1	0.5	78	290

[*]Calculated assuming radionuclide ratios of 0.9 for ^{90}Sr/^{90}Y:^{137}Cs, 0.003 for ^{238}Pu:^{137}Cs ratio and 0.001 for ^{239}Pu:^{137}Cs and ^{241}Am:^{137}Cs. Absorption to blood was assumed to be 1% for ^{137}Cs, 0.01% for ^{90}Sr and 0.001% for ^{238}Pu, ^{239}Pu, ^{241}Am and ^{90}Y.

[†]RBM: red bone marrow.

[‡]BS: bone surfaces.

[§]E: committed effective dose.

Tables 5.3 – 5.6 show the radionuclide contributions to committed equivalent doses to organs / tissues of adult males and one year-old children after ingestion of 10^5 and 10^8 Bq ^{137}Cs particles. The combined contributions from the beta / gamma emitters, ^{137}Cs, ^{90}Sr and ^{90}Y dominate doses to all tissues except bone surfaces, for which alpha emissions from the actinide isotopes contribute 60 – 70% of the committed equivalent dose.

Table 5.3. Radionuclide contributions to committed equivalent doses to organs / tissues of an adult male after ingestion of a 10^5 Bq ^{137}Cs particle, μSv[*]

Organ/ tissue	^{137}Cs	^{90}Sr	^{90}Y	Total βγ	^{238}Pu	^{239}Pu	^{241}Am	Total α
Stomach	58	15	140	220	0.08	0.03	0.03	0.1
Colon	170	140	310	610	0.08	0.03	0.03	0.1
RBM[†]	25	5	0.003	30	2	0.8	0.6	4
BS[‡]	19	13	0.003	32	45	16	18	79
Liver	19	0.02	0.003	19	9	4	1	14
Gonads	76	0.02	0.0002	76	0.6	0.2	0.4	1

[*]Calculated assuming radionuclide ratios of 0.9 for ^{90}Sr/^{90}Y:^{137}Cs, 0.003 for ^{238}Pu:^{137}Cs ratio and 0.001 for ^{239}Pu:^{137}Cs and ^{241}Am:^{137}Cs. Absorption to blood was assumed to be 1% for ^{137}Cs, 0.01% for ^{90}Sr and 0.001% for ^{238}Pu, ^{239}Pu, ^{241}Am and ^{90}Y.

[†]RBM = red bone marrow.

[‡]BS = bone surfaces.

Table 5.4. Radionuclide contributions to committed equivalent doses to organs / tissues of a one year-old child after ingestion of a 10^5 Bq ^{137}Cs particle, μSv[a]

Organ/ tissue	^{137}Cs	^{90}Sr	^{90}Y	Total βγ	^{238}Pu	^{239}Pu	^{241}Am	Total α
Stomach	210	110	620	940	0.3	0.1	0.08	0.4
Colon	630	580	1200	2400	0.3	0.1	0.08	0.4
RBM[b]	37	10	0.03	47	6	2	2	10
BS[c]	37	16	0.02	53	42	15	17	74
Liver	50	0.1	0.02	50	15	5	2	22
Gonads	310	0.1	0.003	310	1	0.4	0.5	2

*Calculated assuming radionuclide ratios of 0.9 for ^{90}Sr/^{90}Y:^{137}Cs, 0.003 for ^{238}Pu:^{137}Cs ratio and 0.001 for ^{239}Pu:^{137}Cs and ^{241}Am:^{137}Cs. Absorption to blood was assumed to be 1% for ^{137}Cs, 0.01% for ^{90}Sr and 0.001% for ^{238}Pu, ^{239}Pu, ^{241}Am and ^{90}Y.

†RBM = red bone marrow.

‡BS = bone surfaces.

Table 5.5. Radionuclide contributions to committed equivalent doses to organs / tissues of an adult male after ingestion of a 10^8 Bq ^{137}Cs particle, mSv*

Organ/ tissue	^{137}Cs	^{90}Sr	^{90}Y	Total βγ	^{238}Pu	^{239}Pu	^{241}Am	Total α
Stomach	42	3	70	120	0.08	0.03	0.03	0.1
Colon	140	60	140	350	0.08	0.03	0.03	0.1
RBM†	25	5	0.003	30	2	0.8	0.6	4
BS‡	19	13	0.003	32	45	16	18	79
Liver	19	0.02	0.003	19	9	4	1	14
Gonads	76	0.02	0.0002	76	0.6	0.2	0.4	1

*Calculated assuming radionuclide ratios of 0.9 for ^{90}Sr/^{90}Y:^{137}Cs, 0.003 for ^{238}Pu:^{137}Cs ratio and 0.001 for ^{239}Pu:^{137}Cs and ^{241}Am:^{137}Cs. Absorption to blood was assumed to be 1% for ^{137}Cs, 0.01% for ^{90}Sr and 0.001% for ^{238}Pu, ^{239}Pu, ^{241}Am and ^{90}Y.

†RBM = red bone marrow.

‡BS = bone surfaces.

Table 5.7 shows the results of calculations of committed equivalent doses to organs / tissues and committed effective dose for ingestion by an adult male of an MTR particle with solubility characteristics corresponding to those exhibited *in vitro* by particle MTR113 (section 3.4.1). The committed effective dose is about 2 mSv from a 10^5 Bq ^{137}Cs particle, on the basis of standard assumptions for radionuclide ratios and absorption to blood of 60% of the particle content of ^{137}Cs, 15% of ^{90}Sr and 0.03% of the actinides and ^{90}Y. Tissue doses are dominated by contributions from beta / gamma emissions from ^{137}Cs, ^{90}Sr and ^{90}Y. Committed equivalent doses to the alimentary tract (stomach and colon) contribute about 15% of the committed effective dose while skeletal tissues (red bone marrow and bone surfaces) contribute about 60%. Doses to a one year-old child would be about two to four times greater than to an adult male.

Table 5.6. Radionuclide contributions to committed equivalent doses to organs / tissues of a one year-old child after ingestion of a 10^8 Bq ^{137}Cs particle, mSv[*]

Organ/ tissue	^{137}Cs	^{90}Sr	^{90}Y	Total βγ	^{238}Pu	^{239}Pu	^{241}Am	Total α
Stomach	140	13	310	460	0.3	0.1	0.08	0.4
Colon	520	220	580	1300	0.3	0.1	0.08	0.4
RBM[b]	37	10	0.03	47	6	2	2	10
BS[c]	37	16	0.02	53	42	15	17	74
Liver	50	0.1	0.02	50	15	5	2	22
Gonads	310	0.1	0.003	310	1	0.4	0.5	2

[*]Calculated assuming radionuclide ratios of 0.9 for ^{90}Sr/^{90}Y:^{137}Cs, 0.003 for ^{238}Pu:^{137}Cs ratio and 0.001 for ^{239}Pu:^{137}Cs and ^{241}Am:^{137}Cs. Absorption to blood was assumed to be 1% for ^{137}Cs, 0.01% for ^{90}Sr and 0.001% for ^{238}Pu, ^{239}Pu, ^{241}Am and ^{90}Y.

[†]RBM = red bone marrow.

[‡]BS = bone surfaces.

Table 5.7. Committed equivalent doses to organs / tissues and committed effective dose to an adult male from the ingestion of soluble MTR particle 113, μSv[*]

Organ/ tissue	^{137}Cs	^{90}Sr	^{90}Y	Total βγ	$^{238/239}$Pu	^{241}Am	Total α	Total
Stomach	830	50	150	1030	3	0.8	4	1030
Colon	910	170	310	1390	3	0.8	4	1400
RBM[†]	790	8050	0.1	8840	90	20	110	8950
BS[‡]	830	18400	0.1	19230	1800	540	2340	21600
Liver	820	28	0.1	850	390	34	420	1270
Gonads	880	28	0.003	910	30	11	41	950
E[§]	820	1200	54	2070	56	12	68	2140

[*]Calculated assuming radionuclide ratios of 0.9 for ^{90}Sr/^{90}Y:^{137}Cs, 0.003 for ^{238}Pu:^{137}Cs ratio and 0.001 for ^{239}Pu:^{137}Cs and ^{241}Am:^{137}Cs. Absorption to blood was assumed to be 60% ^{137}Cs, 15% ^{90}Sr and 0.03% for the actinides and yttrium.

[†]RBM = red bone marrow.

[‡]BS = bone surfaces.

[§]E: committed effective dose.

For particles containing ^{60}Co, colon doses were discussed briefly in Chapter 3 and estimates of effective dose have also been made. As noted in Chapter 3, gut doses from ^{60}Co were calculated using the ICRP HAT model as described in section 3.2 without regard for self-absorption within the particle. Absorption to blood was assumed to be the same as for ^{90}Sr absorption from typical MTR particles, that is 10^{-4} of the ingested activity. On this basis, estimated values of committed effective dose per Bq ^{60}Co were greater than those for unit activity of ^{137}Cs (together with the associated activities of ^{90}Sr and ^{90}Y) by about 30% for a 10^5 Bq particle and 60% for a 10^8 Bq particle. The higher value for the larger particle reflects the conservative nature of the calculation for large particles in which self-absorption is ignored. Thus, within the uncertainties associated with such estimates of dose, committed effective doses from a particle containing only ^{60}Co (e.g. #86037, 8.5 x 10^6 Bq) can be taken to be approximately equal to the results obtained for a particle of similar ^{137}Cs activity (Table 5.2). Due to the high proportion of photon emissions produced by ^{60}Co, only about 50% of the effective dose is attributable to gut doses.

5.4.2 Particle inhalation

As discussed in Chapter 4, inhaled particles with effective diameters of 300 μm (approximate size of 10^5 Bq ^{137}Cs particles) and aerodynamic diameters of about 400 μm are too large to reach the bronchial airways of the lungs and will deposit in extrathoracic (ET) airways. While lung tissues are important sites of radiation-induced cancer, this does not apply to extrathoracic tissue. Doses to the AI region of the lung from 10^5 and 10^8 Bq ^{137}Cs particles deposited in the ET region were given in Table 4.4 (section 4.4.2) for an adult male as 3 μGy and 3 mGy, respectively. As shown in Figure 4.2, deposition in ET_1 (the front of the nose) and ET_2 (all other extrathoracic airways) is considered to be followed by rapid removal, either to the exterior environment (ET_1) or to the alimentary tract (ET_2), with rates of 1 d^{-1} and 100 d^{-1}, respectively. Consequently, there will be little time for dissolution and absorption to blood while particles remain in the ET region and it appears reasonable to assume that intestinal absorption will dominate uptake to blood. Thus, the doses shown in Table 5.2 will apply to inhaled particles deposited in the extrathoracic airways (other than ET1) and the additional lung dose will make negligible contributions (< 1%) to committed effective doses.

This analysis ignores the current ICRP methodology which assigns half the remainder w_T (see 5.1) to an individual remainder tissue, such as ET, in situations where its dose exceeds doses to all named tissues. This so-called splitting rule is not relevant to the consideration of risks of cancer and hereditary effects from exposure to Dounreay particles and is to be dropped following the introduction of new recommendations (www.icrp.org).

5.4.3 Particles on skin

ICRP (1991) relates the risk of skin cancer to the average dose to the total area of skin, 1.9 m^2 in adult man and 0.48 m^2 for a one year old child (ICRP, 2002). A number of animal studies, mainly using skin exposures of mice and rats, have evaluated the carcinogenic risk of hot particles in comparison with spatially uniform radiation exposures. For the same average dose there is little evidence, within a factor of ± 3, of any dependence of cancer risk on spatial dose distribution (Charles *et al*. 2003). The overall finding is that the use of mean dose to predict carcinogenic risks, as advocated by the ICRP, is appropriate for hot particle exposures.

A dose of 2 Gy to 1 cm^2 of skin, referred to in Chapter 2 as a threshold for observable ulceration, corresponds to an equivalent dose to the skin for the assessment of cancer risk of 0.1 mSv in adults and 0.4 mSv in one year old children. The effective dose is then the equivalent dose to skin multiplied by the w_T for skin of 0.01: that is, 1 μSv for adults and 4 μSv for one year old children. There will be a larger contribution to the effective dose from Dounreay fuel fragments located at the body surface due to a small whole body exposure from the gamma emitter ^{137}Cs. Walters *et al*. (1999) have evaluated this to be between 0.2 – 3.8 μSv h^{-1} MBq^{-1}, depending on the location of the radioactive source on the body. This dose from ^{137}Cs will increase estimated effective doses corresponding to 2 Gy to 1 cm^2 of skin to maximum values of about 4 μSv in adults and about 25 μSv in one year old children.

5.5 Discussion

The ICRP dose quantity, committed effective dose, provides a convenient method for the summation of doses from different radionuclides and external sources, for the purposes of comparison with dose limits set on the basis of risks of cancer and hereditary effects. It should be noted, however, as discussed also in Chapter 2, that the ICRP dose limits apply to controlled sources and are not intended to apply to existing situations in which the only available protective action takes the form of an intervention (ICRP, 1991a), as is the case in the control of potential public exposure to Dounreay particles. Nevertheless, the limits provide values with which to compare possible doses from Dounreay particles and the calculated doses can be used to provide approximate estimates of cancer risk and total detriment (see below).

The estimates of committed effective dose obtained in this section for the ingestion of typical 10^5 and 10^8 Bq ^{137}Cs MTR particles are 0.1 mSv and 80 mSv, respectively, for an adult male, and 0.5 mSv and 300 mSv, respectively, for a one year-old child. For each of these values, the results showed that doses are dominated (>70%) by contributions from committed equivalent doses to the alimentary tract, particularly the colon. While doses are not directly proportional to the activity of the ingested particles, because of energy attenuation within larger particles, deviation from proportionality is small compared with uncertainties associated with dose estimation. Committed effective doses of 0.1 mSv and 0.5 mSv from 10^5 Bq ^{137}Cs particles are below the dose limit of 1 mSv for members of the public.

As discussed in Chapter 3, an important factor determining colon doses from ingested particles is the assumed transit time of material through the colon. While there are good data supporting the central values of transit times used in the ICRP model, there are also many data showing that transit time is typically increased by a factor of 2 – 3 in constipated individuals and can be increased by factors of up to 10 in extreme cases. A threefold increase in the transit time of a 10^5 Bq ^{137}Cs particle through the colon of a one year-old child would increase the committed effective dose by a factor of two to 1 mSv and a tenfold increase would increase the dose by a factor of 6 to 3 mSv.

Doses have also been calculated for a 10^5 Bq ^{137}Cs particle on the basis of the uncharacteristic solubility in simulated gut fluids exhibited by MTR113. The *in vitro* data obtained for this particle suggested that more than half of the radionuclide content was dissolved from the particle and would therefore be available for intestinal absorption, compared with typical solubility of 1% or less. The committed effective dose to an adult male following ingestion of a 10^5 Bq ^{137}Cs particle of such high solubility was estimated as about 2 mSv. In this case, committed equivalent doses to the alimentary tract (stomach and colon) contributed only about 15% of the committed effective dose while skeletal tissues (red bone marrow and bone surfaces) contributed about 60%. Doses to a one year-old child would be about two to four times greater than to an adult male.

Values of committed effective dose allow the approximate estimation of overall risks of fatal cancer and of total detriment, relating to averaged values for a population of 0.05 Sv^{-1} and 0.07 Sv^{-1}, respectively (see Section 5.1). These values take account of evidence of greater risk following irradiation during early childhood than in adulthood by estimated factors of two to three. Thus the dose limit of 1 mSv corresponds to an

overall fatal cancer risk of 5 x 10^{-5} and the dose estimate of 0.1 mSv for an adult following ingestion of a typical insoluble 10^5 Bq ^{137}Cs MTR particle (Table 5.2) implies a fatal cancer risk of 5 x 10^{-6}. The information provided in this chapter on doses to individual organs and tissues also allows the estimation of specific cancer risks, using the risk estimates published by ICRP (1991a) or estimates made specifically for the UK population (Muirhead *et al*. 1993). For example, the committed equivalent dose of 0.61 mSv to the colon of an adult from the ingestion of a 10^5 Bq ^{137}Cs MTR particle (Table 5.2) implies a fatal cancer risk of 3 x 10^{-6}, on the basis of a risk estimate for colon cancer of 5 x 10^{-3} Sv^{-1} (Muirhead *et al*. 1993).

Separate consideration of the possibility of inhalation of particles is not important in the context of effective dose. The deposition in extrathoracic airways of particles with activities of 10^5 Bq ^{137}Cs or more will result in a dose to the lungs that will make a negligible contribution to effective dose compared with doses resulting from the subsequent clearance of particles to the alimentary tract. Equivalent and effective doses from a particle on skin are very small and the associated cancer risk is very low. An equivalent dose of 0.1 mSv to the skin of an adult, corresponding to a local dose of 2 Gy to 1 cm^2, implies a risk of fatal cancer of 2 x 10^{-8} on the basis of a risk estimate of 1.6 x 10^{-4} Sv^{-1} (Muirhead *et al*. 1993). The risk of non-fatal skin cancer is between two and three orders of magnitude greater because of the high success rate in the treatment of basal cell carcinoma, the principal type of skin cancer associated with exposure to ionising radiation. Skin cancer risk associated with possible exposure to Dounreay particles can be regarded as of low importance in comparison with considerations of local dose and the possibility of skin ulceration.

6 REFERENCES

Arhan P, Devroede G, Jehannin B, Lanza M, Faverdin C, Dornic C, Persoz B, Tetreault L, Perey B and Pellerin D (1981). Segmental colonic transit time. *Dis Colon Rectum* **24**, 625-629.

Aydarous AS (2003). Development of imaging techniques for determining dose distributions around discrete radioactive particles found in the environment. PhD thesis. School of Physics and Astronomy, University of Birmingham.

Aydarous AS, Darley PJ and Charles MW (2001). A wide dynamic range, high spatial resolution readout system for radiochromic dye films. *Phys Med Biol* **46**, 1379-1389.

Bailey MR, Harrison JD, Jones KA, Marsh JW and Prosser SL (1997). Uncertainties in aspects of internal dosimetry relevant to accident consequence assessment codes. Chilton, NRPB-M763.

Barabanova A and Osanov DP (1990). The dependence of skin lesions on the depth-dose distribution of beta-irradiation of people in the Chernobyl nuclear power plant accident. *Int J Radiat Biol* **57**, 775-782.

Bautista Casasnovas A, Varela Cives R, Villanueva Jeremias A, Castro-Gago M, Cadranel S and Tojo Sierra R (1991). Measurement of colonic transit time in children. *J Pediatr Gastroenterol Nutr* **13**, 42-45.

Benninga MA, Buller HA, Tytgat GN, Akkermans LM, Bossuyt PM and Taminiau JA (1996). Colonic transit time in constipated children: does pediatric slow-transit constipation exist? *J Pediatr Gastroenterol Nutr* **23**, 241-251.

Bond VP, Fliedner TM and Archambeau JO (1965). Mammalian radiation lethality: a disturbance in cellular kinetics. Academic Press, New York.

Bouchoucha M and Thomas SR (2000). Error analysis of classic colonic transit time estimates. *Am J Physiol Gastrointest Liver Physiol* **279**, G520-G527.

Brandao-Mello CE, Oliverira AR, Valverde NJ, Farina R and Cordeiro JM (1991). Clinical and haematological aspects of ^{137}Cs: the Goiania radiation accident. *Health Phys* **60**, 31-39.

Bridges BA and Knill J (1995). Report on potential health effects and possible sources of radioactive particles found in the vicinity of the Dounreay Nuclear Establishment. Joint COMARE/ RWMAC Report. London, HMSO.

Briesmeister JF (Ed). (1997) MCNP - A General Monte Carlo N-Particle Transport Code, version 4C. Los Alamos National Laboratory LA-12625-M, Los Alamos, New Mexico.

Briesmeister JF (Ed). (2000) MCNP - A General Monte Carlo N-Particle Transport Code, version 4C. Los Alamos National Laboratory LA-13709-M, Los Alamos, New Mexico.

Cai WB, Roberts SA, Bowley E, Hendry JH and Potten CS (1997). Differential survival of murine small and large intestinal crypts following ionising radiation. *Int J Radiat Biol* **71**, 145-55.

Cember H and Stemmer K (1964). Lung cancer from radioactive cerium chloride. *Health Phys* **10**, 43-8.

Charles MW (1990). General considerations of the choice of dose limits, averaging areas and weighting factors for the skin in the light of revised skin cancer risk figures and experimental data on non-stochastic effects. *International Journal of Radiation Biology* **57**, 841-858.

Charles, M. W. (1991) The Hot Particle Problem. Radiat. Prot. Dosim. **39**, 39-47.

Charles, M. W. (1997) Physical and Radiobiological Considerations in Eye Dosimetry. NATO Advance Research Workshop. Ocular Radiation Risk Assessment in Population Exposed to Environmental Radiation Contamination.

Charles, M. W. (2004) The skin in radiological protection - Recent advances and residual unresolved issues. Radiat. Prot. Dosim. **109**, 323-330.

Charles MW and Brown NA (1975). Dimensions of the Human Eye Relevant to radiation Protection. *Phys Med Biol* **20**, 202.

Charles MW, Mill AJ and Darley PJ (2003) Carcinogenic risk of hot particle exposures. *J Radiol Prot* **23**, 5-28.

COMARE (1999). Committee on Medical Aspects of Radiation in the Environment. Sixth Report: A reconsideration of the possible health implications of the radioactive particles found in the general environment around the Dounreay Nuclear Establishment in the light of the work undertaken since 1995 to locate their source. NRPB, Chilton.

Cristy M and Eckerman KF (1987). Specific absorbed fractions of energy at various ages from internal photon sources. Oak Ridge National Laboratory, Oak Ridge, Tennessee. ORNL/TM-8381/v1-7.

Cristy M and Eckerman KF (1993). SEECAL: Program to calculate age-dependent specific effective energies. ORNL/TM-12351. Oak Ridge National Laboratory, Oak Ridge, Tennessee, USA.

Cross, F.T., Endres, G.W.R. and Sullivan, M.F. (1978). Dose to the GI tract from ingested insoluble beta emitters. Radiat. Res. 73, 37-50.

Culling CFA (1974). Handbook of histopathological and histochemical techniques. 3rd Edn. Butterworths, London.

Darley PJ (2001). Improved dose estimates for Dounreay fuel fragment particles. UBIRM/UKAEA/DOUNREAY-002. University of Birmingham, School of Physics and Astronomy.

Darley PJ, Charles MW, Fell TP and Harrison JD (2003). Doses and risks from the ingestion of Dounreay fuel fragments. *Radiat Prot Dosim* **105**, 49-54.

Dean PN, Langham J and Holland LM (1970). Skin response to a point source of fissioned uranium-235 carbide. *Health Phys* **19**, 3-7.

Eckerman KF, Westfall RJ, Ryman JC and Cristy M (1994). Availability of nuclear decay data in electronic form, including beta spectra not previously published. *Health Phys* **67**, 338-345.

Endo A, Yamaguchi Y and Eckerman KF (2003). Development and assessment of a new radioactive decay database use for dosimetry calculation. *Radiat Prot Dosim* **105**, 565-569.

Endo A, Yamaguchi Y and Eckerman KF (2004). Nuclear decay data for dosimetry calculation. Revised data of ICRP Publication 38. To be published as a Japanese Atomic Energy Research Institute (JAERI) report.

Evans JS, Abrahamson S, Bender MA, Boecker BB, Gilbert ES and Scott BR (1993). Health effects models for nuclear power plant accident consequence analysis. Washington DC, Nuclear Regulatory Commission, NUREG/CR-4214, Rev. 2, Part 1.

Evans JM, Fleming KC, Talley NJ, Schleck CD, Zinsmeister AR and Melton LJ (1998). Relation of colonic transit to functional bowel disease in older people: a population-based study. *J Amer Geriatr Soc* **46**, 83-87.

Eve IS (1966). A review of the physiology of the gastrointestinal tract in relation to radiation doses from radioactive materials. *Health Phys* **12**, 131-161.

Fallingborg, J., Christensen, L. A., Ingeman-Nielsen, M., Jacobsen, B. A., Abildgaard, K. and Rasmussen, H. H. (1989) pH-profile and regional transit times of the normal gut measured by a radiotelemetry device. Aliment. Pharmacol. Ther. **3**, 605-613.

Fallingborg J, Christensen LA, Ingeman-Nielsen M, Jacobsen BA, Abildgaard K, Rasmussen HH and Rasmussen SN (1990). Measurement of gastrointestinal pH and regional transit times in normal children. *J Pediatr Gastroenterol Nutr* **11**, 211-214.

Ferrara A, Pemberton, J H, Grotz R L and Hanson RB (1994). Prolonged ambulatory recording of anorectal motility in patients with slow-transit constipation. *Am J Surg* **167**, 73-79.

Fill UA, Zankl M, Petoussi-Henss N, Siebert M and Regulla D (2004). Adult female voxel models of different stature and photon conversion coefficients for radiation protection. *Health Phys* **86**, 253-272.

Furchner JE and Richmond CR (1962). Effect of stable Cs on the retention of Cs-137 by rats. *Proc Soc Exp Biol Med* **110**, 185-187.

Gran FC (1960). Studies on calcium and strontium-90 metabolism in rats. *Acta Physiol Scand* **48** (Suppl. No.167).

Hall P, Granath F, Lundell M, Olssen K and Holm L-E (1999). Lenticular opacities in individuals exposed to ionising radiation in infancy. *Radat Res* **152**, 190-195.

Hamlet R, Herjet JC, Hopewell JW, Wells J and Charles MW (1986). Late Changes in Pig Skin after Irradiation from Beta Emitting Sources of Different Energy. *British Journal of Radiology* **19**, 51-54.

Harrison JD and Stather JW (1982). The tissue distribution and excretion of actinides absorbed from the gastrointestinal tract of rodents. *Health Phys* **43**, 283-5.

Hendry JH, Potten CS, Ghafoor A, Moore JV, Roberts SA and Williams PC (1989). The response of murine intestinal crypts to short-range promethium-147 beta irradiation: deductions concerning clonogenic cell numbers and positions. *Radiat Res* **118**, 364-74.

Hendry JH, Roberts SA and Potten CS (1992). The clonogenic content of murine intestinal crypts: dependence on radiation dose used in its determination. *Radiat Res* **132**, 115-119.

Hobbs CH, Barnes JE, McClellan RO, Chiffelle TL, Jones RK, Lundgren DL, Mauderley JL, Pickrell JA and Rypka EW (1977). Toxicity in the dog of ^{90}Y in fused clay particles: early biological effects. *Radiat Res* **49**, 430-60.

Hopewell JW, Coggle JE, Wells J, Hamlet R, Williams JP and Charles MW (1986). The acute effects of different energy beta emitters on pig and mouse skin. *Brit J Radiol Suppl* **19**, 47-51.

Hopewell JW (1991) Biological Effects of Irradiation on Skin and Recommended Dose Limits. *Radiat Prot Dosim* **39**, 11-24.

Horan R (1966). Major health physics experiences during 15 years of reactor testing. In 'Proceedings of the first International Congress of Radiation Protection', pp.541-546. W S Snyder et al, Eds., Pergamon Press, New York.

Hume WJ and Potten CS (1979). Advances in epithelial kinetics-an oral view. *J Oral Pathol* **8**, 3-22.

IAEA (1987). The Radiological Accident in Goiania. International Atomic Energy Agency, PO Box 100, A-1400 Vienna, Austria.

ICRP (1977). Recommendations of the International Commission on Radiological Protection, ICRP Publication 26. Ann. ICRP **1** (3). Pergamon Press, Oxford.

ICRP (1979). Limits for Intakes of Radionuclides by Workers. ICRP Publication 30 Part 1. Ann. ICRP **2** (3/4). Pergamon Press, Oxford.

ICRP (1980) Limits for Intakes of Radionuclides by Workers. ICRP Publication 30 Part 2. Ann. ICRP **4** (3/4). Pergamon Press, Oxford.

ICRP (1989). Age-Dependent Doses to Members of the Public from Intake of Radionuclides: Part 1. ICRP Publication 56. Ann. ICRP **20** (2). Pergamon Press, Oxford.

ICRP (1991a) 1990 Recommendations of the International Commission on Radiological Protection. ICRP Publication 60. Ann. ICRP **21** (1-3), Pergamon Press, Oxford.

ICRP (1991b). The biological basis for skin dose limitation. ICRP Publication 59. Ann. ICRP **22** (2). Pergamon Press, Oxford.

ICRP (1993) Age-Dependent Doses to Members of the Public from Intake of Radionuclides: Part 2. ICRP Publication 67. Ann ICRP **23** (3/4). Pergamon Press, Oxford.

ICRP (1994a) Human Respiratory Tract Model for Radiological Protection. ICRP Publication 66. Ann. ICRP **24** (1-3). Elsevier Science Ltd, Oxford.

ICRP (1994b) Dose Coefficients for Intake of Radionuclides by Workers. ICRP Publication 68. Ann. ICRP **24** (4). Elsevier Science Ltd, Oxford.

ICRP (1995) Age-dependent Doses to Members of the Public from Intake of Radionuclides: Part 4. Inhalation Dose Coefficients. ICRP Publication 71. Ann. ICRP **25** (3/4), Elsevier Science Ltd, Oxford.

ICRP (1996) Age-dependent Doses to Members of the Public from Intake of Radionuclides: Part 5 Compilation of Ingestion and Inhalation Dose Coefficients. ICRP Publication 72. Ann. ICRP **26** (1), Elsevier Science Ltd, Oxford.

ICRP (2001) Doses to the embryo and fetus from intakes of radionuclides by the mother. ICRP Publication 88. Ann. ICRP **31** (1-3), Elsevier Sciences Ltd, Oxford.

ICRP (2002). Basic anatomical and physiological data for use in radiological protection: Reference values. ICRP Publication 89. Ann. ICRP, **32** (3-4). Elsevier Sciences Ltd, Oxford.

ICRP (2005) Human Alimentary Tract Model for Radiological Protection. ICRP Publication 99. Elsevier Sciences Ltd, Oxford. (To be published.)

ICRU (1997) Dosimetry of external beta rays for radiation protection. ICRU Report 56. Bethesda, MD, USA.

Jarvis NS, Birchall A, James AC, Bailey MR and Dorrian M-D (1996). LUDEP 2.0 Personal computer program for calculating internal doses using the ICRP Publication 66 respiratory tract model. Chilton, NRPB-SR287.

Jones PW, Taylor DM and Williams DR (2001). Chemical speciation of neptunium in the small intestine: A comparison of an in vitro model and a computer modelling investigation. Presentations at the 6th International Symposium on Applied Bioinorganic Chemistry, Cardiff, June 2001, London, the Royal Society of Chemistry.

Jurgenliemk-Schulz IM, Hartman LJC, Roeesink JM, Tesrsteeg RJHA, Tweel I, Kal HB, Mourtis MP and Wyrdeman HK (2004). Prevention of pterygium recurrence by postoperative single-dose beta-irradiation: A prospective randomized clinical double-blind trial. *Int J Radiat Oncol Biol Phys* **59**, 1138-1147.

Karam SM, Straiton T, Hassan WM, Leblond CP (2003). Defining epithelial cell progenitors in the human oxyntic mucosa. *Stem Cells* **21**, 322-36.

Kaurin DGL, Baum JW, Carsten AL, Schaefer CW and Forbes PD (2001a). Scab diameters on pig skin resulting from hot particle exposures under varying conditions. *Health Phys* **81**, 35-46.

Kaurin, D. G. L., Baum, J. W., Carsten, A. L. & Schaefer, C. W. (2001b) Scab incidence on pig skin resulting from hot particle exposures under varying conditions. Health Phys. **81**, 47-56.

Kaurin DGL, Baum JW, Charles MW, Darley PJ, Durham JS and Scannell MJ (1997). Hot particle dosimetry: Intercomparisons. In Appendix to NUREG Report ' Effects of radioactive hot particles on pig skin'. US Nuclear Regulatory Commission NUREG Report: NUREG/CR-6531.

Klauser AG, Voderholzer WA, Heinrich CA, Schindlbeck NE and Muller-Lissner SA (1990). Behavioural modification of colonic function. Can constipation be learned? *Dig Dis Sci* **35**, 1271-1275.

Kolster J, de Kolter CC, Castro J and Carvajal A (1991). Study of colonic transit time with radiopaque markers in patients with chronic constipation. *G E N* **45**, 14-22.

MacDonald A, Baxter JN, Bessent RG, Gray HW and Finlay IG (1997). Gastric emptying in patients with constipation following childbirth and due to idiopathic slow transit. *Brit J Surg* **84**, 1141-1143.

Maisin J, Maisin JR and Dunjic A (1971). The gastrointestinal tract. In: C.C. Berjis, (Eds.) Pathology of Irradiation. William and Wilkins, Baltimore. p.296.

Mauderley JL, Pickrell JA, Hobbs CH, Benjamin SA, Hahn FF, Jones RK and Barnes JE (1973). The effects of inhaled 90Y fused clay aerosol on pulmonary function and related parameters of the beagle dog. *Radiat Res* **56**, 83-96.

Mazeron JJ, Chalie R, Zeller J, Marinello G, Marin L, Raynal M, Bourgeois JP and Pierquin B (1986). Radiation therapy for carcinoma of the pinna using iridium 192 wires. A series of 70 patients. *Int J Radiat Oncol Biol Phys* **12**, 1757-1763.

McClellan RO, Boecker BB, Cuddihy RG, Griffith WC, Hahn FF, Muggenburg BA, Scott BR and Seiler FA (1982). Health effects from internally deposited radionuclides released in nuclear disasters. In: The control of exposure of the public to ionising radiation in the event of accident or attack. Proc. NCRP Symp. Reston, Virginia. NCRP, Washington DC. pp.28-39.

Metcalf AM, Phillips SF, Zinsmeister AR, MacCarty RL, Beart RW and Wolff BG (1987). Simplified assessment of segmental colonic transit. *Gastroenterol* **92**, 40-47.

Minamoto A, Taniguchi H, Yoshitani N, Mukai S, Yokoyama T, Kumagami T, Tsuda Y, Mishima HK, Ameiya T, Nakashima E, Neriisha K, Hida A, Fujiwara S, Suzuki G and Akahoshi M (2004). Cataract in atomic bomb survivors. *Int J Radiat Biol* **80**, 339-345.

Modlin IM, Kidd M, Lye KD and Wright NA (2003). Gastric stem cells: an update. *Keio J Med* **52**, 134-7.

Muirhead CR, Cox R, Stather JW, MacGibbon BH, Edwards AA and Haylock RG (1993). Estimates of late radiation risks to the UK population. Doc. NRPB **4** (4). HMSO, London.

NCRP (1989). Limit for exposure to 'hot particles' on the skin. NCRP Report No.106. National Council on Radiation Protection and Measurements, Bethesda, Washington DC.

NCRP (1999). Biological effects and exposure limits for 'hot particles'. NCRP Report No. 130. National Council on Radiation Protection and Measurements, Bethesda, Washington DC.

NRPB (1996). Risk from deterministic effects of ionising radiation. Doc. NRPB **7** (3). HMSO, London.

NRPB (1997). Assessment of skin doses. Doc. NRPB, **8** (3). HMSO, London.

NUDAT (2000). Evaluated numerical nuclear data (NUDAT). www.nndc.bnl.gov National Nuclear Data Centre. Upton, New York: Brookhaven National Laboratory.

Penna FJ, Hill ID, Kingston D, Roberston K, Slavin G and Shiner M (1981). Jejunal mucosal morphometry in children with and without gut symptoms and in normal adults. *J Clin Pathol* **34**, 386-392.

Philips TL and Margolis L (1972). Radiation pathology and the clinical response of lung and oesophagus. *Front Radiat Ther Oncol* **6**, 254-73.

Potten CS (1990). A comprehensive study of the radiobiological response of the murine (BDF1) small intestine. *Int J Radiat Biol* **58**, 925-973.

Potten CS (1995). Structure, function and proliferative organisation of mammalian gut. P1-31 in: Radiation and Gut. eds C S Potten and J H Hendry, Elsevier, Amsterdam.

Potten CS (2003). Personal communication to the ICRP Task Group revising the dosimetric model for the human alimentary tract.

Rao SSC, Read NW, Brown C, Bruce C and Holdsworth CD (1987) Studies on the mechanism of bowel disturbance in ulcerative colitis. *Gastroenterol* **93**, 934-940.

Reece WD, Poston JW and McFarlane DL (1994). Skin injuries from discrete radioactive particles: A summary of EPRI sponsored experiments. TR-104781. Electric Power Research Institute, Palo Alto, California.

Roberts SA, Hendry JH and Potten CS (1995). The deduction of the clonogen content of intestinal crypts: a direct comparison of fractionated-dose and graded-dose methodologies. *Radiat Res* **141**, 303.108.

Roberts SA, Hendry JH and Potten CS (2003). Intestinal crypt clonogens: a new interpretation of radiation survival curve shape and clonogenic cell number. *Cell Prolif* **36**, 215-231.

Scott BR and Hahn FF (1985). Early occurring and continuing effects. In: Health effects models for nuclear power plant accident consequence analysis. (Edited by JS Evans, JW Moeller and DW Cooper) Washington DC, Nuclear Regulatory Commission. NUREG/CR-4214 (SAND85-7185).

Smith KR, Bedwell P, Etherington G, Youngman M and Wilkins BT (2005). The impact of fragments of irradiated fuel on Sandside beach. SEPA Report.

Sontag W (1987). Dosimetry of alpha-emitting radionuclides in bone -a practical approach. *Health Phys* **53**, 495-501.

Stabin MG, Watson EE, Cristy M, et al (1995). Mathematical models and specific absorbed fractions of photon energy in the nonpregnant adult female and at the end of each trimester of pregnancy. Oak Ridge National Laboratory, Oak Ridge, Tennessee. ORNL/TM-12907.

Stather JW, Muirhead CR, Edwards AA, Harrison JD, Lloyd DC and Wood NR (1988). Health effects models developed from the 1988 UNSCEAR Report. Chilton. NRPB-R226.

Stenling R, Fredrikzon B, Nyhlin H and Helander HF (1984). Surface ultrastrucure of the small intestine mucosa in healthy children and adults: a scanning electron microscopic study with some methodological aspects. *Ultrastruct Pathol* **6**, 131-140.

Stephen AM, Wiggins HS and Cummings JH (1987).Effect of changing transit time on colonic microbial metabolism in man. *Gut* **28**, 601-609.

Stewart A, Cook GT and MacKenzie AB (2003) Simulation of human stomach and intestine leaching of Dounreay hot particles. Scottish Universities Research and Reactor Centre Contract Report to SEPA.

Stromme O (1955). In the absorption of particulate allergens as pollen through the nasal mucosa and some remarks on bacterial nasal allergy. Acta Allergol. VIII, 283-8.

Stuart BO, Casey WH and Bair WJ (1964). Acute and chronic effects of inhaled ^{144}CeO2 in dogs. *Health Phys* **10**, 1203-9.

Stubbs JB (1992).Results from a new mathematical model of gastrointestinal transit that incorporates age- and gender-dependent physiological parameters. *Radiat Prot Dosim* **41**, 63-69.

Sullivan MF, Marks S, Hackett PL and Thompson RC (1959).X-irradiation of the exteriorised or in situ intestine of the rat. *Radiat Res* **73**, 653-666.

Sullivan MF, Hackett PL and George LA (1960). Irradiation of the intestine by radioisotopes. *Radiat Res* **13**, 343-355.

Sullivan MF, Ruemmler PS, Reamer JL *et al.* (1978). Acute toxicity of beta-emitting radionuclides that may be released in a reactor accident and ingested. *Radiat Res* **73**, 21-36.

Talley NJ, Phillips SF, Haddad A, Miller LJ, Twomey C, Zinsmeister AR, MacCarty RL and Ciociola A (1990).GR 38032F (ondansetron), a selective 5HT3 receptor antagonist, slows colonic transit in healthy man. *Dig Dis Sci* **35**, 477-480.

Taylor DM, Duffield JR and Proctor JA (1986).The chemical form of plutonium in the gastrointestinal tract. In: R. A. Bulman and J. R. Cooper (Eds.) Speciation of Fission and Activation Products in the Environment, Elsevier, London. pp.208-212.

Thomas RL, Scott JK and Chiffelle TL (1972). Metabolism and toxicity of inhaled 144CeO2 in rats. *Radiat Res* **49**, 589-610.

Thomas RL, Storb R and Clift RA (1975). Bone marrow transplantation. *New England J Med* **292**, 832-44.

Tossavainen K (1990). Radioactive metal particle gets in the eye of a worker. In 'Operation of Finnish Power Plants, Quarterly report (2nd quarter)', pages 20-21. National Technical Information Service, Springfield, Virginia.

UNSCEAR (1988) United Nations Scientific Committee on the Effects of Atomic Radiation). Sources, Effects and Risks of Ionizing Radiation. UN, New York.

Van Dyk J, Keane TJ, Kan S, Rider WD and Fryer CJ (1981). Radiation pneumonitis following large single dose irradiation: a re-evaluation based on absolute dose to lung. *Int J Radiat Oncol Biol Phys* **7**, 461-7.

Vattimo A, Burroni L, Bertelli P, Messina M, Meucci D and Tota G (1993). Total and segmental colon transit time in constipated children assessed by scintigraphy with 111In-DTPA given orally. *J Nucl Biol Med* **37**, 218-222.

Waller SL (1975). Differential measurement of small and large bowel transit times in constipation and diarrhoea: A new approach. *Gut* **16**, 372-378.

Walters MD, Miller WH, Casey SL and Graham C (1999). Effective dose equivalent due to gamma-ray emissions from hot particles. *Health Phys* **76,** 564-566.

Webb LM (1998). Computer Modelling of the Chemical Speciation of Lanthanides and Actinides in the Human Gastrointestinal Tract. PhD Thesis, University of Wales, Cardiff.

Wilkins BT, Fry FA, Burgess PH, Fayers CA, Haywood SM, Bexon AP and Tournette C (1998). Radiological implications of the presence of fragments of irradiated fuel in the sub-tidal zone at Dounreay. Chilton, NRPB-M1005.

Young RW (1987). Acute radiation syndrome. In: Military Radiobiology. (Eds. J.J. Conklin and R.I. Walker). Academic Press, New York.

Zankl M, Fill U, Petoussi-Henss N and Regulla D (2002). Organ dose conversion coefficients for external photon irradiation of male and female voxel models. *Phys Med Biol* **47**, 2367-2385.

Zankl M, Petoussi-Henss N, Fill U and Regulla D (2003). The application of voxel phantoms to the internal dosimetry of radionuclides. *Radiat Prot Dosim* **105**, 539-548.

Zaslavsky C, da Silveira TR and Maguilnik I (1998). Total and segmental colonic transit time with radio-opaque markers in adolescents with functional constipation. *J Pediatr Gastroenterol Nutr* **27**, 138-142.